DETAILED MODELING AND CONTROL OF A 2-DOF GIMBAL SYSTEM

A THESIS SUBMITTED TO
THE GRADUATE SCHOOL OF NATURAL AND APPLIED SCIENCES
OF
MIDDLE EAST TECHNICAL UNIVERSITY

BY

ERHAN POYRAZOĞLU

IN PARTIAL FULFILLMENT OF THE REQUIREMENTS
FOR
THE DEGREE OF MASTER OF SCIENCE
IN
ELECTRICAL AND ELECTRONICS ENGINEERING

JANUARY 2017

Approval of the thesis:

DETAILED MODELING AND CONTROL OF A 2-DOF GIMBAL SYSTEM

submitted by **ERHAN POYRAZOĞLU** in partial fulfillment of the requirements for the degree of **Master of Science in Electrical and Electronics Engineering Department, Middle East Technical University** by,

Prof. Dr. Gülbin Dural Ünver _____
Dean, Graduate School of **Natural and Applied Sciences**

Prof. Dr. Tolga Çiloğlu _____
Head of Department, **Electrical and Electronics Engineering**

Prof. Dr. Kemal Leblebicioğlu _____
Supervisor, **Electrical and Electronics Engineering Department, METU**

Examining Committee Members:

Prof. Dr. Mustafa Kuzuoğlu _____
Electrical and Electronics Engineering Department, METU

Prof. Dr. M. Kemal Leblebicioğlu _____
Electrical and Electronics Engineering Department, METU

Prof. Dr. M. Kemal Özgören _____
Mechanical Engineering Department, METU

Prof. Dr. Mehmet Önder Efe _____
Computer Engineering Department, Hacettepe University

Assist. Prof. Dr. Emre Özkan _____
Electrical and Electronics Engineering Department,METU

Date: _____

I hereby declare that all information in this document has been obtained and presented in accordance with academic rules and ethical conduct. I also declare that, as required by these rules and conduct, I have fully cited and referenced all material and results that are not original to this work.

Name, Last Name: ERHAN POYRAZOĞLU

Signature :

ABSTRACT

DETAILED MODELING AND CONTROL OF A 2-DOF GIMBAL SYSTEM

Poyrazoğlu, Erhan

M.S., Department of Electrical and Electronics Engineering

Supervisor : Prof. Dr. Kemal Leblebicioğlu

January 2017, 111 pages

Gimbal systems are used in various engineering applications such as military systems. Their configurations are designed according to the types of application and desired performance requirements. The essential aim of these systems is to compensate the disturbance effects in order to stabilize LOS and positioning to the desired point.

In this thesis, first, a detailed mathematical model of a 2-DOF gimbal system containing some nonlinear dynamic effects such as friction, static and dynamic mass unbalance is obtained by Newton-Euler approach. Next, three different controllers that are cascade proportional-integral (PI), global and local linear quadratic integral (LQI) have been constructed. The mathematical model and the controllers have been implemented in MATLAB and their performances have been investigated.

In the final part of this study, in order to visualize and track a target in simulation, a 3-D virtual environment is constructed within MATLAB/Simulink 3-D Toolbox

and a simple target tracking algorithm is designed to detect and track targets. All of these operations are simulated on MATLAB/Simulink environment.

Keywords: Mathematical Model, Stabilization, Target Tracking, Gimbal, VRML

ÖZ

İKİ EKSEN BİR GİMBAL SİSTEMİNİN DETAYLI MODELLEMESİ VE KONTROLÜ

Poyrazoğlu, Erhan
Yüksek Lisans, Elektrik ve Elektronik Mühendisliği Bölümü
Tez Yöneticisi : Prof. Dr. Kemal Leblebicioğlu

Ocak 2017 , 111 sayfa

Gimbal sistemleri çeşitli mühendislik uygulamalarında kullanılmaktadır. Uygulama alanları ve performans isterleri göz önüne alınarak bu sistemlerin yapısal konfigürasyonları tasarlanmaktadır. Bu sistemlerin temel hedefleri bir hedefe bakarken hareket eden bir platform üzerinde sistemin stabilize olması ve istenen konumlara yönlenmesidir.

Bu tezde ilk olarak sürtünme, statik ve dinamik kütle dengesizliği gibi doğrusal olmayan dinamikler içeren iki eksen bir gimbal sisteminin detaylı matematiksel modeli Newton-Euler yaklaşımı ile elde edilmiştir. Ardından üç farklı kontrol yöntemi kurulmuştur. matematiksel model ve kontrolörler MATLAB'da uygulanmış ve performansları incelenmiştir.

Son olarak benzetim ortamını görselleştirmek ve hedef takibi yapabilmek için MAT-

LAB/Simulink 3-D Toolbox ile üç boyutlu sanal bir ortam kurulmuş ve basit bir hedef takip algoritması tasarlanmıştır. Tüm benzetim çalışmaları MATLAB/Simulink ortamında yapılmıştır.

Anahtar Kelimeler: Matematiksel Model, Stabilizasyon, Hedef Takip, Gimbal, VRML

To my family

ACKNOWLEDGMENTS

I would like to thank my supervisor Professor Kemal Leblebicioğlu for his guidance and friendship. It was a great honor to work with him and our cooperation influenced my academical view highly.

My family also provided invaluable support for this work. I would like to thank especially to my mother Nezihe Poyrazoğlu and my brother Furkan Poyrazoğlu. They always make me feel loved and cared.

I would like to thank Mehmet Sami Büyüksarıkulak, Irmak Ece Şener, Kamil Alper Yalçınkaya and Elif Yavuztürk who supported this work and their contributions were most valuable. Furthermore I would like to thank my dear friends for their fellowships and endless supports; Selin Akboğa, Ahmet Furkan Oruç, Onur Aydın, Oğuz Kırbıyık, Murat Karabıyık, Deniz Genlik, Dilara Uğurlu, Merve Tiftik, Neslihan Küçük, Ozan Can Sarıoğlu and Hayrettin Karadağ.

TABLE OF CONTENTS

LIST OF TABLES

TABLES

LIST OF FIGURES

FIGURES

LIST OF ABBREVIATIONS AND SYMBOLS

ISU	Inertially stabilized platform
LOS	Line of sight
IMU	Inertial measurement unit
CG	Center of gravity
DOF	Degree of freedom
FOV	Field of view
PID	Proportional integral derivative
POI	Product of inertia
VRC	Variance ratio criterion
LQI	Linear quadratic integral
LTI	Linear time invariant
MIMO	Multiple input and multiple output
2-D	Two dimensional
3-D	Three dimensional
VRML	Visual reality modeling language
(e)	Reference frame fixed to the earth (Inertial frame)
(m), (n)	Reference frames defining platform base motion between earth and gimbal base
(B)	Reference frame fixed to the gimbal base
(O)	Reference frame fixed to the outer gimbal
(I)	Reference frame fixed to the inner gimbal
P	Pivot point
$\mathbb{I}_1$	The identity matrix
J	Cost function
$\mathbb{M}_\Omega$	Skew-symmetric matrix which is connected with the angular velocity vector $\mathbf{\Omega}$
$\mathbb{T}_{ab}$	Transformation matrix from the reference frame (a) to the reference frame (b)
ψ, θ, ϕ	Yaw, pitch and roll angles of the platform motion

η	Angular position of the outer gimbal
η_{ref}	Angular position reference of the outer gimbal
ϵ	Angular position of the inner gimbal
ϵ_{ref}	Angular position reference of the inner gimbal
$\boldsymbol{\Omega}_{ab}$	Angular velocity vector of the reference frame (a) relative to the reference frame (b) in the reference frame (a)
Ω_{ab_x}, Ω_{ab_y}, Ω_{ab_z}	Components of the angular velocity vector $\boldsymbol{\Omega}_{ab}$ on x, y and z axes of the reference frame (a)
$\boldsymbol{\alpha}_{ab}$	Angular acceleration vector of the reference frame (a) relative to the reference frame (b) in the reference frame (a)
α_{ab_x}, α_{ab_y}, α_{ab_z}	Components of the angular acceleration vector $\boldsymbol{\alpha}_{ab}$ on x, y and z axes of the reference frame (a)
T_C	Coulomb friction torque
T_S	Static friction torque
v_s	Stribeck velocity
δ	Stribeck shape factor
$T_{fr_{ab}}$	Friction torque between the reference frame (a) and reference frame (b)
σ_0, σ_1, σ_2	Stiffness, damping and viscous damping coefficients of friction models
R_m	Resistance of motor
L_m	Inductance of motor
I_{m_I}, I_{m_O}	Inner and outer gimbal rotor moment of inertia
K_m	Torque constant
K_e	Back EMF constant
T_p	Peak torque of motor
T_{fr_m}	Friction motor torque
T_r	Torque ripple
T_{m_I}, T_{m_O}	Motor torques transmitted to the inner and outer gimbal
m_I, m_O	Inner and outer gimbal masses
$\boldsymbol{A}_{G_I}$, $\boldsymbol{A}_{G_O}$	Linear acceleration vector of the the inner and outer gimbal CG
$\boldsymbol{F}_{ab}$	Linear force vector applied from the reference frame (a) to reference frame (b)
$\boldsymbol{g}$	Gravity vector
$\boldsymbol{H}_{I,P}$	Angular momentum vector of the inner gimbal about pivot point P relative to the inner gimbal reference frame (I)

$\boldsymbol{H}_{O,P}$	Angular momentum vector of the outer gimbal about pivot point P relative to the outer gimbal reference frame (I)
$\mathbb{I}_P^I$, $\mathbb{I}_P^O$	Inertia tensors of the decoupled inner and outer gimbal calculated about pivot point P relative to the earth frame (e)
$\boldsymbol{M}_{ab}$	Moment vector applied from reference frame (a) to the reference frame (b)
$\boldsymbol{D}^I_{staticUnb}$	Disturbance moment vector caused by static mass unbalance on the inner gimbal
$\boldsymbol{D}^O_{staticUnb}$	Disturbance moment vector caused by static mass unbalance on the outer gimbal
$\boldsymbol{D}^I_{dynamicUnb}$	disturbance moment vector caused by dynamic mass unbalance on the inner gimbal
$\boldsymbol{D}^O_{dynamicUnb}$	disturbance moment vector caused by dynamic mass unbalance on the outer gimbal
$\boldsymbol{r}_{PG_I}$, $\boldsymbol{r}_{PG_O}$	Position vectors from pivot point to the CG of inner and outer gimbal
$\boldsymbol{x}_a$	State vector of gimbal model (a)
$\boldsymbol{u}_a$	Control input vector of gimbal model (a)
$\boldsymbol{w}_a$	Disturbance vector of gimbal model (a)
$\boldsymbol{n}_a$	Gyroscope noise vector of gimbal model (a)
$\boldsymbol{y}_a$	Output vector of gimbal model (a)
$\boldsymbol{A}_a$	State matrix of gimbal model (a)
$\boldsymbol{B}_a$	Control input matrix of gimbal model (a)
$\boldsymbol{C}_a$	Output matrix of gimbal model (a)
$\boldsymbol{G}_a$	Disturbance state matrix of gimbal model (a)
$\boldsymbol{P}_a$	Disturbance output matrix of gimbal model (a)
$\hat{\boldsymbol{S}}_a$	Matrix used to collect all the first order derivative terms of states on the left of state equation of gimbal model (a)
Γ_a	Equilibrium points of gimbal model (a)
CH_k	The Calinski-Harabasz index
SS_B	Overall between-cluster variance
SS_W	Overall within-cluster variance
$\boldsymbol{\delta}_x$	Deviation of state variables
K_p	Proportional gain of PID controller
K_i	Integral gain of PID controller
K_d	Derivative gain of PID controller

$\boldsymbol{K}$	State feedback gain matrix of linear quadratic control problem
$\boldsymbol{\xi}$	Integral of error signal vector of linear quadratic control problem
$\hat{\boldsymbol{Q}}$, $\hat{\boldsymbol{R}}$	LQI controller matrices
w_u	Scalar weight constant of control signal of a LTI subsystem
d	Euclidean distance
q_i	ith pixel of the image
$I_x(q_i)$	Partial derivative of q_i on x axis
$I_y(q_i)$	Partial derivative of q_i on y axis
$I_t(q_i)$	Partial derivative of q_i with respect to time
$\boldsymbol{v}$	Optical flow vector
V_x	Optical flow in horizontal direction
V_y	Optical flow in vertical direction
$x_{Est.PlaneLoc}$	Estimated translational position of the plane on the x axis of virtual world
$y_{Est.PlaneLoc}$	Estimated translational position of the plane on the y axis of virtual world
$z_{Est.PlaneLoc}$	Estimated translational position of the plane on the z axis of virtual world
x_{LOS}, y_{LOS}, z_{LOS}	Projection of LOS onto the x,y and z axes of virtual world

CHAPTER 1

INTRODUCTION

1.1 Background

Inertial stabilization platforms (ISPs) are used in lots of various engineering applications such as weapon systems, telescopes and cameras. Their configurations are designed according to the types of application and desired performance requirements [20]. The essential aim of these systems is to compensate the maneuvers, platform motions, vibrations and nonlinearity based disturbances such as friction, static mass unbalance, dynamic mass unbalance and torque ripple in order to stabilize, or hold steady, a pointing vector, namely line-of-sight (LOS), in an inertial space by means of electro-optic sensors such as inertial measurement units (IMUs), encoders and cameras [25]. All of these disturbances cause decreasing the pointing accuracy of the ISPs [27].

This thesis consists of three main parts which are modeling, control and animation of an inertially stabilized 2-DOF gimbal system being developed by ASELSAN. Configuration of this system has two gimbals which are mounted on each other with orthogonal pivot axes: The inner gimbal contains two cameras, one laser designator, one IMU, one brushed DC motor to drive the inner gimbal and one encoder mounted on motor. The outer gimbal has only one brushed DC motor and one encoder.

When the gimbal is yet to be constructed, simulation studies gain more importance for control system designers. There are lots of applications and softwares to simulate the dynamic characteristics of control systems [15], [40], [44]. Mathematical mod-

eling of the gimbal takes the most importance for this study because this system is still in preliminary design phase. If we construct a detailed system model, designers can observe the performances of control algorithms even if the physical system is not present. Moreover, simulation studies are faster, desired data can be acquired easily and system scenarios can be simulated any number of times. Mathematical modeling study of our gimbal has been started with the geometrical model shown in Figure 1.1, which is a detailed CAD drawing of the physical model to be constructed.

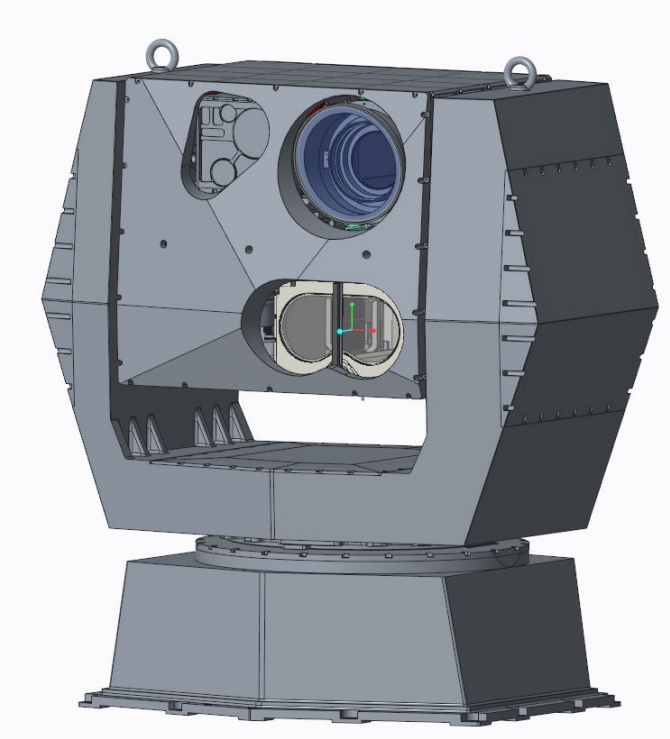

Figure 1.1: CAD drawing of a stabilized 2-DOF gimbal system developing by ASEL-SAN

1.2 Literature Survey

During the modeling study of the gimbal system, gimbal frame transformations, kinematics and dynamics of a gimbal system have been investigated, [4], [39] and [16]. When we examine [39] and [10] which focus on modeling of a gimbal system, it has been observed that static and dynamic mass unbalance effects are neglected in their gimbal models and all gimbals are decoupled, which results in unsatisfactory gimbal

models, which are used for many purposes. [1] explains static and dynamic mass unbalance dynamics of a 2-DOF gimbal system in detail. On the purpose of observing mass unbalance effects on a gimbal, they are included in the dynamic equations in this thesis. Furthermore, static friction models in these studies are unable to capture most of the friction phenomena and their success in simulation can not be guaranteed in practice. To construct a realistic friction model for friction compensation study, [42] compares lots of static and dynamic friction models. According to the result of this comparison, we decided to use Dahl friction model due to a number of advantages it provides, instead of the other static and dynamic friction models. Generally, simple DC motor models are combined by linear electrical and mechanical components [17]. It has been decided that two nonlinear terms are to be incorporated with the motor models; motor friction and torque ripple effects, based on the formulation provided in [35]. A nonlinear 2-DOF gimbal is described as a multiple-input, multiple-output (MIMO) system. In order to the resultant MIMO system via a linear compensator, a state space representation of the gimbal is obtained, equilibrium points are computed and these system models which are represented in state space are linearized about equilibrium points. There are two different approaches for the state space representation of the gimbal model in this study: In the first approach, inner and outer gimbals are coupled with each other and one gimbal model is obtained in state space. In the second approach, inner and outer gimbals are decoupled and their state space representations are expressed separately. These three nonlinear state space models contain lots of equilibrium points; these points are partitioned into clusters according to their similarities by means of K-means algorithm [33] and Calinski-Harabasz criterion [7] to reduce the number of linear models. [36] helps formulation of the gimbal models in state space, calculation of equilibrium points and linearization of nonlinear system models about clustered equilibrium points.

After mathematical models are constructed, two main control methods are examined. Firstly, [29] introduces PID control method, discusses whether the controller parameters in performance and some handicaps when integral and derivative terms are not fine-tuned. In this thesis, we have constructed a cascade PI control structure whose design procedure has been explained in detail for both inner and outer gimbals, coupled with each other. Secondly, the linear quadratic regular problem is formulated

in [36] and its benefits are discussed in [41]. However, linear tracking problem, proposed in [28], is more convenient than a regulator problem. In addition, none of our linearized subsystems have integrators present and integrator inclusions in controllers have been investigated. In literature, [36] presents and integrator-inserted LQI controller between error signals and the plant, which satisfies all the design requirements. In order to determine LQI controller parameters, [5] offers a very successful method to obtain the best performance control system. It is observed in this study that linear gimbal models represented in state space have more than one LTI subsystem. Thus, control inputs of subsystems are weighted by a gain scheduling algorithm for each subsystem and the sum of their outputs gives the overall system response.

After modeling and designing controller of the system is completed, Virtual Reality Modeling Language (VRML) technology [8] is used to generate a 3-D virtual world and capture video frames in camera frame frequency (rate) on MATLAB/Simulink environment [22]. The main aim of building a virtual reality world is to realize system scenarios for tracking a plane by looking from a distance when platform motion is carried out at the gimbal. To understand how to build a virtual world by using VRML and utilize Simulink blocks for target tracking in video frame sequence, especially [32], published by MATLAB, is a very helpful document which explains all examples and key parts of the utilization in detail. In [22], a virtual car, a static video camera and a virtual world having obstacles are built and Horn-Schunck optical flow method [21] is used for image processing and target tracking. In this thesis, discrete Kalman filter [9] is used to be able to track a target in the virtual world, based on motion estimation. [11] explains and formulates this algorithm in detail. To run the target tracking algorithm, blob analysis has been utilized in Simulink environment, [31].

1.3 Outline of Thesis

This thesis is organized as follows:

Chapter 2 presents detailed mathematical modeling of the 2-DOF gimbal system for

the purpose of constructing a model as realistic as possible. In the modeling process of the gimbal system, first, reference frames are described, transformation matrices and their first order derivatives are computed. Second, kinematic equations are incorporated. Third, the most realistic friction and actuator models are provided. Then, dynamic equations with friction models and mass unbalance effects are formulated. Lastly, both coupled and decoupled 2-DOF gimbal models are represented in a state space and their LTI models are obtained by Jacobian linearization technique.

Chapter 3 focuses on the two main control strategies implemented in nonlinear gimbal models on MATLAB/Simulink environment and their performances are compared in consideration of desired criteria. One of them is cascade PI control which is composed of rate and position controllers utilizing stabilization and pointing of the system, respectively. The other is linear quadratic integral control which is designed with LTI subsystems of both coupled 2-DOF gimbal and decoupled gimbals. Also gain scheduling is implemented into LQI control to weight the control signal of each LTI subsystems of coupled and decoupled gimbals.

In Chapter 4, a 3-D simulation environment is designed by means of the virtual reality modeling language (VRML) on MATLAB/Simulink. In addition, a tracker algorithm combined by discrete Kalman filter and image processing techniques is used to estimate motion of the target via video outputs of the constructed virtual world and it produces inner and outer position commands for the nonlinear gimbal system model with PI control method.

Finally in Chapter 5, the summary of the thesis and some suggestions for future studies have been presented.

CHAPTER 2

MATHEMATICAL MODELING OF THE 2-DOF GIMBAL SYSTEM

Detailed mathematical model of the 2-DOF gimbal system is examined in order to construct a realistic simulation environment in this chapter. Gimbal model has some nonlinearities such as friction, torque ripple, motor friction torque, static and dynamic mass unbalances. The main advantage of obtaining a realistic system model is the possibility of applying control methods in the lack of the physical system.

In the modeling study of the gimbal system, first, reference frames and transformation matrices are described. Second, kinematic equations are formulated. Then, friction effects between the gimbals, brushed DC actuators and sensor noises of the gyroscopes are modeled. After that, dynamic equations containing the friction and mass unbalance effects are formulated for the inner and outer gimbals. In addition, two decoupling methods for the gimbal platform are proposed and outputs of the coupled 2-DOF and decoupled gimbals are compared.

Nonlinear gimbal systems can be described as multiple-input, multiple-output (MIMO) systems. In the modeling study, we have also obtained nonlinear state space models of the coupled and decoupled gimbals. After that, their equilibrium points are found and they are clustered. Last, all nonlinear state space models are linearized about the cluster centers.

2.1 Reference Frames and Transformations

The mathematical model of the 2-DOF gimbal platform includes the outer gimbal, inner gimbal and gimbal base. Angular motions of the outer and inner gimbals are yaw (η) and pitch (ϵ) directions on their own reference frames, respectively. Moreover the gimbal base motion referring to the disturbances, caused by the sea waves, is a yaw-pitch-roll sequence. Angular displacements of the base motions in yaw (ψ), pitch (θ) and roll (ϕ) directions are called Euler angles. It is assumed that all reference frames are orthogonal and their origins are overlapped (in Figure 2.1). Frame transformations used to analyze the motion are summed up below:

(e):	Reference frame fixed to the earth (inertial) frame
(m), (n):	Reference frames defining platform base motion between the earth and gimbal base
(B):	Reference frame fixed to the gimbal base
(O):	Reference frame fixed to the outer gimbal
(I):	Reference frame fixed to the inner gimbal

and the unit direction vectors about the x, y and z axes are:

$$\boldsymbol{u}_x = \begin{bmatrix} 1 \\ 0 \\ 0 \end{bmatrix}, \boldsymbol{u}_y = \begin{bmatrix} 0 \\ 1 \\ 0 \end{bmatrix}, \boldsymbol{u}_z = \begin{bmatrix} 0 \\ 0 \\ 1 \end{bmatrix} \tag{2.1}$$

Moreover, rotational relations of the reference frames between the earth and inner gimbal are given in Figure 2.2. These transformations are highly important for computing kinematic and dynamic equations of the system.

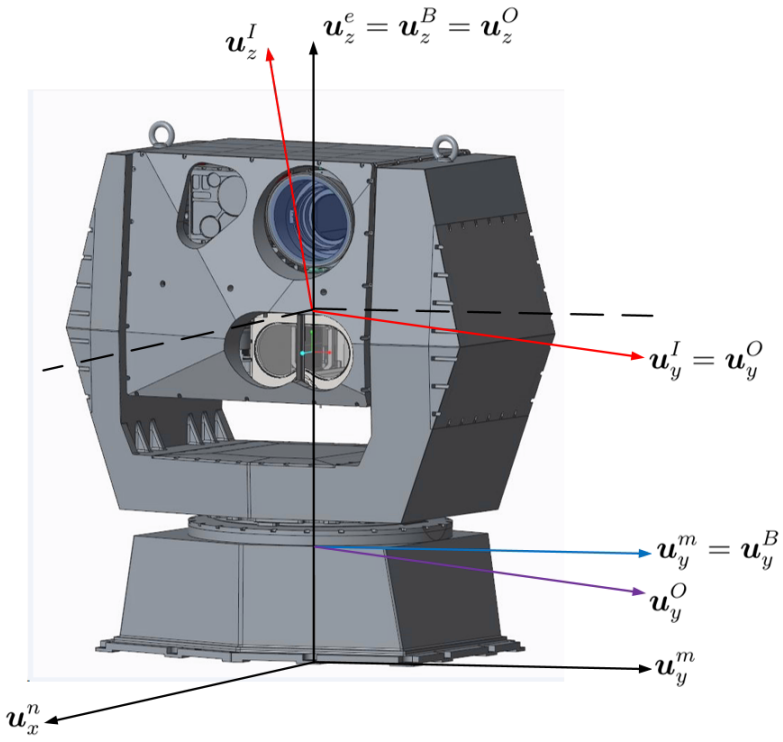

Figure 2.1: Rotational directions of a 2-DOF gimbal

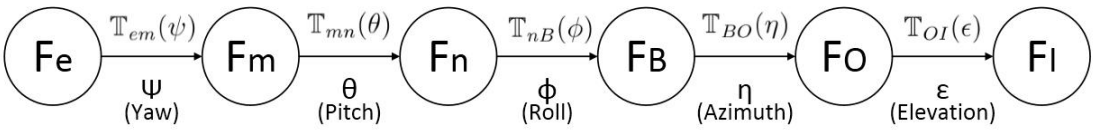

Figure 2.2: Reference frames and their rotational relations

In [4], theory of the transformation matrices between reference frames and computation of their first order derivatives with respect to time are examined in detail. A transformation matrix is expressed by $\mathbb{T}_{ab}$ which is used to project a vector from the reference frame (a) to the reference frame (b). Transformation matrices between reference frames in a sequence are expressed as follows:

$$\mathbb{T}_{em}(\psi) = \mathbb{T}_{me}^{T}(\psi) = \begin{bmatrix} \cos(\psi) & -\sin(\psi) & 0 \\ \sin(\psi) & \cos(\psi) & 0 \\ 0 & 0 & 1 \end{bmatrix} \tag{2.2}$$

$$\mathbb{T}_{mn}(\theta) = \mathbb{T}_{nm}^{T}(\theta) = \begin{bmatrix} \cos(\theta) & 0 & \sin(\theta) \\ 0 & 1 & 0 \\ -\sin(\theta) & 0 & \cos(\theta) \end{bmatrix} \tag{2.3}$$

$$\mathbb{T}_{nB}(\phi) = \mathbb{T}_{Bn}^{T}(\phi) = \begin{bmatrix} 1 & 0 & 0 \\ 0 & \cos(\phi) & -\sin(\phi) \\ 0 & \sin(\phi) & \cos(\phi) \end{bmatrix} \tag{2.4}$$

$$\mathbb{T}_{BO}(\eta) = \mathbb{T}_{OB}^{T}(\eta) = \begin{bmatrix} \cos(\eta) & -\sin(\eta) & 0 \\ \sin(\eta) & \cos(\eta) & 0 \\ 0 & 0 & 1 \end{bmatrix} \tag{2.5}$$

$$\mathbb{T}_{OI}(\epsilon) = \mathbb{T}_{IO}^{T}(\epsilon) = \begin{bmatrix} \cos(\epsilon) & 0 & \sin(\epsilon) \\ 0 & 1 & 0 \\ -\sin(\epsilon) & 0 & \cos(\epsilon) \end{bmatrix} \tag{2.6}$$

One property of the transformation matrices is that product of the transformation matrices and their transpose are equal to the identity matrix due to the orthogonality of frames. Therefore the first order derivatives of the transformation matrices with respect to time can be formulated by:

$$\frac{d\mathbb{T}^{T}}{dt}\mathbb{T} + \mathbb{T}^{T}\frac{d\mathbb{T}}{dt} = 0$$

and $\mathbb{T}^{T}\frac{d\mathbb{T}}{dt}$ term is a skew-symmetric matrix expressed by $\mathbb{M}_{\Omega}$.

$$\mathbb{M}_{\Omega} = \begin{bmatrix} 0 & -\Omega_z & \Omega_y \\ \Omega_z & 0 & -\Omega_x \\ -\Omega_y & \Omega_x & 0 \end{bmatrix} \tag{2.7}$$

The matrix $\mathbb{M}_{\Omega}$ is related with the angular velocity vector $\mathbf{\Omega} = \begin{bmatrix} \Omega_x & \Omega_y & \Omega_z \end{bmatrix}^{T}$. Hence the derivative of a transformation matrix is represented as:

$$\frac{d\mathbb{T}}{dt} = \mathbb{M}_{\Omega} \cdot \mathbb{T} \tag{2.8}$$

Consequently, the first order derivatives of all transformation matrices are written

(based on Eqs. 2.7 and 2.8) as:

$$\dot{\mathbb{T}}_{IO} = \mathbb{M}_{\Omega_{IO}} \mathbb{T}_{IO} = \begin{bmatrix} 0 & -\Omega_{IO_z} & \Omega_{IO_y} \\ \Omega_{IO_z} & 0 & -\Omega_{IO_x} \\ -\Omega_{IO_y} & \Omega_{IO_x} & 0 \end{bmatrix} \begin{bmatrix} \cos(\epsilon) & 0 & -\sin(\epsilon) \\ 0 & 1 & 0 \\ \sin(\epsilon) & 0 & \cos(\epsilon) \end{bmatrix}$$
$$= \begin{bmatrix} \Omega_{IO_y} \sin(\epsilon) & -\Omega_{IO_z} & \Omega_{IO_y} \cos(\epsilon) \\ \Omega_{IO_z} \cos(\epsilon) - \Omega_{IO_x} \sin(\epsilon) & 0 & -\Omega_{IO_z} \sin(\epsilon) - \Omega_{IO_x} \cos(\epsilon) \\ \Omega_{IO_y} \cos(\epsilon) & \Omega_{IO_x} & \Omega_{IO_y} \sin(\epsilon) \end{bmatrix} \tag{2.9}$$

$$\dot{\mathbb{T}}_{OB} = \mathbb{M}_{\Omega_{OB}} \mathbb{T}_{OB} = \begin{bmatrix} 0 & -\Omega_{OB_z} & \Omega_{OB_y} \\ \Omega_{OB_z} & 0 & -\Omega_{OB_x} \\ -\Omega_{OB_y} & \Omega_{OB_x} & 0 \end{bmatrix} \begin{bmatrix} \cos(\eta) & \sin(\eta) & 0 \\ -\sin(\eta) & \cos(\eta) & 0 \\ 0 & 0 & 1 \end{bmatrix}$$
$$= \begin{bmatrix} \Omega_{OB_z} \sin(\eta) & -\Omega_{OB_z} \cos(\eta) & \Omega_{OB_y} \\ \Omega_{OB_z} \cos(\eta) & \Omega_{OB_z} \sin(\eta) & -\Omega_{OB_x} \\ -\Omega_{OB_y} \cos(\eta) - \Omega_{OB_x} \sin(\eta) & -\Omega_{OB_y} \sin(\eta) + \Omega_{OB_x} \cos(\eta) & 0 \end{bmatrix} \tag{2.10}$$

$$\dot{\mathbb{T}}_{Bn} = \mathbb{M}_{\Omega_{Bn}} \mathbb{T}_{Bn} = \begin{bmatrix} 0 & -\Omega_{Bn_z} & \Omega_{Bn_y} \\ \Omega_{Bn_z} & 0 & -\Omega_{Bn_x} \\ -\Omega_{Bn_y} & \Omega_{Bn_x} & 0 \end{bmatrix} \begin{bmatrix} 1 & 0 & 0 \\ 0 & \cos(\phi) & \sin(\phi) \\ 0 & -\sin(\phi) & \cos(\phi) \end{bmatrix}$$
$$= \begin{bmatrix} 0 & -\Omega_{Bn_z} \cos(\phi) - \Omega_{Bn_y} \sin(\phi) & -\Omega_{Bn_z} \sin(\phi) + \Omega_{Bn_y} \cos(\phi) \\ \Omega_{Bn_z} & \Omega_{Bn_x} \sin(\phi) & -\Omega_{Bn_x} \cos(\phi) \\ -\Omega_{Bn_y} & \Omega_{Bn_x} \cos(\phi) & \Omega_{Bn_x} \sin(\phi) \end{bmatrix} \tag{2.11}$$

$$\dot{\mathbb{T}}_{nm} = \mathbb{M}_{\Omega_{nm}} \mathbb{T}_{nm} = \begin{bmatrix} 0 & -\Omega_{nm_z} & \Omega_{nm_y} \\ \Omega_{nm_z} & 0 & -\Omega_{nm_x} \\ -\Omega_{nm_y} & \Omega_{nm_x} & 0 \end{bmatrix} \begin{bmatrix} \cos(\theta) & 0 & -\sin(\theta) \\ 0 & 1 & 0 \\ \sin(\theta) & 0 & \cos(\theta) \end{bmatrix}$$
$$= \begin{bmatrix} \Omega_{nm_y} \sin(\theta) & -\Omega_{nm_z} & \Omega_{nm_y} \cos(\theta) \\ \Omega_{nm_z} \cos(\theta) - \Omega_{nm_x} \sin(\theta) & 0 & -\Omega_{nm_z} \sin(\theta) - \Omega_{nm_x} \cos(\theta) \\ \Omega_{nm_y} \cos(\theta) & \Omega_{nm_x} & \Omega_{nm_y} \sin(\theta) \end{bmatrix} \tag{2.12}$$

2.2 Kinematic Equations of Gimbal

Kinematics of the gimbal represent the angular velocity and acceleration terms. There are twelve kinematics of the 2-DOF gimbal relative to the earth frame. Transformations between the reference frames are related in kinematics. In order to project the inner and outer gimbal kinematics into the earth frame, first, they are transformed to the reference frame of the gimbal base. Then these are rotated by an amount of ϕ, θ and ψ Euler angles about the x, y and z axes, respectively [6].

2.2.1 Angular Velocity

Firstly, angular velocity vector of the outer gimbal $\boldsymbol{\Omega}_{Oe} = \begin{bmatrix} \Omega_{Oe_x} & \Omega_{Oe_y} & \Omega_{Oe_z} \end{bmatrix}^T$ relative to the earth frame (e) and represented in the outer gimbal frame (O) is:

$$\boldsymbol{\Omega}_{Oe} = \boldsymbol{\Omega}_{OB} + \boldsymbol{\Omega}_{Bn} + \boldsymbol{\Omega}_{nm} + \boldsymbol{\Omega}_{me}$$

and

$$\begin{aligned} \boldsymbol{\Omega}_{Oe} &= \dot{\eta}\boldsymbol{u}_z + \dot{\phi}\mathbb{T}_{OB}\boldsymbol{u}_x + \dot{\theta}\mathbb{T}_{OB}\mathbb{T}_{Bn}\boldsymbol{u}_y + \dot{\psi}\mathbb{T}_{OB}\mathbb{T}_{Bn}\mathbb{T}_{nm}\boldsymbol{u}_z \\ &= \begin{bmatrix} 0 \\ 0 \\ \dot{\eta} \end{bmatrix} + \mathbb{T}_{OB}\begin{bmatrix} \dot{\phi} \\ 0 \\ 0 \end{bmatrix} + \mathbb{T}_{OB}\mathbb{T}_{Bn}\begin{bmatrix} 0 \\ \dot{\theta} \\ 0 \end{bmatrix} + \mathbb{T}_{OB}\mathbb{T}_{Bn}\mathbb{T}_{nm}\begin{bmatrix} 0 \\ 0 \\ \dot{\psi} \end{bmatrix} \end{aligned}$$

where η is the angular position of the outer gimbal about the z axis. By substituting transformation matrices into $\boldsymbol{\Omega}_{Oe}$, components of this velocity expression about the x, y and z axes are:

$$\Omega_{Oe_x} = \dot{\phi}\cos\phi + \dot{\theta}\cos\phi\sin\eta + \dot{\psi}(\cos\theta\sin\eta\sin\phi - \cos\eta\sin\theta) \tag{2.13}$$

$$\Omega_{Oe_y} = -\dot{\phi}\sin\phi + \dot{\theta}\cos\phi\cos\eta + \dot{\psi}(\sin\eta\sin\theta + \cos\eta\cos\theta\sin\phi) \tag{2.14}$$

$$\Omega_{Oe_z} = \dot{\eta} + \Omega_{dist_{O_z}} \tag{2.15}$$

where $\Omega_{dist_{O_z}}$ is disturbance velocity effect about the z axis of the outer gimbal.

$$\Omega_{dist_{O_z}} = -\dot{\theta}\sin\phi + \dot{\psi}\cos\phi\cos\theta$$

Secondly, angular velocity of the inner gimbal $\boldsymbol{\Omega}_{Ie} = \begin{bmatrix}\Omega_{Ie_x} & \Omega_{Ie_y} & \Omega_{Ie_z}\end{bmatrix}^T$ relative to the earth frame and represented in the inner gimbal frame (I) is:

$$\begin{aligned}\boldsymbol{\Omega}_{Ie} &= \dot{\epsilon}\boldsymbol{u}_y + \mathbb{T}_{IO}\boldsymbol{\Omega}_{Oe} \\ &= \begin{bmatrix}0\\ \dot{\epsilon}\\ 0\end{bmatrix} + \mathbb{T}_{IO}\begin{bmatrix}0\\ 0\\ \dot{\eta}\end{bmatrix} + \mathbb{T}_{IO}\mathbb{T}_{OB}\begin{bmatrix}\dot{\phi}\\ 0\\ 0\end{bmatrix} + \mathbb{T}_{IO}\mathbb{T}_{OB}\mathbb{T}_{Bn}\begin{bmatrix}0\\ \dot{\theta}\\ 0\end{bmatrix} + \mathbb{T}_{IO}\mathbb{T}_{OB}\mathbb{T}_{Bn}\mathbb{T}_{nm}\begin{bmatrix}0\\ 0\\ \dot{\psi}\end{bmatrix}\end{aligned} \tag{2.16}$$

where ϵ is the angular position of the inner gimbal. When transformation matrices substituted into Eq. 2.16, components of $\boldsymbol{\Omega}_{Ie}$ about the x, y and z axes are written as follows:

$$\begin{aligned}\Omega_{Ie_x} = {} & \dot{\phi}\cos\epsilon\cos\eta - \dot{\psi}(\sin\epsilon\cos\phi - \cos\epsilon\sin\eta\sin\phi) + \dot{\theta}(\sin\epsilon\sin\phi + \cos\epsilon\sin\eta\cos\phi) \\ & - \dot{\eta}\sin\epsilon\end{aligned} \tag{2.17}$$

$$\Omega_{Ie_y} = \dot{\epsilon} + \Omega_{dist_{I_y}} \tag{2.18}$$

where $\Omega_{dist_{I_y}}$ is the disturbance velocity about the y axis of the inner gimbal.

$$\Omega_{dist_{I_y}} = -\dot{\phi}\sin\eta + \dot{\theta}\cos\eta\cos\phi + \dot{\psi}\cos\eta\sin\phi$$

$$\begin{aligned}\Omega_{Ie_z} = {} & \dot{\phi}\sin\epsilon\cos\eta + \dot{\psi}(\cos\epsilon\cos\phi + \sin\epsilon\sin\eta\sin\phi) - \dot{\theta}(\cos\epsilon\sin\phi - \sin\epsilon\sin\eta\cos\phi) \\ & + \dot{\eta}\cos\epsilon\end{aligned} \tag{2.19}$$

2.2.2 Angular Acceleration

Angular acceleration of the 2-DOF gimbal is obtained by the first order derivative of angular velocity of the same gimbal reference frame with respect to time. Angular acceleration of the outer gimbal relative to the earth frame (e) described by $\boldsymbol{\alpha}_{Oe} =$

$\begin{bmatrix} \alpha_{Oe_x} & \alpha_{Oe_y} & \alpha_{Oe_z} \end{bmatrix}^T$ can be calculated by:

$$\begin{aligned} \boldsymbol{\alpha}_{Oe} &= \ddot{\eta}\boldsymbol{u}_z \\ &+ \ddot{\phi}\mathbb{T}_{OB}\boldsymbol{u}_x \\ &+ \ddot{\theta}(\mathbb{T}_{OB}\mathbb{T}_{Bn})\boldsymbol{u}_y \\ &+ \ddot{\psi}(\mathbb{T}_{OB}\mathbb{T}_{Bn}\mathbb{T}_{nm})\boldsymbol{u}_z \\ &+ \dot{\phi}\dot{\mathbb{T}}_{OB}\boldsymbol{u}_x \\ &+ \dot{\theta}(\dot{\mathbb{T}}_{OB}\mathbb{T}_{Bn} + \mathbb{T}_{OB}\dot{\mathbb{T}}_{Bn})\boldsymbol{u}_y \\ &+ \dot{\psi}(\dot{\mathbb{T}}_{OB}\mathbb{T}_{Bn}\mathbb{T}_{nm} + \mathbb{T}_{OB}\dot{\mathbb{T}}_{Bn}\mathbb{T}_{nm} + \mathbb{T}_{OB}\mathbb{T}_{Bn}\dot{\mathbb{T}}_{nm})\boldsymbol{u}_z \end{aligned} \tag{2.20}$$

where the first order derivatives of the transformation matrices are:

$$\dot{\mathbb{T}}_{OB} = \mathbb{M}_{\Omega_{OB}}\mathbb{T}_{OB} = \dot{\eta}\begin{bmatrix} \sin\eta & -\cos\eta & 0 \\ \cos\eta & \sin\eta & 0 \\ 0 & 0 & 0 \end{bmatrix}$$

$$\dot{\mathbb{T}}_{Bn} = \mathbb{M}_{\Omega_{Bn}}\mathbb{T}_{Bn} = \dot{\phi}\begin{bmatrix} 0 & \sin^2\phi & -cos\phi\sin\phi \\ 0 & \cos\phi\sin\phi & -\cos^2\phi \\ \sin\phi & \cos^2\phi & \cos\phi\sin\phi \end{bmatrix}$$

$$\begin{aligned} \dot{\mathbb{T}}_{nm} &= \mathbb{M}_{\Omega_{nm}}\mathbb{T}_{nm} \\ &= \dot{\theta}\begin{bmatrix} \cos\eta\cos\phi\sin\theta & \sin\phi & \cos\eta\cos\phi\cos\theta \\ -\cos\theta\sin\phi - \cos\phi\sin\eta\sin\theta & 0 & \sin\phi\sin\theta - \cos\phi\cos\theta\sin\eta \\ -\cos\eta\cos\phi\cos\theta & \cos\phi\sin\eta & \cos\eta\cos\phi\sin\theta \end{bmatrix} \end{aligned}$$

and angular acceleration of the inner gimbal $\alpha_{Ie} = \begin{bmatrix} \alpha_{Ie_x} & \alpha_{Ie_y} & \alpha_{Ie_z} \end{bmatrix}^T$ relative to

the earth frame (e) and represented in the inner gimbal reference frame (I) is:

$$
\begin{aligned}
\boldsymbol{\alpha}_{Ie} = & \ddot{\epsilon}\boldsymbol{u}_y \\
& + \ddot{\eta}\mathbb{T}_{IO}\boldsymbol{u}_z \\
& + \dot{\eta}\dot{\mathbb{T}}_{IO}\boldsymbol{u}_z \\
& + \ddot{\phi}(\mathbb{T}_{IO}\mathbb{T}_{OB})\boldsymbol{u}_x \\
& + \ddot{\theta}(\mathbb{T}_{IO}\mathbb{T}_{OB}\mathbb{T}_{Bn})\boldsymbol{u}_y \\
& + \ddot{\psi}(\mathbb{T}_{IO}\mathbb{T}_{OB}\mathbb{T}_{Bn}\mathbb{T}_{nm})\boldsymbol{u}_z \\
& + \dot{\phi}(\dot{\mathbb{T}}_{IO}\mathbb{T}_{OB} + \mathbb{T}_{IO}\dot{\mathbb{T}}_{OB})\boldsymbol{u}_x \\
& + \dot{\theta}(\dot{\mathbb{T}}_{IO}\mathbb{T}_{OB}\mathbb{T}_{Bn} + \mathbb{T}_{IO}\dot{\mathbb{T}}_{OB}\mathbb{T}_{Bn} + \mathbb{T}_{IO}\mathbb{T}_{OB}\dot{\mathbb{T}}_{Bn})\boldsymbol{u}_y \\
& + \dot{\psi}(\dot{\mathbb{T}}_{IO}\mathbb{T}_{OB}\mathbb{T}_{Bn}\mathbb{T}_{nm} + \mathbb{T}_{IO}\dot{\mathbb{T}}_{OB}\mathbb{T}_{Bn}\mathbb{T}_{nm} + \mathbb{T}_{IO}\mathbb{T}_{OB}\dot{\mathbb{T}}_{Bn}\mathbb{T}_{nm} + \mathbb{T}_{IO}\mathbb{T}_{OB}\mathbb{T}_{Bn}\dot{\mathbb{T}}_{nm})\boldsymbol{u}_z
\end{aligned}
\tag{2.21}
$$

where

$$
\dot{\mathbb{T}}_{IO} = \mathbb{M}_{\Omega_{IO}}\mathbb{T}_{IO} = \dot{\epsilon}\begin{bmatrix} \sin\epsilon & 0 & \cos\epsilon \\ 0 & 0 & 0 \\ -\cos\epsilon & 0 & \sin\epsilon \end{bmatrix}
$$

By substituting transformation matrices into Eq. 2.20 and Eq. 2.21, components of $\boldsymbol{\alpha}_{Oe}$ and $\boldsymbol{\alpha}_{Ie}$ about the x, y and z axes are given in Eqs. A.1 - A.6.

2.3 Friction Model

Friction term can be described as the resistance to the motion between two surfaces sliding against each other. It is a natural phenomenon which is quite hard to model and it is not yet completely understood [14]. The main goal of modeling of the friction is to observe uncertainty of the mechanical systems. There are two main types of friction models which are static and dynamic in simulation studies.

The classic friction models can be accepted the most basic friction models, including Coulomb, viscous, stiction, Stribeck effect and their all possible combinations. These types of frictions depend statically on the applied load and relative velocity [42]. Hence classical models are described by static maps between velocity and friction torque [14].

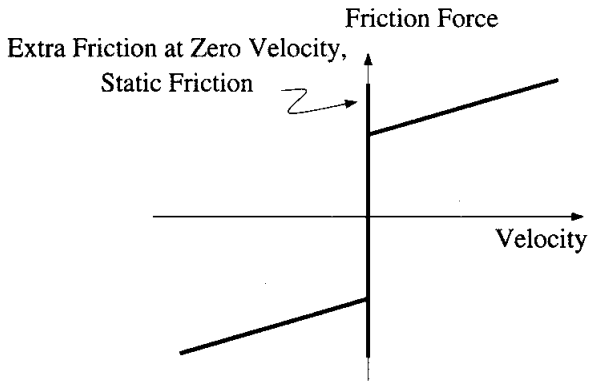

Figure 2.3: Combination of Coulomb, viscous and static friction [2]

The Stribeck effect [2] is expressed as nonlinear continuous transition from the static friction to the dynamic friction for lubricated and dry surfaces. The Stribeck velocity v_s can be defined as the velocity where dip point of the Stribeck curve, shown in Figure 2.4. Stribeck effect is formulated by:

$$s(v) = (T_C + (T_S - T_C)e^{-(v/v_s)^\delta})sgn(v) \tag{2.22}$$

where T_C is Coulomb friction torque, T_S is stiction torque, v is relative velocity, v_s is the Stribeck velocity and δ is the Stribeck shape factor.

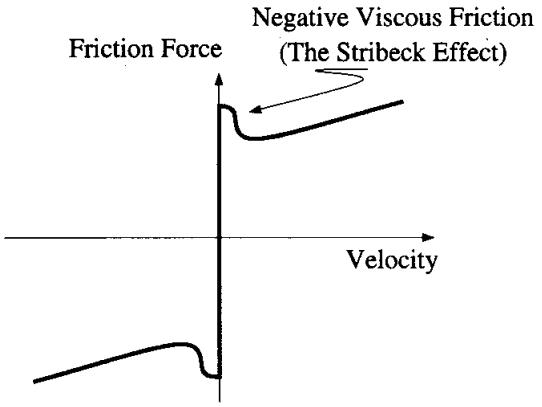

Figure 2.4: Combination of Coulomb, viscous, static friction and Stribeck effect [2]

The main limitations of the classical friction models are zero crossing of velocity and non-uniqueness of the solution between $-T_S$ and $+T_S$ at zero velocity [3]. To solve these problems, Karnopp friction model which is capable of detecting zero velocity with high accuracy is proposed in [24]. Although Karnopp model is efficient in simu-

lation studies, it is strongly coupled with the rest of system and external torque which is one of the friction input terms which can not be described explicitly. Therefore, the success in simulation may fail in practical applications [42]. When all problems and limited capabilities of static models are taken into account, these models are not able to satisfy the friction phenomenon accurately. On the other hand, dynamic models can solve all problems of static models and capture some friction phenomena. Consequently, the dynamic models are preferred instead of static models.

The Dahl friction model [12], which is the simplest dynamic model, is used to simulate servo systems with ball bearing friction [37]. This model depends on Coulomb friction, sign of velocity and angular displacement. It captures hysteresis effects and solves all problems of static friction models. In addition, the Dahl model is very successful in both simulation and practical applications [14]. On the other hand, the Dahl neither captures the Stribeck effect, depending on angular velocity, nor the stick-slip motion. Description of the Dahl model in time domain is formulated by:

$$T_{fr} = \sigma_0 z \tag{2.23}$$

$$\frac{dz}{dt} = v - \frac{\sigma_0 |v|}{T_C} z \tag{2.24}$$

where T_{fr} is friction torque, T_C is Coulomb friction, v is relative angular velocity and σ_0 is stiffness.

Table2.1: Parameters of Dahl friction model effect on inner and outer gimbals

Parameters	**Units**	**Symbol**	$T_{fr_{BO}}$ **values**	$T_{fr_{IO}}$ **values**
Coulomb friction torque	N.m	T_C	18.1	2.7
Stiffness coefficient	N.m/rad	σ_0	80	90

The LuGre friction model includes all advantages of the Dahl model. In addition, this model can capture the Stribeck effect, stick-slip motion, friction lag in sliding regime, hysteresis curve in pre-sliding and it can estimate the break-away force at transition from pre-sliding to sliding regime [42]. The LuGre friction model is based on representation of the elastic bristles visualized between two rigid bodies [18]. Modeling of LuGre is built on the average deflection of the bristles. When a tangential force is applied, the bristles will deflect like springs. If deflection is sufficiently large the

bristles start to slip [14], [37].

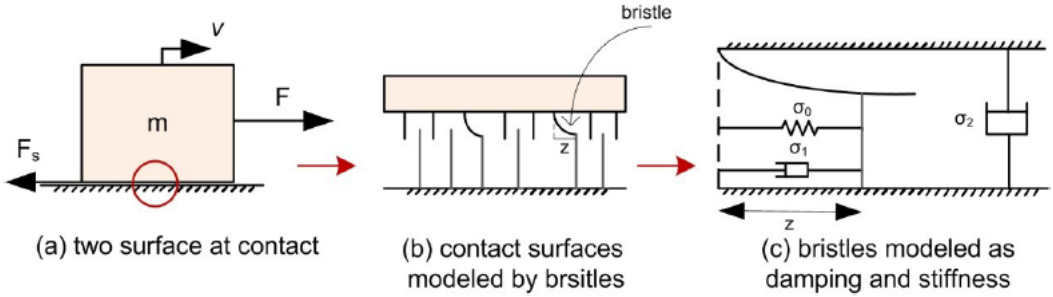

Figure 2.5: Physical explanation of the LuGre friction model [42]

LuGre friction model is in the following form:

$$\frac{dz}{dt} = v - \frac{|v|}{g(v)}z \tag{2.25}$$

$$T_{fr} = \sigma_0 z + \sigma_1 \frac{dz}{dt} + \sigma_2 v \tag{2.26}$$

where z is average deflection of the bristles, v is relative velocity between two surfaces, σ_0 is stiffness coefficient, σ_1 is damping coefficient, σ_2 is viscous damping coefficient and $g(v)$ function is used to obtain Stribeck effect formulated by:

$$\sigma_0 g(v) = T_C + (T_S - T_C)e^{-(v/v_s)^\delta} \tag{2.27}$$

where T_C is the Coulomb friction torque, T_S is the stiction torque, v_s is the Stribeck velocity and δ is the Stribeck shape factor. Values of parameters of LuGre friction models on inner and outer gimbals are given in Table 2.2. With these values of parameters, hysteresis curves of frictions between gimbals are shown below.

Table2.2: Parameters of LuGre friction model effect on inner and outer gimbals

Parameters	**Units**	**Symbol**	T_{frBO} **values**	T_{frIO} **values**
Coulomb friction torque	N.m	T_C	18.1	2.7
Static friction torque	N.m	T_S	22.6	3.4
Stribeck velocity	rad/sec	v_s	0.001	0.001
Stribeck shape factor	-	δ	2	2
Stiffness coefficient	N.m/rad	σ_0	80	90
Damping coefficient	N.m/rad	σ_1	8.9	9.48
Viscous damping coefficient	N.m sec/rad	σ_2	0	0

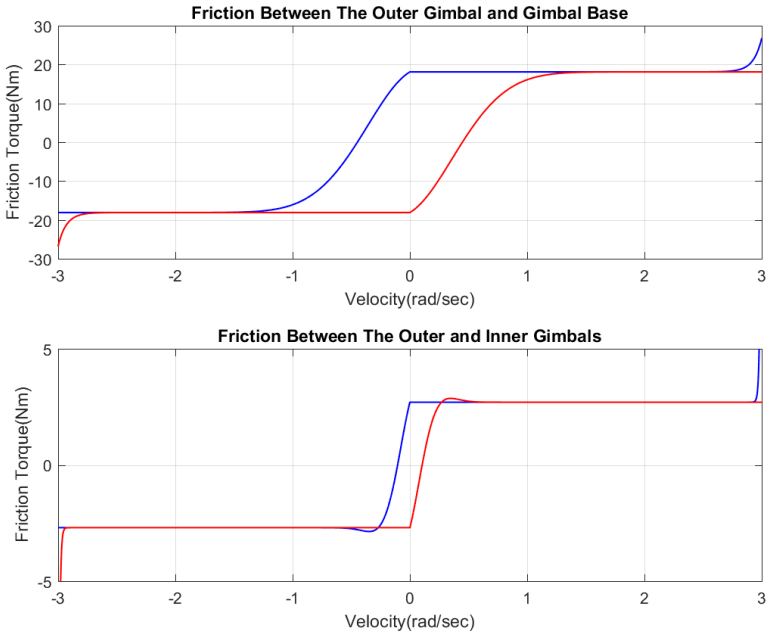

Figure 2.6: Hysteresis curves of the LuGre friction models

In order to decide the most convenient dynamic friction model for simulation studies, outputs of Dahl and LuGre are examined for different angular velocity inputs.

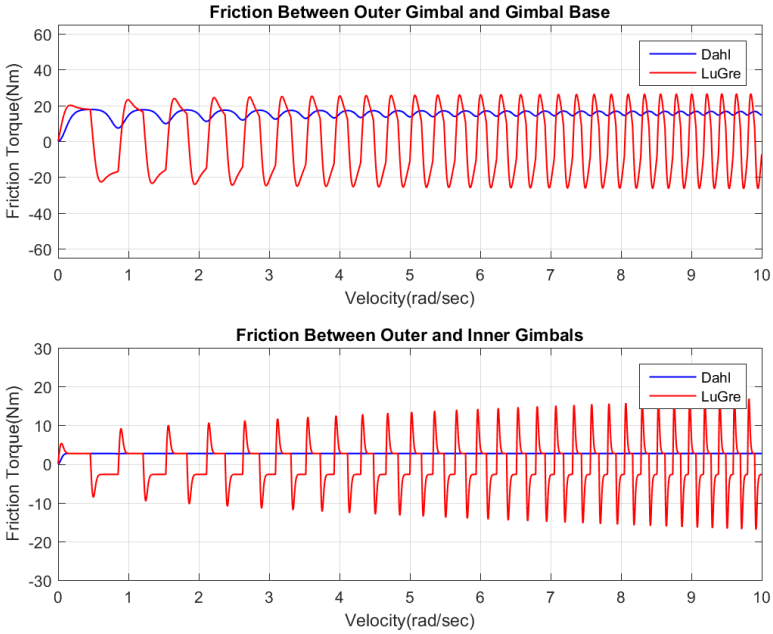

Figure 2.7: Chirp responses of the Dahl and LuGre friction models

In [42], LuGre friction model is chosen for friction compensation instead of the other static and dynamic models. It can capture many friction phenomena and the number

of LuGre parameters is less than Leuven and GMS models for identification. In mechanical design of our system, ball bearings are used on the purpose of decreasing friction effects between weighty gimbals. Although LuGre has many advantages on obtaining a realistic friction model, Dahl model is more suitable to use in this study.

2.4 DC Motor Model

Actuators of the inner and outer gimbals are chosen as brushed DC motors from KOLLMORGEN Company. Mathematical model of the DC motor, constructed by electrical and mechanical parts, is strengthened in a lot of scientific paper [17]. Electrical part parameters are inductance L_m, motor resistance R_m and back EMF constant K_e. On the other hand, mechanical part parameters of the brushed DC motor are rotor moment of inertia I_m, motor friction torque T_{fr_m}, torque ripple T_r and torque constant K_m.

Mathematical model of the DC actuator contains both linear and nonlinear effects. In [1], simplest linear DC motor model is used for the mathematical model of the gimbal. In this study, Coulomb motor friction torque and torque ripple effect, caused by lots of reasons such as coupling of magnetic field, cogging torque and mechanical unbalances of motor, are implemented into the linear motor model. Torque ripple causes acoustic noise, mechanical vibrations and inaccuracy for position and speed control [43]. As shown in Figure 2.8, characteristic of the torque ripple is a sine wave function of the ripple frequency and angular displacement. Value of the torque ripple can be described as the percent change from the peak value to the average value of motor torque. Besides, ripple frequency refers to the number of ripple cycles in one revolution of the motor. Indeed, number of ripple cycles in one revolution is equal to the number of commutator bars [35].

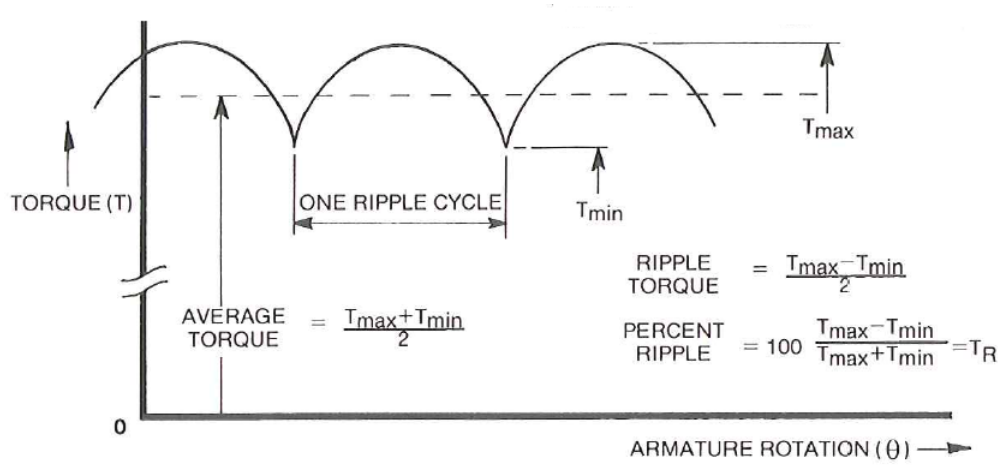

Figure 2.8: Torque ripple effect [35]

In Simulink model of the actuator, given in Figure B.3, relative angular velocity comes from the first order derivative of angular displacement measured by encoder. In addition, torque ripple depend on angular displacement. Last, saturation block ensures the operation of the motor in torque limits.

Table2.3: Parameters of the motor models for the inner and outer gimbals

Parameters	**Units**	**Symbols**	**Inner gimbal**	**Outer gimbal**
Resistance	ohms	R_m	0.83	1.2
Inductance	mH	L_m	0.91	4
Rotor moment of inertia	kg.m^2	I_m	0.149	0.0168
Torque constant	N.m/amp	K_m	5.11	1.5
Back EMF constant	V per rad/s	K_b	5.11	1.5
Peak torque	N.m	T_p	203	35.3
Motor friction torque	N.m	T_{frm}	2.71	0.54
Torque ripple, Ave. to peak	percent	T_r	4	4
Ripple cycles per rev.	cycles/rev	-	181	91

2.5 Gyroscope Model

Stabilization studies focuses on handling disturbances applied to the system. Fiber optic inertial measurement units (IMUs) which contain three gyroscopes measuring angular velocities about x, y and z axes of gimbals relative to the earth reference frame

have main role in stabilization. However, there are some problems of gyroscopes which can be handled by means of sensor fusion algorithms such as bias, angular random walk, scale factor and misalignment. In this study, angular random walk of used gyroscope is lower than $0.013°/\sqrt{hr}$ and its bandwidth frequency at higher that 440 Hz. White noise characteristic of the gyroscopes is shown in Figure 2.9.

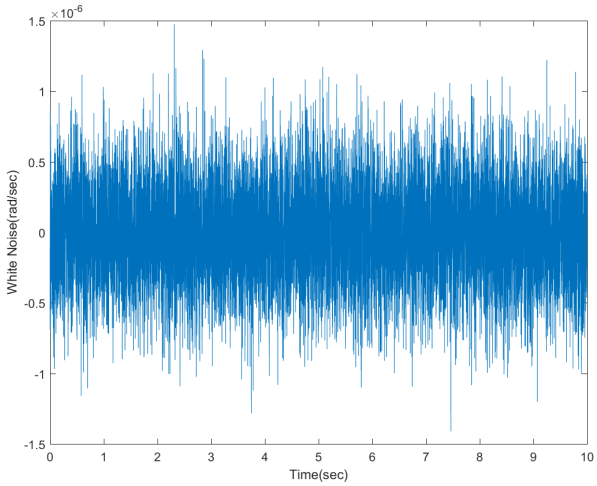

Figure 2.9: White noise of the gyroscope used

2.6 Dynamic Equations of Gimbal

There are lots of formulation in order to construct mathematical models of gimbal platforms but none of these are capable of capturing most of the dynamics [39]. In this study, dynamic equations of the 2-DOF gimbal system is written by the Newton-Euler equations about inner and outer gimbal motion axes. Linear forces applied to the center of rotational axes of the inner and outer gimbals can not create any net torque on either of the gimbals. Hence only Euler's equations, representing rotational motions, are examined to obtain a mathematical model of this system [10]. This section especially focuses on capturing nonlinearities and disturbances of the system. After that, block diagram of the equation of motion and values of parameters for both gimbals are given to be used in controller design phase.

Frictions and mass unbalances of the inner and outer gimbals are the essential dis-

turbance sources on the system. Especially, it can be said that friction is the more dominant effect against mass unbalance. There are two types of mass unbalances of the gimbals. One of them is the dynamic mass unbalance caused by the asymmetric mass distribution, called product of inertia (POI) [38]. Inertia matrices (tensors) demonstrate the dynamic unbalance states of the gimbals. If the gimbal has symmetrical mass distribution with respect to the its frame axis, dynamic mass unbalance will be nonexistent and inertia tensor of the gimbal becomes a diagonal matrix. The other disturbance source is the static mass unbalance caused by the offset between the intersection (pivot) point of the rotation axes and the center of gravity (CG) of gimbals. The gravitational and base motion acceleration act on the CG of gimbals and disturbance torques about the pivot point occur [1].

Table2.4: Values of parameters of the outer and inner gimbals

Gimbal	**Parameters**	**Units**	**Symbols**	**Values**
Outer	Inertia matrix elements	kg.m^2	I^O_{xx}	18.667
			I^O_{yy}	25.025
			I^O_{zz}	9.9024
			$I^O_{yz} = I^O_{zy}$	0.0006029
			$I^O_{xy} = I^O_{yx}$	0
			$I^O_{xz} = I^O_{zx}$	-4.7643
	Distance between pivot point and CG of gimbal	m	$r_{PG_{O_x}}$	-0.0957
			$r_{PG_{O_y}}$	-0.0000245
			$r_{PG_{O_z}}$	-0.3318
	Mass of outer gimbal	kg	m_O	93.48
Inner	Inertia matrix elements	kg.m^2	I^I_{xx}	14.508
			I^I_{yy}	2.8813
			I^I_{zz}	14.409
			$I^I_{yz} = I^I_{zy}$	0.3639
			$I^I_{xy} = I^I_{yx}$	0.067255
			$I^I_{xz} = I^I_{zx}$	0.051688
	Distance between pivot point and CG of gimbal	m	$r_{PG_{I_x}}$	-0.003269
			$r_{PG_{I_y}}$	0.3477
			$r_{PG_{I_z}}$	-0.008242
	Mass of inner gimbal	kg	m_I	82.07

In this thesis, values of parameters of the system are obtained by CAD drawings. It is an important point about the determination of values of these parameters that both gimbals have to be decoupled in CAD drawings.

2.6.1 Inner Gimbal

Newton's equation which yields translational motion for the inner gimbal is:

$$\boldsymbol{F}_{OI} = m_I(\boldsymbol{A}_{CG_I} - \boldsymbol{g}) \tag{2.28}$$

where m_I is the inner gimbal mass, $\boldsymbol{A}_{CG_I}$ is the linear acceleration of the CG of the inner gimbal, $\boldsymbol{F}_{OI}$ is the linear force applied from the outer gimbal to the CG of the inner gimbal and $\boldsymbol{g}$ is the gravity vector.

Angular momentum of the inner gimbal about the pivot point P relative to the inner gimbal frame $\boldsymbol{H}_{I,P}$ is:

$$\boldsymbol{H}_{I,P} = \mathbb{I}_P^I \cdot \boldsymbol{\Omega}_{Ie} \tag{2.29}$$

where $\mathbb{I}_P^I$ and $\boldsymbol{\Omega}_{Ie}$ express the inertia tensor of the decoupled inner gimbal calculated about the pivot point and angular velocity vector of the inner gimbal relative to the earth frame, respectively. Total moment applied to the inner gimbal is formulated by the first order derivative of inner gimbal angular momentum with respect to time. With some calculations in [4], Euler's equation of the inner gimbal about the pivot point is formulated by:

$$\mathbb{I}_P^I \cdot \boldsymbol{\alpha}_{Ie} + \boldsymbol{\Omega}_{Ie} \times \mathbb{I}_P^I \cdot \boldsymbol{\Omega}_{Ie} = \boldsymbol{M}_{OI} + \boldsymbol{D}_{staticUnb}^I \tag{2.30}$$

where

$\mathbb{I}_P^I$: Inertia tensor of the decoupled inner gimbal about the pivot point

$\boldsymbol{\alpha}_{Ie}$: Angular acceleration of the inner gimbal frame relative to the earth frame

$\boldsymbol{\Omega}_{Ie}$: Angular velocity of the inner gimbal frame relative to the earth frame

$\boldsymbol{M}_{OI}$: Moment applied from the outer gimbal on the inner gimbal

$\boldsymbol{D}_{staticUnb}^I$: Disturbance moment caused by static mass unbalance on the inner gimbal

To calculate disturbance torque caused by static mass unbalance on gimbals, the gravitational effect and the gimbal base motion acceleration should be transformed into the reference frames of the gimbals. However, the base motion acceleration is neglected in these equations. The gravity vector relative to the earth reference frame is $\boldsymbol{g}^e = -g\boldsymbol{u}_z$ which is projected into the inner gimbal reference frame.

$$\boldsymbol{g}^I = -g\mathbb{T}_{IO}(\boldsymbol{u}_z)^e_{Oe} = -g(\mathbb{T}_{IO}\mathbb{T}_{OB}\mathbb{T}_{Bn}\mathbb{T}_{nm}\mathbb{T}_{me})\boldsymbol{u}_z$$

Thus

$$\boldsymbol{g}^I = -g\begin{bmatrix} -\cos\eta\sin\theta\cos\epsilon + \sin\eta_z\sin\phi\cos\theta\cos\epsilon - \cos\phi\cos\theta\sin\epsilon \\ \sin\eta\sin\theta + \cos\eta\sin\phi\cos\theta \\ -\cos\eta\sin\theta\sin\epsilon + \sin\eta\sin\phi\cos\theta\sin\epsilon + \cos\phi\cos\theta\cos\epsilon \end{bmatrix} \tag{2.31}$$

Equation of the static mass unbalance torque of the inner gimbal is:

$$\boldsymbol{D}^I_{staticUnb} = \boldsymbol{r}_{PG_I} \times (m_I\{\boldsymbol{g}\}^I) \tag{2.32}$$

where m_I is the mass of inner gimbal. Position vector from the pivot point to the CG of the inner gimbal is:

$$\boldsymbol{r}_{PG_I} = \begin{bmatrix} r_{PG_{I_x}} & r_{PG_{I_y}} & r_{PG_{I_z}} \end{bmatrix}^T \tag{2.33}$$

Besides, the moment term transfered into the inner gimbal can be expressed by:

$$\boldsymbol{M}_{OI} = \begin{bmatrix} M_{OI_x} \\ T_{m_I} + T_{fr_{OI}} \\ M_{OI_z} \end{bmatrix} \tag{2.34}$$

where T_{m_I} is the motor torque transmitted into the inner gimbal and $T_{fr_{OI}}$ is the friction torque between the inner and outer gimbals. $T_{m_I} + T_{fr_{OI}}$ is transfered into the inner gimbal along the y axis so that components of the moment, which is applied from the outer gimbal on the inner gimbal, about the x and z axes are neglected. Inertia tensor of the inner gimbal is:

$$\mathbb{I}^I_P = \begin{bmatrix} I^I_{xx} & I^I_{xy} & I^I_{xz} \\ I^I_{yx} & I^I_{yy} & I^I_{yz} \\ I^I_{zx} & I^I_{zy} & I^I_{zz} \end{bmatrix} \tag{2.35}$$

If Euler's equation of the inner gimbal is rewritten with above terms

$$\begin{bmatrix} I^I_{xx} & I^I_{xy} & I^I_{xz} \\ I^I_{yx} & I^I_{yy} & I^I_{yz} \\ I^I_{zx} & I^I_{zy} & I^I_{zz} \end{bmatrix} \begin{bmatrix} \alpha_{Ie_x} \\ \alpha_{Ie_y} \\ \alpha_{Ie_z} \end{bmatrix} + \begin{bmatrix} \Omega_{Ie_x} \\ \Omega_{Ie_y} \\ \Omega_{Ie_z} \end{bmatrix} \times \begin{bmatrix} I^I_{xx} & I^I_{xy} & I^I_{xz} \\ I^I_{yx} & I^I_{yy} & I^I_{yz} \\ I^I_{zx} & I^I_{zy} & I^I_{zz} \end{bmatrix} \begin{bmatrix} \Omega_{Ie_x} \\ \Omega_{Ie_y} \\ \Omega_{Ie_z} \end{bmatrix}$$
$$= \begin{bmatrix} 0 \\ T_{m_I} + T_{fr_{OI}} \\ 0 \end{bmatrix} + \begin{bmatrix} r_{PG_{I_x}} \\ r_{PG_{I_y}} \\ r_{PG_{I_z}} \end{bmatrix} \times -(m_I g) \begin{bmatrix} \cos(\epsilon)\sin(\theta) + \cos(\theta)\sin(\epsilon) \\ 0 \\ \sin(\epsilon)\sin(\theta) - \cos(\epsilon)\cos(\theta) \end{bmatrix} \tag{2.36}$$

This equation can be expanded into three equations of the inner gimbal with respect to the angular accelerations α_{Ie_x}, α_{Ie_y}, α_{Ie_z} and the angular velocities Ω_{Ie_x}, Ω_{Ie_y}, Ω_{Ie_z}. These scalar equations are given in Eq. A.7 - A.9, explicitly. If dynamic equation of the inner gimbal about the y axis, given by Eq. A.8, is rewritten:

$$I^I_{yy}\alpha_{Ie_y} + D^I_{dynamicUnb_y} = T_{m_I} + T_{fr_{OI}} + D^I_{staticUnb_y} \tag{2.37}$$

where disturbance torques caused by the dynamic and static mass unbalance are:

$$\begin{aligned} D^I_{dynamicUnb_y} &= I^I_{xy}\alpha_{Ie_x} + I^I_{yz}\alpha_{Ie_z} + \Omega_{Ie_z}(I^I_{xx}\Omega_{Ie_x} + I^I_{xy}\Omega_{Ie_y} + I^I_{xz}\Omega_{Ie_z}) \\ &\quad - \Omega_{Ie_x}(I^I_{xz}\Omega_{Ie_x} + I^I_{yz}\Omega_{Ie_y} + I^I_{zz}\Omega_{Ie_z}) \\ D^I_{staticUnb_y} &= gm_I(r_{PG_{I_x}}(\cos\epsilon\cos\theta - \sin\epsilon\sin\theta) + r_{PG_{I_z}}(\cos\epsilon\sin\theta + \cos\theta\sin\epsilon)) \end{aligned}$$

Block diagram of the inner gimbal model is shown in Figure 2.10.

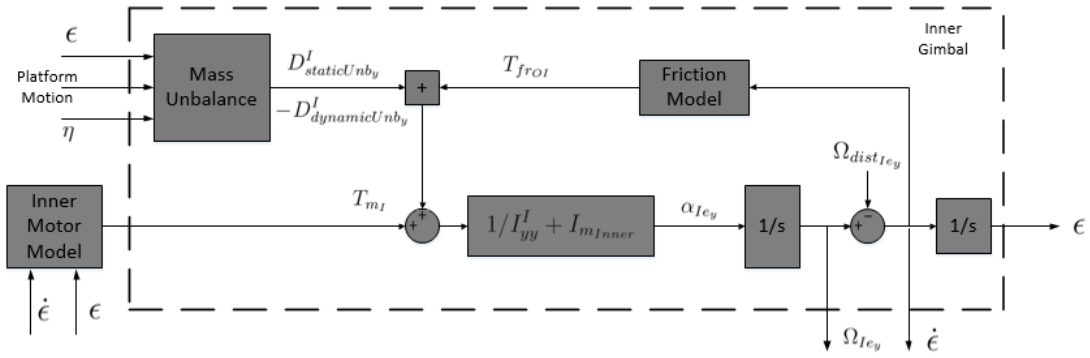

Figure 2.10: Block diagram of the inner gimbal

Angular velocity Ω_{Ie_y} and angular position ϵ are measured by the gyroscope and

encoder sensors, respectively. Moreover, angular velocity term $\Omega_{dist_{Ie_y}}$ represents the platform motion affect on the inner gimbal. Relative velocity $\dot{\epsilon}$ can be defined as changing rate of the angular displacement [39]. Total inertia of the inner gimbal is computed by the sum of motor inertia I_{m_I} and inner gimbal inertia I^I_{yy} along the y axis. Then, only the friction model is required to determine the relative velocity of the inner gimbal $\dot{\epsilon}$ whereas mass unbalance block gets platform motion, angular positions of the inner ϵ and outer η gimbals. Last, motor model requires angular position and relative velocity of the inner gimbal.

2.6.2 Outer Gimbal

Newton's equations of the outer gimbal is:

$$\boldsymbol{F}_{IO} = -\boldsymbol{F}_{OI} \tag{2.38}$$

$$\boldsymbol{F}_{BO} + \boldsymbol{F}_{IO} = (m_O + m_I)(\boldsymbol{A}_{G_O} - \boldsymbol{g}) \tag{2.39}$$

where m_O is the outer gimbal mass, $\boldsymbol{A}_{G_O}$ is linear acceleration of the CG of the outer gimbal, $\boldsymbol{F}_{BO}$ is linear force applied from the gimbal base to the CG of the outer gimbal, $\boldsymbol{F}_{IO}$ is linear force applied from the inner gimbal to the CG of the outer gimbal.

The angular momentum of the outer gimbal about the pivot point P relative to the outer gimbal frame $\boldsymbol{H}_{O,P}$ is formulated by:

$$\boldsymbol{H}_{O,P} = \mathbb{I}^O_P \cdot \boldsymbol{\Omega}_{Oe} + \mathbb{T}_{IO} \cdot \mathbb{I}^I_P \cdot \boldsymbol{\Omega}_{Ie} \tag{2.40}$$

where $\mathbb{I}^O_P$ is the inertia tensor of the decoupled outer gimbal and $\boldsymbol{\Omega}_{Oe}$ is angular velocity vector of the outer gimbal relative to the earth frame. Euler's equation of the outer gimbal about the pivot point is:

$$\begin{aligned} \mathbb{I}^O_P \cdot \boldsymbol{\alpha}_{Oe} + \dot{\mathbb{T}}_{IO} \cdot \mathbb{I}^I_P \cdot \boldsymbol{\Omega}_{Ie} + \mathbb{T}_{IO} \cdot \mathbb{I}^I_P \cdot \boldsymbol{\alpha}_{Ie} + \boldsymbol{\Omega}_{Oe} \times (\mathbb{I}^O_P \cdot \boldsymbol{\Omega}_{Oe} + \mathbb{T}_{IO} \cdot \mathbb{I}^I_P \cdot \boldsymbol{\Omega}_{Ie}) \\ = \boldsymbol{M}_{BO} + \boldsymbol{M}_{IO} + \boldsymbol{D}^O_{staticUnb} \end{aligned} \tag{2.41}$$

where

$\mathbb{I}^I_P$: Inertia tensor of the decoupled inner gimbal about pivot point

$\mathbb{I}_P^O$: Inertia tensor of the decoupled outer gimbal about pivot point

$\boldsymbol{\alpha}_{Ie}$: Angular acceleration of the inner gimbal frame relative to the earth frame

$\boldsymbol{\alpha}_{Oe}$: Angular acceleration of the outer gimbal frame relative to the earth frame

$\boldsymbol{\Omega}_{Ie}$: Angular velocity of the inner gimbal frame relative to the earth frame

$\boldsymbol{\Omega}_{Oe}$: Angular velocity of the outer gimbal frame relative to the earth frame

$\boldsymbol{M}_{BO}$: Moment applied from the gimbal base to the outer gimbal

$\boldsymbol{M}_{IO}$: Moment applied from the inner gimbal to the outer gimbal

$\boldsymbol{D}^O_{staticUnb}$: Disturbance torque caused by static mass unbalance on the outer gimbal

Equation of the static mass unbalance torque on the outer gimbal is:

$$\boldsymbol{D}^O_{staticUnb} = \boldsymbol{r}_{PG_O} \times ((m_O + m_I)\{\boldsymbol{g}\}^O) \tag{2.42}$$

where m_I and m_O are the mass of inner and outer gimbals, respectively. Position vector from the pivot point to the CG of the outer gimbal is expressed by $\boldsymbol{r}_{PG_O}$:

$$\boldsymbol{r}_{PG_O} = \begin{bmatrix} r_{PG_{O_x}} & r_{PG_{O_y}} & r_{PG_{O_z}} \end{bmatrix}^T \tag{2.43}$$

and the gravity vector $\{\boldsymbol{g}\}^O$ projected into the outer gimbal is:

$$\{\boldsymbol{g}\}^O = -g(\boldsymbol{u}_z)^e_{Oe} = -g(\mathbb{T}_{OB}\mathbb{T}_{Bn}\mathbb{T}_{nm}\mathbb{T}_{me})\boldsymbol{u}_z$$

Furthermore

$$\boldsymbol{g}^O = -g \begin{bmatrix} -\cos\eta\sin\theta + \sin\eta\sin\phi\cos\theta \\ \sin\eta\sin\theta + \cos\eta\sin\phi\cos\theta \\ \cos\phi\cos\theta \end{bmatrix} \tag{2.44}$$

The moment terms transfered into the outer gimbal can be written as:

$$\boldsymbol{M}_{IO} = \begin{bmatrix} M_{IO_x} \\ M_{IO_y} \\ T_{fr_{IO}} \end{bmatrix}, \qquad \boldsymbol{M}_{BO} = \begin{bmatrix} M_{BO_x} \\ M_{BO_y} \\ T_{m_O} + T_{fr_{BO}} \end{bmatrix} \tag{2.45}$$

where $T_{fr_{BO}}$ is the friction torque between the gimbal base and the outer gimbal, $T_{fr_{IO}}$ is friction torque between the inner and outer gimbals and T_{m_O} is motor torque applied to the outer gimbal. Rotations of the joints between the gimbal base and outer gimbal are overlapped along the same z axis. Thus $T_{m_O} + T_{fr_{BO}}$ is transfered into the outer gimbal directly whereas $T_{fr_{IO}}$ is the friction torque transfered indirectly.

Inertia tensor of outer gimbal is defined by:

$$\mathbb{I}_P^O = \begin{bmatrix} I_{xx}^O & I_{xy}^O & I_{xz}^O \\ I_{yx}^O & I_{yy}^O & I_{yz}^O \\ I_{zx}^O & I_{zy}^O & I_{zz}^O \end{bmatrix} \tag{2.46}$$

When we rewrite Euler's equation of outer gimbal and substitute above terms into this equation with assuming $M_{IO_x} = M_{IO_y} = 0$ and $M_{BO_x} = M_{BO_y} = 0$,

$$\begin{aligned}
&\begin{bmatrix} I_{xx}^O & I_{xy}^O & I_{xz}^O \\ I_{yx}^O & I_{yy}^O & I_{yz}^O \\ I_{zx}^O & I_{zy}^O & I_{zz}^O \end{bmatrix} \begin{bmatrix} \alpha_{Oe_x} \\ \alpha_{Oe_y} \\ \alpha_{Oe_z} \end{bmatrix} + \begin{bmatrix} \sin\epsilon & 0 & cos\epsilon \\ 0 & 0 & 0 \\ -\cos\epsilon & 0 & \sin\epsilon \end{bmatrix} \begin{bmatrix} I_{xx}^I & I_{xy}^I & I_{xz}^I \\ I_{yx}^I & I_{yy}^I & I_{yz}^I \\ I_{zx}^I & I_{zy}^I & I_{zz}^I \end{bmatrix} \begin{bmatrix} \Omega_{Ie_x} \\ \Omega_{Ie_y} \\ \Omega_{Ie_z} \end{bmatrix} \\
&+ \begin{bmatrix} \cos\epsilon & 0 & \sin\epsilon \\ 0 & 1 & 0 \\ -\sin\epsilon & 0 & \cos\epsilon \end{bmatrix} \begin{bmatrix} I_{xx}^I & I_{xy}^I & I_{xz}^I \\ I_{yx}^I & I_{yy}^I & I_{yz}^I \\ I_{zx}^I & I_{zy}^I & I_{zz}^I \end{bmatrix} \begin{bmatrix} \alpha_{Ie_x} \\ \alpha_{Ie_y} \\ \alpha_{Ie_z} \end{bmatrix} \\
&+ \begin{bmatrix} \Omega_{Oe_x} \\ \Omega_{Oe_y} \\ \Omega_{Oe_z} \end{bmatrix} \times \left(\begin{bmatrix} I_{xx}^O & I_{xy}^O & I_{xz}^O \\ I_{yx}^O & I_{yy}^O & I_{yz}^O \\ I_{zx}^O & I_{zy}^O & I_{zz}^O \end{bmatrix} \begin{bmatrix} \Omega_{Oe_x} \\ \Omega_{Oe_y} \\ \Omega_{Oe_z} \end{bmatrix} + \begin{bmatrix} \cos\epsilon & 0 & \sin\epsilon \\ 0 & 1 & 0 \\ -\sin\epsilon & 0 & \cos\epsilon \end{bmatrix} \begin{bmatrix} I_{xx}^I & I_{xy}^I & I_{xz}^I \\ I_{yx}^I & I_{yy}^I & I_{yz}^I \\ I_{zx}^I & I_{zy}^I & I_{zz}^I \end{bmatrix} \begin{bmatrix} \Omega_{Ie_x} \\ \Omega_{Ie_y} \\ \Omega_{Ie_z} \end{bmatrix} \right) \\
&= \begin{bmatrix} 0 \\ 0 \\ T_{m_O} + T_{fr_{BO}} \end{bmatrix} + \begin{bmatrix} 0 \\ 0 \\ T_{fr_{IO}} \end{bmatrix} \\
&+ \begin{bmatrix} r_{PG_{O_x}} \\ r_{PG_{O_y}} \\ r_{PG_{O_z}} \end{bmatrix} \times -g(m_O + m_I) \begin{bmatrix} -\cos\eta\sin\theta + \sin\eta\sin\phi\cos\theta \\ \sin\eta\sin\theta + \cos\eta\sin\phi\cos\theta \\ \cos\phi\cos\theta \end{bmatrix}
\end{aligned} \tag{2.47}$$

This matrix is decomposed into three scalar equations of outer gimbal with respect to angular accelerations α_{Oe_x}, α_{Oe_y}, α_{Oe_z} and angular velocities Ω_{Oe_x}, Ω_{Oe_y}, Ω_{Oe_z}. These equations are written in Eq. A.10 - A.12, explicitly. The equation of motion

for the outer gimbal on the z axis is given in Eq. A.12. If we write again this equation

$$I^O_{zz}\alpha_{Oe_z} + D^O_{dynamicUnb_z} = T_{m_O} + T_{fr_{BO}} + T_{fr_{IO}} + D^O_{staticUnb_z} \tag{2.48}$$

where dynamic and static mass unbalance terms are:

$$\begin{aligned}
D^O_{dynamicUnb_z} &= I^O_{xz}\alpha_{Oe_x} + I^O_{yz}\alpha_{Oe_y} \\
&+ \alpha_{Ie_x}(I^I_{xz}\cos\epsilon + I^I_{xx}\sin\epsilon) + \alpha_{Ie_y}(I^I_{yz}\cos\epsilon + I^I_{xz}\sin\epsilon) \\
&+ \alpha_{Ie_z}(I^I_{zz}\cos\epsilon + I^I_{xz}\sin\epsilon) \\
&+ \Omega_{Oe_x}(\Omega_{Oe_x}(I^I_{xy} + I^O_{xy}) + \Omega_{Oe_y}(I^I_{yy} + I^O_{yy}) + \Omega_{Oe_z}(I^I_{yz} + I^O_{yz})) \\
&- \Omega_{Oe_y}(\Omega_{Oe_x}(I^O_{xx} + I^I_{xx}\cos\epsilon - I^I_{xz}\sin\epsilon) + \Omega_{Oe_y}(I^O_{xy} + I^I_{xy}\cos\epsilon - I^I_{yz}\sin\epsilon) \\
&+ \Omega_{Oe_z}(I^O_{xz} + I^I_{xz}\cos\epsilon - I^I_{zz}\sin\epsilon)) \\
&- \Omega_{Ie_x}\dot{\epsilon}(I^I_{xx}\cos\epsilon - I^I_{xz}\sin\epsilon) - \Omega_{Ie_y}\dot{\epsilon}(I^I_{xy}\cos\epsilon - I^I_{yz}\sin\epsilon) \\
&- \Omega_{Ie_z}\dot{\epsilon}(I^I_{xz}\cos\epsilon - I^I_{zz}\sin\epsilon) \\
D^O_{staticUnb_z} &= g(m_O + m_I)((-\cos\eta\sin\theta + \sin\eta\sin\phi\cos\theta)r_{PG_{O_y}} \\
&- (\sin\eta\sin\theta + \cos\eta\sin\phi\cos\theta)r_{PG_{O_x}})
\end{aligned}$$

Block diagram of outer gimbal is shown in Figure 2.11. The angular velocity Ω_{Oe_z} and η are measured by gyroscope and encoder sensors, respectively.

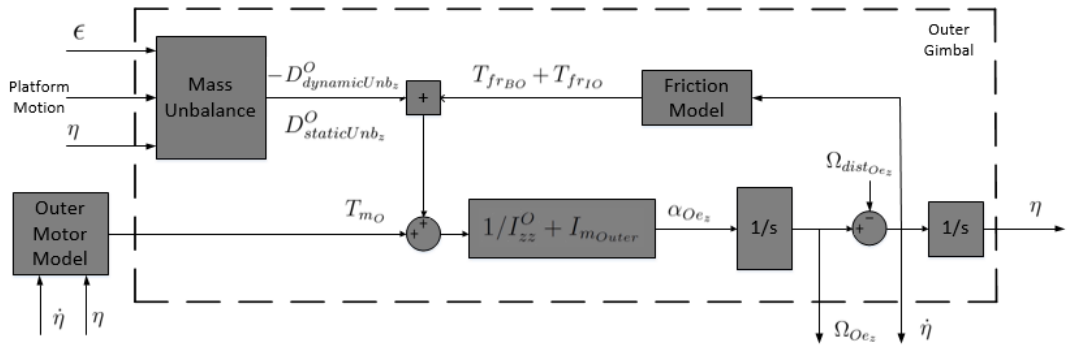

Figure 2.11: Block diagram of the outer gimbal

Angular velocity $\Omega_{dist_{Oe_z}}$ expresses platform motion disturbance on the outer gimbal and $\dot{\eta}$ is relative velocity of outer gimbal. Total inertia of the outer gimbal is computed by the sum of motor inertia I_{m_O} and outer gimbal inertia I^O_{zz} along the z axis. Further, motor model requires angular position and relative velocity of the outer gimbal. Moreover, inputs of the friction models are relative velocities of the gimbals whereas

inputs of the mass unbalance block are platform motion and angular positions of both inner and outer gimbals.

2.7 Verification of the Decoupling of the Gimbals

The stabilized gimbal system has the inner and outer gimbals controlled separately. However, if two separate controllers are implemented to control the two gimbals, these one has to verify that decoupling is realistic [39].

There are two methods in order to decouple mechanically coupled two gimbals. In the first proposed method, if dynamic equations of the gimbal includes the inertia and mass terms of the other gimbal, these expressions have to be neglected. In addition to the ignored terms of the first method, each gimbal is fixed to the other and angular position of the other gimbal is set to zero in the second method. When motor torques as chirp signals are applied to inner and outer gimbals, angular position and velocity outputs of the systems are shown below.

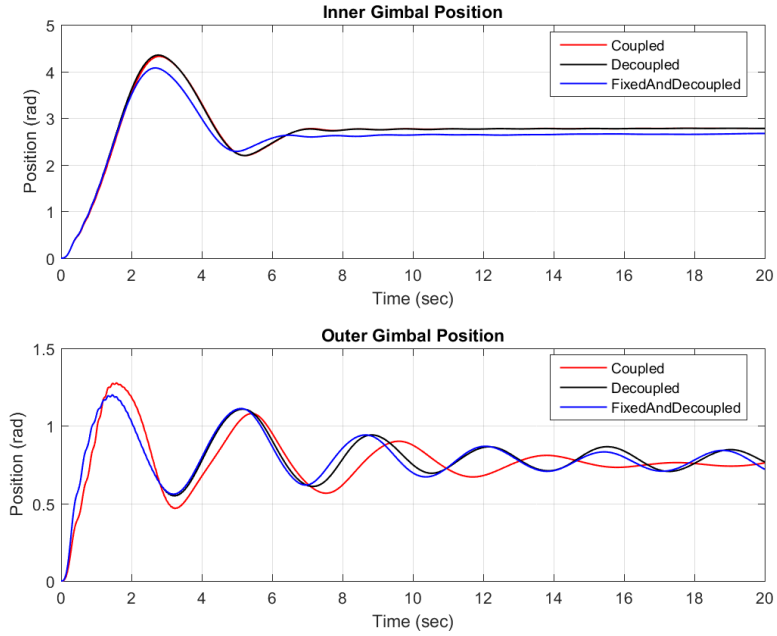

Figure 2.12: Position outputs of coupled and decoupled gimbals

These figures shows that decoupling approaches are unable to respond with the same

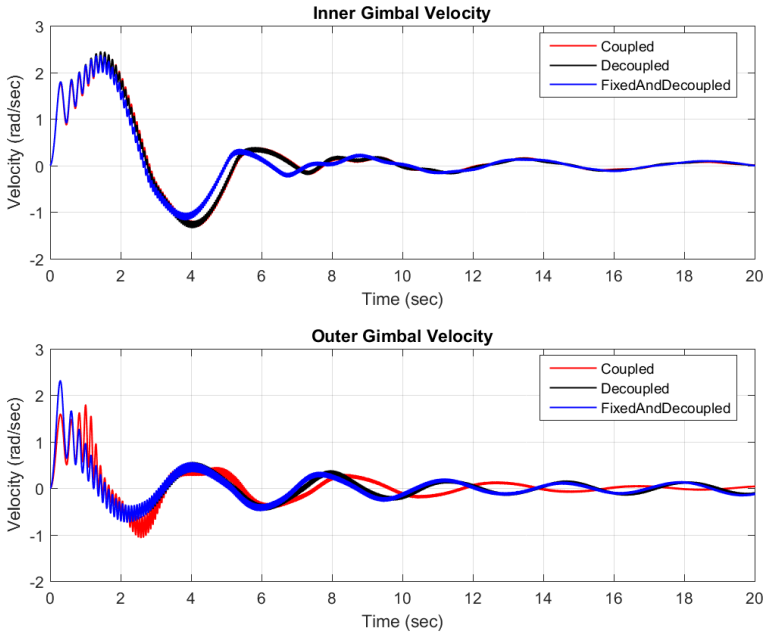

Figure 2.13: Velocity outputs of coupled and decoupled gimbals

coupled 2-DOF gimbal. Even though outputs of the coupled and decoupled inner gimbal with the first decoupling approach are about same, they are much different in all the other cases. In this study, the first approach is used to obtain state space models of the decoupled gimbals. After that local LQI controllers, discussed in the next chapter, are designed for these decoupled models and linear quadratic controllers for models of the coupled and decoupled gimbals are compared.

2.8 State Space Representation of Gimbal

The nonlinear 2-DOF gimbal is described as a multiple-input, multiple-output system. Different from the conventional control theory, modern control theory allows to construct MIMO system model and helps to implement different control strategies such as H_∞ and linear quadratic regulator in state space [36]. In this section, state space representations of the coupled 2-DOF gimbal, decoupled inner and decoupled outer gimbals are examined in order to determine which approach is more convenient in control studies. State and output equations of the gimbals are written from kinematics and dynamics of the system. In addition, platform motion and sensor noise are

also defined in state space. None of system model represented in state space contains mathematical model of the motors.

State variables describe the behavior of the system. Friction state z which is used in the Dahl model, relative angular position and relative angular velocity terms of the inner and outer gimbals are chosen as state variables. Output variables have to be selected as measurable quantities whereas state variables do not have any necessity on being measurable [36]. Hence angular position and velocity responses, measured by encoders and gyroscopes of IMU, for inner and outer gimbals are chosen as the output variables. Motor torques refers to the control input variables, platform motion kinematics and sensor noise are used to define external effects carried out to the system.

The nonlinear state space representation of the system is in the following form:

$$\dot{\boldsymbol{x}} = \boldsymbol{f}(\boldsymbol{x}, \boldsymbol{u}, \boldsymbol{w}) \tag{2.49}$$

$$\boldsymbol{y} = \boldsymbol{h}(\boldsymbol{x}, \boldsymbol{w}, \boldsymbol{n}) \tag{2.50}$$

where $\boldsymbol{x}$ is the state vector, $\boldsymbol{u}$ is the control input vector, $\boldsymbol{w}$ is the disturbance vector referring to platform motion which is carried out to the gimbal base, $\boldsymbol{f}(\boldsymbol{x}, \boldsymbol{u}, \boldsymbol{w})$ is the state equation consisting of dynamic and kinematic equations of the system, $\dot{\boldsymbol{x}}$ is the first order derivative of the state vector, $\boldsymbol{y}$ is the output vector, $\boldsymbol{n}$ is the gyroscope noise vector and $\boldsymbol{h}(\boldsymbol{x}, \boldsymbol{w}, \boldsymbol{n})$ is the output equation which defines the system responses.

2.8.1 Coupled 2-DOF Gimbal

The nonlinear state space representation of the coupled 2-DOF gimbal is:

$$\dot{\boldsymbol{x}}_G = \boldsymbol{f}_G(\boldsymbol{x}_G, \boldsymbol{u}_G, \boldsymbol{w}_G) \tag{2.51}$$

$$\boldsymbol{y}_G = \boldsymbol{h}_G(\boldsymbol{x}_G, \boldsymbol{w}_G, \boldsymbol{n}_G) \tag{2.52}$$

There are six states, two control inputs, eight disturbances, two gyroscope noises and four outputs for the coupled gimbal. State vector consists of two angular positions (η, ϵ), two friction states (z_{OB}, z_{IO}), relative angular velocity between the outer gimbal

and the platform base about the z axis Ω_{OB_z} and relative angular velocity between inner and outer gimbals about the y axis Ω_{IO_y}. Nonetheless control input vector contains two motor torques (T_{m_O}, T_{m_I}) and disturbance vector involves two Euler angles (θ, ϕ), the first order derivatives ($\dot{\psi}$, $\dot{\theta}$, $\dot{\phi}$) and the second order derivatives ($\ddot{\psi}$, $\ddot{\theta}$, $\ddot{\phi}$) of the Euler angles. Noise vector has only gyroscope noise states affecting on angular velocity responses. Output vector has two measurable relative angular positions (η, ϵ) for tracking and two measurable angular velocities relative to the earth reference frame ($\Omega_{Oe_z} + n_z$, $\Omega_{Ie_y} + n_y$) for stabilization.

$$\boldsymbol{x}_G = \begin{bmatrix} \eta & \epsilon & \Omega_{OB_z} & \Omega_{IO_y} & z_{OB} & z_{IO} \end{bmatrix}^T$$

$$\boldsymbol{u}_G = \begin{bmatrix} T_{m_O} & T_{m_I} \end{bmatrix}^T$$

$$\boldsymbol{w}_G = \begin{bmatrix} \theta & \phi & \dot{\psi} & \dot{\theta} & \dot{\phi} & \ddot{\psi} & \ddot{\theta} & \ddot{\phi} \end{bmatrix}^T$$

$$\boldsymbol{y}_G = \begin{bmatrix} \eta & \epsilon & (\Omega_{Oe_z} + n_z) & (\Omega_{Ie_y} + n_y) \end{bmatrix}^T$$

$$\boldsymbol{n}_G = \begin{bmatrix} 0 & 0 & n_z & n_y \end{bmatrix}^T$$

The limits of the state, control input, disturbance and sensor noise variable of the coupled 2-DOF gimbal are given in Table 2.5 and Table 2.6. Boundaries of η and ϵ angular position come from the mechanical limits of the outer and inner gimbal, respectively. Angular velocity limits are determined from the maximum acceleration in a second in the case of disturbances are neglected. Further, boundaries of T_{m_O} and T_{m_I} inputs refers to the peak torque values of the outer and inner gimbal motors. On the other hand, limiting ranges of disturbance and friction state variables are chosen arbitrarily.

Table2.5: Boundaries of the state variables of the coupled 2-DOF gimbal

States	**Units**	**Lower**	**Upper**
x_{G_1}	rad	$-\pi$	π
x_{G_2}	rad	$-\frac{\pi}{9}$	$\frac{4\pi}{9}$
x_{G_3}	rad/sec	-20	20
x_{G_4}	rad/sec	-12	12
x_{G_5}	-	-10	10
x_{G_6}	-	-10	10

Table2.6: Boundaries of the disturbance, sensor noise and control input variables of the coupled 2-DOF gimbal

Inputs	**Units**	**Lower**	**Upper**
u_{G_1}	$N.m$	-203	203
u_{G_2}	$N.m$	-35.3	35.3
w_{G_1}	rad	$-\frac{\pi}{20}$	$\frac{\pi}{20}$
w_{G_2}	rad	$-\frac{\pi}{8}$	$\frac{\pi}{8}$
w_{G_3}	rad/sec	$-\frac{\pi}{180}$	$\frac{\pi}{180}$
w_{G_4}	rad/sec	$-\frac{\pi}{60}$	$\frac{\pi}{60}$
w_{G_5}	rad/sec	$-\frac{\pi}{18}$	$\frac{\pi}{18}$
w_{G_6}	rad/sec^2	$-\frac{\pi}{180}$	$\frac{\pi}{180}$
w_{G_7}	rad/sec^2	$-\frac{\pi}{60}$	$\frac{\pi}{60}$
w_{G_8}	rad/sec^2	$-\frac{\pi}{18}$	$\frac{\pi}{18}$
n_{G_3}	rad/sec	-0.000001	0.000001
n_{G_4}	rad/sec	-0.000001	0.000001

In order to obtain state equations, first, we rewrite the first order derivatives of relative angular positions for both gimbals.

$$\dot{\eta} = \Omega_{OB_z}$$

$$\dot{\epsilon} = \Omega_{IO_y}$$

Hence $\dot{\eta}$ and $\dot{\epsilon}$ are written in terms of state variables as follows:

$$\dot{x}_{G_1} = x_{G_3} \tag{2.53}$$

$$\dot{x}_{G_2} = x_{G_4} \tag{2.54}$$

Secondly, the first order derivatives of $\dot{\Omega}_{OB_z}$ and $\dot{\Omega}_{IO_y}$ are:

$$\dot{\Omega}_{OB_z} = \ddot{\eta}$$

$$\dot{\Omega}_{IO_y} = \ddot{\epsilon}$$

To obtain $\dot{\Omega}_{OB_z}$, Eq. A.3 is written again:

$$\dot{\Omega}_{OB_z} = \alpha_{Oe_z} - \alpha_{dist_{O_z}}$$

where α_{Oe_z} is the angular acceleration of outer gimbal relative to the earth reference frame about the z axis and $\alpha_{dist_{O_z}}$ is disturbance angular acceleration. By using Euler

equation of the outer gimbal about the z axis, given in Eq. 2.48, and friction torque equation, given in Eq. 2.23, $\dot{\Omega}_{OB_z}$ can be written as follows:

$$\dot{\Omega}_{OB_z} = -\frac{1}{I^O_{zz}} D^O_{dynamicUnb_z} + \frac{1}{I^O_{zz}} T_{m_O} + \frac{1}{I^O_{zz}} T_{fr_{BO}} + \frac{1}{I^O_{zz}} T_{fr_{IO}} + \frac{1}{I^O_{zz}} D^O_{staticUnb_z} - \alpha_{dist_{O_z}}$$

This equation is written in terms of state and input variables with values of system parameters, given in Table 2.4, and friction parameters, given in Table 2.2, as follows:

$$\dot{x}_{G_3} = -0.1 D^O_{dynamicUnb_z} + 0.1 u_{G_1} + 0.1 T_{fr_{BO}} + 0.1 T_{fr_{IO}} + 0.1 D^O_{staticUnb_z} - \alpha_{dist_{O_z}} \tag{2.55}$$

where the dynamic mass unbalance is:

$$\begin{aligned} D^O_{dynamicUnb_z} = &+ \dot{x}_{G_3}(14.41 \cos^2 x_{G_2} - 14.51 \sin^2 x_{G_2}) \\ &+ \dot{x}_{G_4}(0.364 \cos x_{G_2} + 0.052 \sin x_{G_2}) \\ &+ \hat{D}^O_{dynamicUnb_z} \end{aligned}$$

with

$$\begin{aligned} \hat{D}^O_{dynamicUnb_z} = &- 4.76 \alpha_{Oe_x} + 0.0006 \alpha_{Oe_y} \\ &+ \alpha_{dist_{I_x}}(0.052 \cos x_{G_2} + 14.51 \sin x_{G_2}) \\ &+ \alpha_{dist_{I_y}}(0.364 \cos x_{G_2} + 0.052 \sin x_{G_2}) \\ &+ \alpha_{dist_{I_z}}(14.41 \cos x_{G_2} + 0.052 \sin x_{G_2}) \\ &+ 0.07 \Omega^2_{Oe_x} - \Omega^2_{Oe_y}(0.07 \cos x_{G_2} - 0.36 \sin x_{G_2}) \\ &+ 0.3606 \Omega_{Oe_x}(x_{G_3} + \Omega_{dist_{O_z}}) \\ &- \Omega_{Oe_y} \Omega_{Oe_x}(-9.235 + 14.41 \cos x_{G_2} - 0.052 \sin x_{G_2}) \\ &- \Omega_{Oe_y}(x_{G_3} + \Omega_{dist_{O_z}})(-4.76 + 0.052 \cos x_{G_2} - 14.41 \sin x_{G_2}) \\ &- \Omega_{Ie_x} x_{G_4}(14.51 \cos x_{G_2} - 0.052 \sin x_{G_2}) \\ &- (x_{G_4} + \Omega_{dist_{I_y}}) x_{G_4}(0.07 \cos x_{G_2} - 0.37 \sin x_{G_2}) \\ &- \Omega_{Ie_z} x_{G_4}(0.052 \cos x_{G_2} - 14.41 \sin x_{G_2}), \end{aligned}$$

the static mass unbalance is:

$$\begin{aligned} D^O_{staticUnb_z} = &- 0.043(-\cos x_{G_1} \sin w_{G_1} + \sin x_{G_1} \sin w_{G_2} \cos w_{G_1}) \\ &+ 164.8(\sin x_{G_1} \sin w_{G_1} + \cos x_{G_1} \sin w_{G_2} \cos w_{G_1}), \end{aligned}$$

the friction torque between the outer gimbal and gimbal base is:

$$T_{fr_{BO}} = 80 x_{G_5}$$

and the friction torque between the inner and outer gimbals is:

$$T_{fr_{IO}} = 90x_{G_6}$$

Then $\dot{\Omega}_{IO_y}$ may be written from Eq. A.5 as:

$$\dot{\Omega}_{IO_y} = \alpha_{Ie_y} - \alpha_{dist_{I_y}}$$

where α_{Ie_y} is the angular acceleration of inner gimbal about the y axis relative to the earth frame and $\alpha_{dist_{I_y}}$ is the disturbance angular acceleration about the y axis. $\dot{\Omega}_{IO_y}$ is written from Euler equation for the inner gimbal, given in Eq. 2.37, and the friction torque equation, given in Eq. 2.23.

$$\dot{\Omega}_{IO_y} = -\frac{1}{I^I_{yy}} D^I_{dynamicUnb_y} + \frac{1}{I^I_{yy}} T_{fr_{OI}} + \frac{1}{I^I_{yy}} T_{m_I} + \frac{1}{I^I_{yy}} D^I_{staticUnb_y} - \alpha_{dist_{I_y}}$$

This equation is rewritten in terms of state and input variables with values of inner gimbal parameters in Table 2.4 and friction parameters in Table 2.1.

$$\dot{x}_{G_4} = -0.35 D^I_{dynamicUnb_y} + 0.35 T_{fr_{OI}} + 0.35 u_{G_2} + 0.35 D^I_{staticUnb_y} - \alpha_{dist_{I_y}} \quad (2.56)$$

where dynamic mass unbalance is:

$$D^I_{dynamicUnb_y} = -0.067 \dot{x}_{G_3} \sin x_{G_2} + 0.364 \dot{x}_{G_3} \cos x_{G_2} + \hat{D}^I_{dynamicUnb_y}$$

with

$$\begin{aligned} \hat{D}^I_{dynamicUnb_y} = &+ 0.067 \alpha_{dist_{I_x}} + 0.364 \alpha_{dist_{I_z}} \\ &+ \Omega_{Ie_z} (14.51 \Omega_{Ie_x} + 0.067 (x_{G_4} + \Omega_{dist_{I_y}}) + 0.052 \Omega_{Ie_z}) \\ &- \Omega_{Ie_x} (0.052 \Omega_{Ie_x} + 0.364 (x_{G_4} + \Omega_{dist_{I_y}}) + 14.41 \Omega_{Ie_z}), \end{aligned}$$

The static mass unbalance is:

$$\begin{aligned} D^I_{staticUnb_y} = &- 2.66 (\cos x_{G_2} \cos w_{G_1} - \sin x_{G_2} \sin w_{G_1}) \\ &- 6.44 (\cos x_{G_2} \sin w_{G_1} + \cos w_{G_1} \sin x_{G_2}) \end{aligned}$$

and friction torque between the inner and outer gimbals is:

$$T_{fr_{OI}} = 90x_{G_6}$$

Lastly, the first order derivatives of friction states from Eq. 2.24 are:

$$\dot{z}_{BO} = \Omega_{BO_z} - \sigma_{0BO} \frac{|\Omega_{BO_z}|}{T_{CBO}} z_{BO}$$

$$\dot{z}_{IO} = \Omega_{IO_y} - \sigma_{0IO}\frac{|\Omega_{IO_y}|}{T_{CIO}} z_{IO}$$

With values of friction parameters in Table 2.1, these equations can be described in terms of state variables:

$$\dot{x}_{G_5} = x_{G_3} - 4.42 \cdot |x_{G_3}| \cdot x_{G_5} \tag{2.57}$$

$$\dot{x}_{G_6} = x_{G_4} - 33.3 \cdot |x_{G_4}| \cdot x_{G_6} \tag{2.58}$$

The first order derivatives of all states have to be on the left side of the state equations. Eq. 2.55 and Eq. 2.56 contain both $\dot{x}_{G_3}$ and $\dot{x}_{G_4}$ terms on the right side of the state equation. Thus Eq. 2.55 and Eq. 2.56 are rewritten after $\dot{x}_{G_3}$ and $\dot{x}_{G_4}$ are substituted on the left side.

$$\begin{aligned}\dot{x}_{G_3}(1 + 1.441\cos^2 x_{G_2} - 1.451\sin^2 x_{G_2}) + \dot{x}_{G_4}(0.0364\cos x_{G_2} + 0.0052\sin x_{G_2}) \\ = -0.1\hat{D}^O_{dynamicUnb_z} + 0.1u_{G_1} + 0.1T_{fr_{BO}} + 0.1T_{fr_{IO}} + 0.1D^O_{staticUnb_z} - \alpha_{dist_{O_z}}\end{aligned} \tag{2.59}$$

$$\begin{aligned}\dot{x}_{G_4} + \dot{x}_{G_3}(-0.02345\sin x_{G_2} + 0.1274\cos x_{G_2}) \\ = -0.35\hat{D}^I_{dynamicUnb_y} + 0.35T_{fr_{OI}} + 0.35u_{G_2} + 0.35D^I_{staticUnb_y} - \alpha_{dist_{I_y}}\end{aligned} \tag{2.60}$$

State equation is rewritten in form $\boldsymbol{S}_G\dot{\boldsymbol{x}}_G = \hat{\boldsymbol{f}}_G(\boldsymbol{x}_G, \boldsymbol{u}_G, \boldsymbol{w}_G)$ where $\boldsymbol{S}_G$ matrix is defined to collect all the first order derivatives of states on the left

$$\boldsymbol{S}_G = \begin{bmatrix} 1 & 0 & 0 & 0 & 0 & 0 \\ 0 & 1 & 0 & 0 & 0 & 0 \\ 0 & 0 & s_{g_1} & s_{g_2} & 0 & 0 \\ 0 & 0 & s_{g_3} & 1 & 0 & 0 \\ 0 & 0 & 0 & 0 & 1 & 0 \\ 0 & 0 & 0 & 0 & 0 & 1 \end{bmatrix}$$

with

$$s_{g_1} = 1 + 1.441\cos^2 x_{G_2} - 1.451\sin^2 x_{G_2}$$

$$s_{g_2} = 0.0364\cos x_{G_2} + 0.0052\sin x_{G_2}$$

$$s_{g_3} = -0.02345\sin x_{G_2} + 0.1274\cos x_{G_2}$$

and $\hat{\boldsymbol{f}}_G(\boldsymbol{x}_G, \boldsymbol{u}_G, \boldsymbol{w}_G)$ vector contains kinematic and dynamic equations without the first order derivatives of state variables.

$$\begin{bmatrix} x_{G_3} \\ x_{G_4} \\ -0.1\hat{D}^O_{dynamicUnb_z} + 0.1u_{G_1} + 0.1T_{fr_{BO}} + 0.1T_{fr_{IO}} + 0.1D^O_{staticUnb_z} - \alpha_{dist_{O_z}} \\ -0.35\hat{D}^I_{dynamicUnb_y} + 0.35u_{G_2} + 0.35T_{fr_{OI}} + 0.35D^I_{staticUnb_y} - \alpha_{dist_{I_y}} \\ x_{G_3} - 4.42 \cdot |x_{G_3}| \cdot x_{G_5} \\ x_{G_4} - 33.3 \cdot |x_{G_4}| \cdot x_{G_6} \end{bmatrix}$$

Some elements of $\boldsymbol{S}_G$ matrix depend on the inner gimbal position. It can be said that $\boldsymbol{S}_G$ matrix has to be invertible in mechanical limits of inner gimbal. As shown in Figure 2.14, all determinants of $\boldsymbol{S}_G$ matrix are nonzero except $x_{G_2} \approx 66.5$ degree. Besides diagonal terms of $\mathbf{S}_G$ matrix are dominant in comparison with the other elements except diagonal term of 3rd row of $\mathbf{S_G}$ if $x_{G_2} > 66.5$ degree.

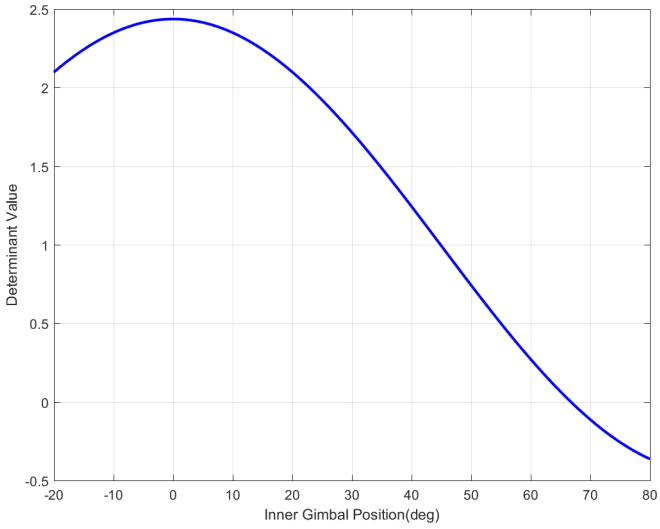

Figure 2.14: Determinants of $\boldsymbol{S}_G$ matrix

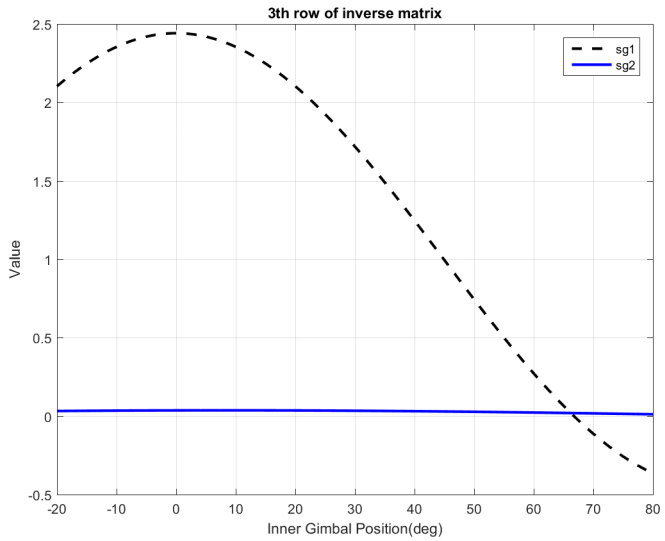

Figure 2.15: Elements of 3rd row of $\mathbf{S_G}$ matrix

To be able to definite this system model for all inner gimbal positions, we describe a new matrix $\hat{\mathbf{S}}_G$:

$$\hat{\mathbf{S}}_G = \begin{cases} \mathbf{S_G} & : x_{G_2} \ \varepsilon \ [-20.0, 66.0) \bigcup (67.0, 80.0] \\ \mathbf{S_G} + \tau_{\mathbf{G}} \cdot \mathbb{I}_{\mathbf{1}} & : x_{G_2} \ \varepsilon \ [66.0, 67.0] \end{cases}$$

where τ_G is a positive constant and $\mathbb{I}_1$ is an identity matrix. As we can see in Figure 2.16, if τ_G is selected 0.01 for inner gimbal angular positions between 66.0 and 67.0 degree, $\hat{\mathbf{S}}_G$ matrix will be nonsingular in the mechanical limits of the inner gimbal. As a result, new state equation of the coupled system becomes $\dot{\mathbf{x}}_G = \hat{\mathbf{S}}_G^{-1} \hat{\boldsymbol{f}}_G(\mathbf{x_G}, \mathbf{u_G}, \mathbf{w_G})$.

Output variables of the coupled gimbal have to be measurable in order to satisfy observability. Angular position outputs η and ϵ are measured by encoder sensors. Moreover, velocity outputs, which are measured by gyroscopes, are written as the sum of the angular velocities of gimbals relative to the earth reference frame and sensor noises.

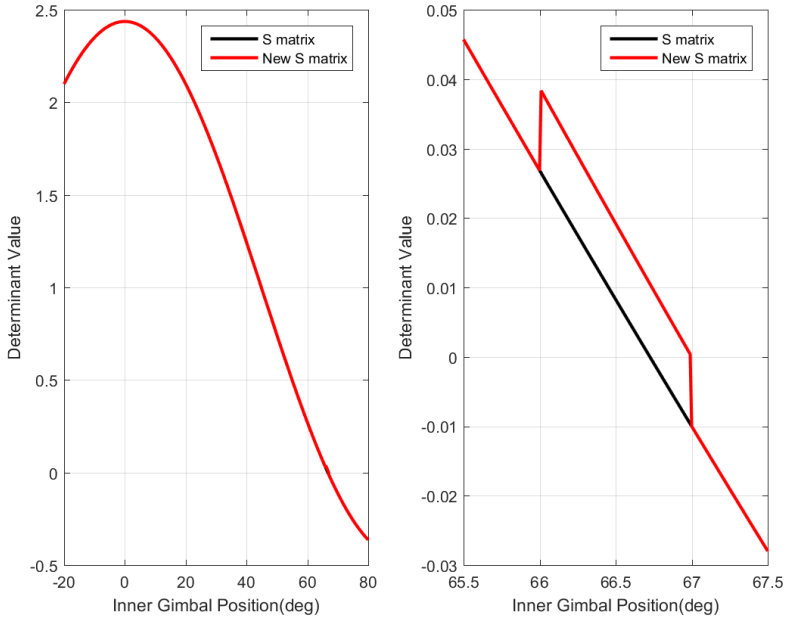

Figure 2.16: Determinants of $\hat{\mathbf{S}}_G$ matrix

Output equation of the coupled gimbal $\boldsymbol{h}_G(\boldsymbol{x}_G, \boldsymbol{w}_G, \boldsymbol{n}_G)$ is formulated by:

$$\begin{bmatrix} x_{G_1} \\ x_{G_2} \\ x_{G_3} - w_{G_4} \sin w_{G_2} + w_{G_3} \cos w_{G_2} \cos w_{G_1} + n_z \\ x_{G_4} - w_{G_5} \sin x_{G_1} + w_{G_4} \cos x_{G_1} \cos w_{G_2} + w_{G_3} \cos x_{G_1} \sin w_{G_2} + n_y \end{bmatrix} \tag{2.61}$$

2.8.2 Decoupled Gimbals

2.8.2.1 Inner Gimbal

The nonlinear state space representation of the decoupled inner gimbal is:

$$\dot{\boldsymbol{x}}_I = \boldsymbol{f}_I(\boldsymbol{x}_I, u_I, \boldsymbol{w}_I) \tag{2.62}$$

$$\boldsymbol{y}_I = \boldsymbol{h}_I(\boldsymbol{x}_I, \boldsymbol{w}_I, \boldsymbol{n}_I) \tag{2.63}$$

There are three state, one control input, eight disturbance, two outputs and one gyroscope noise variables for decoupled inner gimbal. State variables are angular position

ϵ, angular velocity Ω_{IO_y} and friction state z_{IO}. Control input reflects the inner motor torque T_{m_I} and disturbance vectors of the coupled 2-DOF and decoupled inner gimbals are the same. Measurable output variables are angular position ϵ and angular velocity which is the sum of Ω_{Ie_y} and sensor noise n_y.

$$\boldsymbol{x}_I = \begin{bmatrix} \epsilon & \Omega_{IO_y} & z_{IO} \end{bmatrix}^T$$

$$u_I = T_{m_I}$$

$$\boldsymbol{w}_I = \boldsymbol{w}_G = \begin{bmatrix} \theta & \phi & \dot{\psi} & \dot{\theta} & \dot{\phi} & \ddot{\psi} & \ddot{\theta} & \ddot{\phi} \end{bmatrix}^T$$

$$\boldsymbol{y}_I = \begin{bmatrix} \epsilon & (\Omega_{Ie_y} + n_y) \end{bmatrix}^T$$

$$\boldsymbol{n}_I = \begin{bmatrix} 0 & n_y \end{bmatrix}^T$$

State equation of the decoupled inner gimbal may be written from Eq. 2.54, 2.56 and 2.58. Inner gimbal state variables x_{I_1}, x_{I_2}, x_{I_3} and control input variable u_I are substituted into x_{G_2}, x_{G_4}, x_{G_6} and u_{G_2}, respectively. Disturbance vectors of the decoupled inner and coupled 2-DOF gimbals are the same. In order to decouple inner gimbal from outer gimbal, the mass and inertial terms of the outer gimbal have to be neglected.

The first order derivative of state variables are given below. Firstly, $\dot{x}_{I_1}$ is:

$$\dot{x}_{I_1} = x_{I_2} \tag{2.64}$$

Secondly, $\dot{x}_{I_2}$ is:

$$\dot{x}_{I_2} = -0.35 D^I_{dynamicUnb_y} + 0.35 T_{fr_{OI}} + 0.35 u_I + 0.35 D^I_{staticUnb_y} - \alpha_{dist_{I_y}} \tag{2.65}$$

where dynamic mass unbalance is:

$$\begin{aligned} D^I_{dynamicUnb_y} = &+ 0.067\alpha_{dist_{I_x}} + 0.364\alpha_{dist_{I_z}} \\ &+ \Omega_{Ie_z}(14.51\Omega_{Ie_x} + 0.067(x_{I_2} + \Omega_{dist_{I_y}}) + 0.052\Omega_{Ie_z}) \\ &- \Omega_{Ie_x}(0.052\Omega_{Ie_x} + 0.364(x_{I_2} + \Omega_{dist_{I_y}}) + 14.41\Omega_{Ie_z}), \end{aligned}$$

the static mass unbalance is:

$$\begin{aligned} D^I_{staticUnb_y} = &-2.66(\cos x_{I_1}\cos w_{I_1} - \sin x_{I_1}\sin w_{I_1}) \\ &-6.44(\cos x_{I_1}\sin w_{I_1} + \cos w_{I_1}\sin x_{I_1}) \end{aligned}$$

and friction torque between inner and outer gimbals is:

$$T_{fr_{OI}} = 90x_{I_3}$$

Lastly, $\dot{x}_{I_3}$ is:

$$\dot{x}_{I_3} = x_{I_2} - 33.3 \cdot |x_{I_2}| \cdot x_{I_3} \tag{2.66}$$

As a result, state equation of decoupled inner gimbal $\boldsymbol{f}_I(\boldsymbol{x}_I, u_I, \boldsymbol{w}_I)$ is:

$$\begin{bmatrix} x_{I_2} \\ -0.35D^I_{dynamicUnb_y} + 0.35T_{fr_{OI}} + 0.35u_I + 0.35D^I_{staticUnb_y} - \alpha_{dist_{I_y}} \\ x_{I_2} - 33.3 \cdot |x_{I_2}| \cdot x_{I_3} \end{bmatrix}$$

and output equation of decoupled inner gimbal $\boldsymbol{h}_I(\boldsymbol{x}_I, \boldsymbol{w}_I, \boldsymbol{n}_I)$ is:

$$\begin{bmatrix} x_{I_1} \\ x_{I_2} - w_{G_5}\sin\eta + w_{G_4}\cos\eta\cos w_{G_2} + w_{G_3}\cos\eta\sin w_{G_2} + n_y \end{bmatrix} \tag{2.67}$$

where η representing angular position of outer gimbal.

2.8.2.2 Outer Gimbal

The nonlinear state space representation of the decoupled outer gimbal is:

$$\dot{\boldsymbol{x}}_O = \boldsymbol{f}_O(\boldsymbol{x}_O, u_O, \boldsymbol{w}_O) \tag{2.68}$$

$$\boldsymbol{y}_O = \boldsymbol{h}_O(\boldsymbol{x}_O, \boldsymbol{w}_O, \boldsymbol{n}_O) \tag{2.69}$$

There are three state, one control input, eight disturbance, two output and one gyroscope noise variables for outer gimbal. State variables are angular position η, angular velocity Ω_{OB_z} and friction state z_{OB}. Control input is the outer motor torque T_{m_O} and disturbance vectors of coupled 2-DOF and decoupled outer gimbals are the same..

Measurable output variables are angular position η and angular velocity which is the sum of Ω_{Oe_z} and sensor noise n_z.

$$\boldsymbol{x}_O = \begin{bmatrix} \eta & \Omega_{OB_z} & z_{OB} \end{bmatrix}^T$$

$$u_O = T_{m_O}$$

$$\boldsymbol{w}_O = \boldsymbol{w}_G = \begin{bmatrix} \theta & \phi & \dot{\psi} & \dot{\theta} & \dot{\phi} & \ddot{\psi} & \ddot{\theta} & \ddot{\phi} \end{bmatrix}^T$$

$$\boldsymbol{y}_O = \begin{bmatrix} \eta & (\Omega_{Oe_z} + n_z) \end{bmatrix}^T$$

$$\boldsymbol{n}_O = \begin{bmatrix} 0 & n_z \end{bmatrix}^T$$

State equation of decoupled outer gimbal may be written from Eq. 2.53, 2.55 and 2.57. Outer gimbal state variables x_{O_1}, x_{O_2}, x_{O_3} and control input variable u_O are substituted into x_{G_1}, x_{G_3}, x_{G_5} and u_{G_1}, respectively. Disturbance vectors of decoupled outer and coupled 2-DOF gimbals are the same.

The first order derivative of state variables are given below. Firstly, $\dot{x}_{O_1}$ is:

$$\dot{x}_{O_1} = x_{O_2} \tag{2.70}$$

Secondly, $\dot{x}_{O_2}$ is:

$$\dot{x}_{O_2} = -0.1D^O_{dynamicUnb_z} + 0.1u_O + 0.1T_{fr_{BO}} + 0.1T_{fr_{IO}} + 0.1D^O_{staticUnb_z} - \alpha_{dist_{O_z}} \tag{2.71}$$

where dynamic mass unbalance is:

$$\begin{aligned} D^O_{dynamicUnb_z} = &- 4.76\alpha_{Oe_x} + 0.0006\alpha_{Oe_y} \\ &+ \Omega_{Oe_x}(\Omega_{Oe_y}25.025 + 0.0006(x_{O_2} + \Omega_{dist_{O_z}})) \\ &- \Omega_{Oe_y}(\Omega_{Oe_x}18.667 - 4.764(x_{O_2} + \Omega_{dist_{O_z}})), \end{aligned}$$

the static mass unbalance is:

$$\begin{aligned} D^O_{staticUnb_z} = &- 0.023(-\cos x_{O_1} \sin w_{O_1} + \sin x_{O_1} \sin w_{O_2} \cos w_{O_1}) \\ &+ 87.8(\sin x_{O_1} \sin w_{O_1} + \cos x_{O_1} \sin w_{O_2} \cos w_{O_1}), \end{aligned}$$

The friction torque between outer gimbal and gimbal base is:

$$T_{fr_{BO}} = 80x_{O_3}$$

and friction torque between inner and outer gimbals is:

$$T_{fr_{IO}} = 90 z_{IO}$$

Lastly, $\dot{x}_{O_3}$ is:

$$\dot{x}_{O_3} = x_{O_2} - 4.42 \cdot |x_{O_2}| \cdot x_{O_3} \tag{2.72}$$

In Eq. 2.71, the mass of inner gimbal m_I in static mass unbalance expression and all elements of inertia tensor for inner gimbal in dynamic unbalance expression are chosen as zero in order to decouple outer gimbal from inner gimbal. Consequently, state equation of the decoupled outer gimbal $\boldsymbol{f}_O(\boldsymbol{x}_O, u_O, \boldsymbol{w}_O)$ is:

$$\begin{bmatrix} x_{O_2} \\ -0.1 D^O_{dynamicUnb_z} + 0.1 u_O + 0.1 T_{fr_{BO}} + 0.1 T_{fr_{IO}} + 0.1 D^O_{staticUnb_z} - \alpha_{dist_{O_z}} \\ x_{O_2} - 4.42 \cdot |x_{O_2}| \cdot x_{O_3} \end{bmatrix}$$

and output equation of the decoupled outer gimbal $\boldsymbol{h}_O(\boldsymbol{x}_O, \boldsymbol{w}_O, \boldsymbol{n}_O)$ is:

$$\begin{bmatrix} x_{O_1} \\ x_{O_2} - w_{G_4} \sin w_{G_2} + w_{G_3} \cos w_{G_2} \cos w_{G_1} + n_z \end{bmatrix} \tag{2.73}$$

2.8.3 Linearization

2.8.3.1 Finding Equilibrium Points

Equilibrium points of the nonlinear system which are the real roots of Eq. 2.49 can be computed by:

$$\dot{\boldsymbol{x}} = \boldsymbol{f}(\boldsymbol{x}_e, \boldsymbol{u}_e, \boldsymbol{w}_e) = 0 \tag{2.74}$$

where $\boldsymbol{x}_e$ is equilibrium states, $\boldsymbol{u}_e$ is control inputs $\boldsymbol{u}_e$ and $\boldsymbol{w}_e$ is disturbances (platform motions). Equilibrium points can be described as points where values of states and inputs of the system are the same for all time [26]. An equilibrium point set (trimmed condition), expressed by Γ, merges equilibrium state and input variables of the system. As mentioned in previous section, firstly, there are six state equations, six unknown states and eight unknown inputs of the coupled 2-DOF gimbal. Secondly,

decoupled inner gimbal contains three state equations, three unknown states of inner gimbal, two unknown states of outer gimbal and eight unknown inputs. Lastly, decoupled outer gimbal has three state equations, three unknown states of outer gimbal, three unknown states of inner gimbal and eight unknown inputs. Trimmed condition of coupled 2-DOF gimbal Γ_G, trimmed condition of decoupled inner gimbal Γ_I and trimmed condition of decoupled outer gimbal Γ_O can be described as follows:

$$\Gamma_G = [\ x_{G_{1_e}} \quad ... \quad x_{G_{6_e}} \mid u_{G_{1_e}} \quad u_{G_{2_e}} \mid w_{G_{1_e}} \quad ... \quad w_{G_{8_e}}\ ]^T$$
$$\Gamma_I = [\ x_{I_{1_e}} \quad x_{I_{2_e}} \quad x_{I_{3_e}} \mid u_{I_e} \mid w_{I_{1_e}} \quad ... \quad w_{I_{8_e}}\ ]^T$$
$$\Gamma_O = [\ x_{O_{1_e}} \quad x_{O_{2_e}} \quad x_{O_{3_e}} \mid u_{O_e} \mid w_{O_{1_e}} \quad ... \quad w_{O_{8_e}}\ ]^T$$

The number of state equations has to be greater than or equal to the number of unknown variables to be capable of computing equilibrium points. Hence equilibrium states of the gimbals are determined as unknowns and they are calculated for different values of the equilibrium inputs in boundaries. In this computation, each disturbance variable only get its lower boundary, zero and upper boundary. In finding equilibrium points of the coupled system, angular position of the inner gimbal $x_{G_{2_e}}$ and angular position of the outer gimbal $x_{G_{1_e}}$ are split into 11 different values within mechanical limits.

$$x_{G_{1_e}} = -\pi : \frac{\pi}{11} : \pi$$
$$x_{G_{2_e}} = -\frac{\pi}{9} : \frac{5\pi/18}{11} : \frac{4\pi}{9}$$

After we computed equilibrium points of the coupled gimbal, these points were assigned to the equilibrium points of decoupled gimbals. Equilibrium points of the decoupled inner gimbal can be described by:

$$\Gamma_I = [\ x_{G_{2_e}} \quad x_{G_{4_e}} \quad x_{G_{6_e}} \mid u_{G_{2_e}} \mid w_{G_{1_e}} \quad ... \quad w_{G_{8_e}}\ ]^T$$

and equilibrium points of the decoupled outer gimbal is:

$$\Gamma_O = [\ x_{G_{1_e}} \quad x_{G_{3_e}} \quad x_{G_{5_e}} \mid u_{G_{1_e}} \mid w_{G_{1_e}} \quad ... \quad w_{G_{8_e}}\ ]^T$$

Dynamic and kinematic equations of the decoupled gimbals still include unknown

state variables. Dynamic equation of the decoupled inner gimbal, given in Eq. 2.65, contains angular position η, relative angular velocity $\dot{\eta}$ of the outer gimbal. Values of these two unknown variables are chosen the equilibrium points $x_{G_{1_e}}$ and $x_{G_{3_e}}$, respectively. Similar to the inner gimbal, Eq. 2.71 includes ϵ, $\dot{\epsilon}$ and z_{IO} which come from equilibrium points $x_{G_{2_e}}$, $x_{G_{4_e}}$ and $x_{G_{6_e}}$, respectively. In conclusion, the numbers of trimmed conditions of coupled 2-DOF gimbal, decoupled inner and decoupled outer gimbal are $3^8 \times 11 \times 11 = 793881$, $3^8 \times 11 = 72171$ and $3^8 \times 11 = 72171$, respectively.

2.8.3.2 Clustering Trimmed Conditions

Linearization of the system and designing linear controller are computationally expensive for entire trimmed conditions. Hence equilibrium points are partitioned into clusters to reduce the number of linear models. The purpose of cluster analysis is to collect similar observations, equilibrium point sets, into the clusters and isolate from dissimilar ones in some sense. Clustering analysis can be separated into two parts, one of which is the clustering evaluation to determine the optimal number of clusters by means of different criteria such as Davies-Bouldin [13] and Calinski-Harabasz [7], and the other is clustering observations with respect to the optimal number of cluster result of evaluation analysis. In this thesis, K-means clustering algorithm [34] [30], with squared Euclidean distances, along with Calinski-Harabasz clustering evaluation criterion is used in order to find the sufficient number of linearized models.

The Calinski-Harabasz criterion, also named as the variance ratio criterion (VRC), calculates an index value for each number of cluster. The Calinski-Harabasz index value CH_k can be formulated by:

$$CH_k = \frac{n-k}{k-1} \cdot \frac{SS_B(k)}{SS_W(k)} \tag{2.75}$$

where n is the number of trimmed conditions, k is the number of clusters, $SS_B(k)$ term is the overall between-cluster variance and $SS_W(k)$ term is the overall within-cluster variance. $SS_B(k)$ and $SS_W(k)$ variance terms are:

$$SS_B(k) = \sum_{i=1}^{k} n_i ||m_i - m||^2 \tag{2.76}$$

$$SS_W(k) = \sum_{i=1}^{k} \sum_{x \in c_i} ||x - m_i||^2 \tag{2.77}$$

where n_i is the equilibrium point i, m_i is the centroid of cluster i, m is the overall mean of equilibrium points i and x is an equilibrium point.

It can be said that clusters are partitioned successfully if $VRC_B(k)$ variance value is large and $VRC_W(k)$ is small so that success of partition of trimmed conditions depends on how large the Calinski-Harabasz index value is. The optimal number of clusters is determined by the highest Calinski-Harabasz value. Clustering evaluation analysis for equilibrium points of all gimbal models indicates that the optimal number of clusters is two for coupled 2-DOF and decoupled inner gimbal. On the other hand, the optimal number of clusters is three for decoupled outer gimbal, as shown in Figures 2.17 - 2.19.

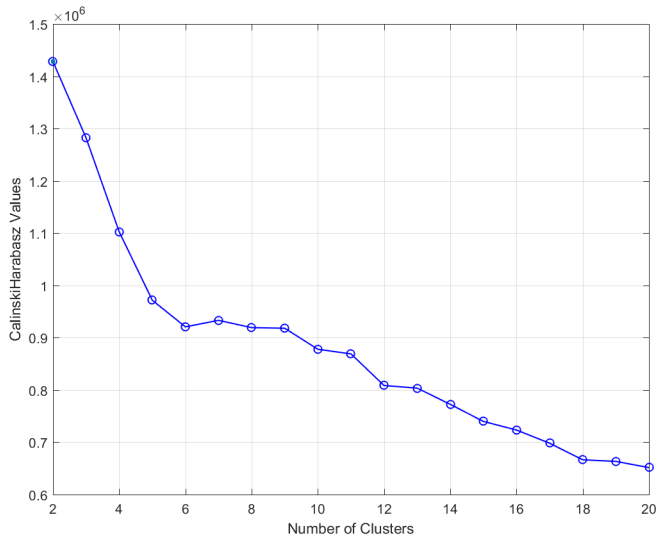

Figure 2.17: Clustering evaluation for coupled gimbal equilibrium points

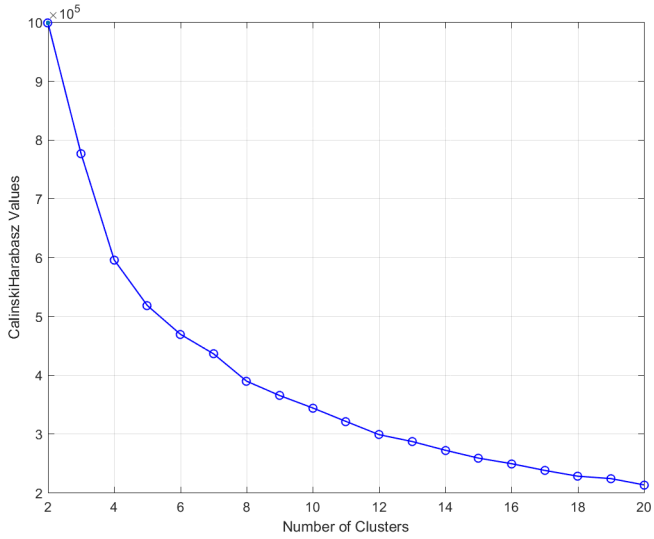

Figure 2.18: Clustering evaluation for decoupled inner gimbal equilibrium points

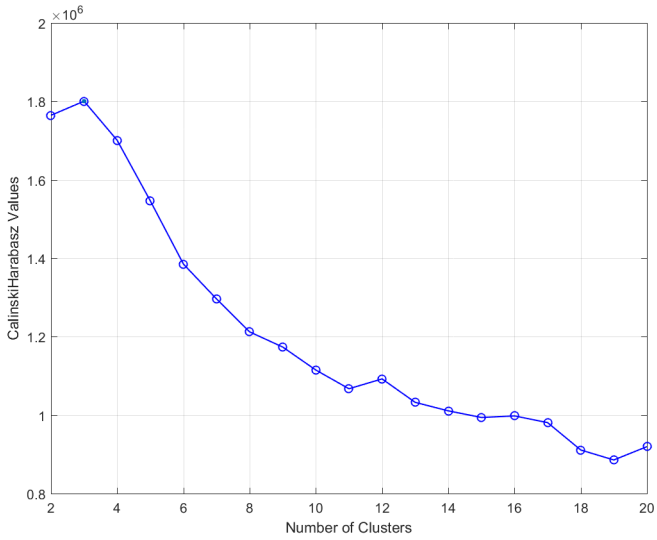

Figure 2.19: Clustering evaluation for decoupled outer gimbal equilibrium points

The K-means clustering is an iterative algorithm that partitions all observations into exactly one of the K groups, or clusters, which is determined by centroids [33]. Observations are assigned into clusters by minimizing of a cost function given by Eq. 2.78.

$$J = \sum_{j=1}^{n} \sum_{i=1}^{k} u_{ij} d(x_j, c_i) \tag{2.78}$$

In this equation, n is the number of observations, K is the number of clusters, u_{ij}, giving the membership of x_j observation to i_{th} cluster, is an element of $K \times n$ partition matrix, x_j is the observation, c_i is the centroid of i_{th} cluster and $d(x_j, c_i) = (x_j - c_i)(x_j - c_i)^T$ is squared Euclidean distance between the observation x_j and the centroid c_i.

In clustering analysis of the equilibrium points of the system models, algorithm gives cluster centroid points and assigns all equilibrium points into a cluster. After that, distances of each equilibrium point to the centroid in the cluster are calculated and the one equilibrium point set which is closest to centroid is selected in order to linearize the system.

2.8.3.3 Obtaining LTI Subsystems

State space representation of a linear time invariant (LTI) system is:

$$\dot{\boldsymbol{x}} = \boldsymbol{A}\boldsymbol{x} + \boldsymbol{B}\boldsymbol{u} + \boldsymbol{G}\boldsymbol{w} \tag{2.79}$$

$$\boldsymbol{y} = \boldsymbol{C}\boldsymbol{x} + \boldsymbol{P}\boldsymbol{w} + \boldsymbol{n} \tag{2.80}$$

where $\boldsymbol{x}$ is state vector, $\boldsymbol{u}$ is control input vector, $\boldsymbol{w}$ is disturbance input vector, $\boldsymbol{y}$ is output vector, $\boldsymbol{n}$ is noise vector, $\boldsymbol{A}$ is state matrix, $\boldsymbol{B}$ is control input matrix, $\boldsymbol{G}$ is disturbance state matrix, $\boldsymbol{C}$ is output matrix and $\boldsymbol{P}$ is disturbance output matrix.

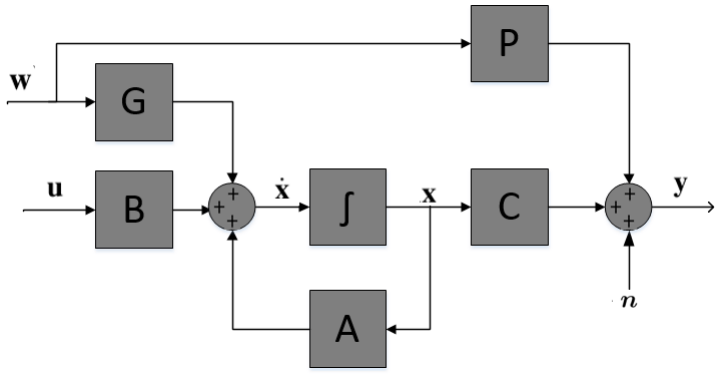

Figure 2.20: Block diagram of the LTI system

State equation (Eq. 2.49) may be written as a Taylor series about equilibrium points.

$$\begin{aligned}\dot{\boldsymbol{x}} = \boldsymbol{f}(\boldsymbol{x}, \boldsymbol{u}, \boldsymbol{w}) = &+ \boldsymbol{f}(\boldsymbol{x}_e, \boldsymbol{u}_e, \boldsymbol{w}_e) \\ &+ \frac{\partial \boldsymbol{f}}{\partial \boldsymbol{x}}\boldsymbol{\delta}_x + \frac{\partial \boldsymbol{f}}{\partial \boldsymbol{u}}\boldsymbol{\delta}_u + \frac{\partial \boldsymbol{f}}{\partial \boldsymbol{w}}\boldsymbol{\delta}_w \\ &+ \frac{1}{2!}\frac{\partial^2 \boldsymbol{f}}{\partial \boldsymbol{x}^2}\boldsymbol{\delta}_x^2 + \frac{1}{2!}\frac{\partial^2 \boldsymbol{f}}{\partial \boldsymbol{u}^2}\boldsymbol{\delta}_u^2 + \frac{1}{2!}\frac{\partial^2 \boldsymbol{f}}{\partial \boldsymbol{w}^2}\boldsymbol{\delta}_w^2 + ...\end{aligned}$$

where deviation variables are

$$\boldsymbol{\delta}_x = \boldsymbol{x} - \boldsymbol{x}_e$$

$$\boldsymbol{\delta}_u = \boldsymbol{u} - \boldsymbol{u}_e$$

$$\boldsymbol{\delta}_w = \boldsymbol{w} - \boldsymbol{w}_e$$

In this equation, $\dot{\boldsymbol{x}}_e = \boldsymbol{f}(\boldsymbol{x}_e, \boldsymbol{u}_e, \boldsymbol{w}_e) = 0$ and the higher-order derivative terms are neglected because these derivatives are multiplied by very small variations raised to, at least second power. State equation of the LTI system can be written by Jacobian linearization method as follows:

$$\dot{\boldsymbol{\delta}}_x = \boldsymbol{A}\boldsymbol{\delta}_x + \boldsymbol{B}\boldsymbol{\delta}_u + \boldsymbol{G}\boldsymbol{\delta}_w$$

where state matrix $\boldsymbol{A}$, control input matrix $\boldsymbol{B}$ and disturbance state matrix $\boldsymbol{G}$ are:

$$\boldsymbol{A} = \left.\frac{\partial \boldsymbol{f}}{\partial \boldsymbol{x}}\right|_{\boldsymbol{x}_e, \boldsymbol{u}_e, \boldsymbol{w}_e} = \begin{bmatrix} \frac{\partial f_1}{\partial x_1} & \cdots & \frac{\partial f_1}{\partial x_n} \\ \cdots & \cdots & \cdots \\ \frac{\partial f_n}{\partial x_1} & \cdots & \frac{\partial f_n}{\partial x_n} \end{bmatrix}_{\boldsymbol{x}_e, \boldsymbol{u}_e, \boldsymbol{w}_e}$$

$$\boldsymbol{B} = \left.\frac{\partial \boldsymbol{f}}{\partial \boldsymbol{u}}\right|_{\boldsymbol{x}_e, \boldsymbol{u}_e, \boldsymbol{w}_e} = \begin{bmatrix} \frac{\partial f_1}{\partial u_1} & \cdots & \frac{\partial f_1}{\partial u_m} \\ \cdots & \cdots & \cdots \\ \frac{\partial f_n}{\partial u_1} & \cdots & \frac{\partial f_n}{\partial u_m} \end{bmatrix}_{\boldsymbol{x}_e, \boldsymbol{u}_e, \boldsymbol{w}_e}$$

$$\boldsymbol{G} = \left.\frac{\partial \boldsymbol{f}}{\partial \boldsymbol{w}}\right|_{\boldsymbol{x}_e, \boldsymbol{u}_e, \boldsymbol{w}_e} = \begin{bmatrix} \frac{\partial f_1}{\partial w_1} & \cdots & \frac{\partial f_1}{\partial w_k} \\ \cdots & \cdots & \cdots \\ \frac{\partial f_n}{\partial w_1} & \cdots & \frac{\partial f_n}{\partial w_k} \end{bmatrix}_{\boldsymbol{x}_e, \boldsymbol{u}_e, \boldsymbol{w}_e}$$

where n is the number of state variables, m is the number of control input variables and k is the number of disturbance input variables.

Taylor series expression of the output equation, given in Eq. 2.50, about the equilibrium points is:

$$\begin{aligned}\boldsymbol{y} = \boldsymbol{h}(\boldsymbol{x}, \boldsymbol{w}, \boldsymbol{n}) = &+ \boldsymbol{h}(\boldsymbol{x}_e, \boldsymbol{w}_e, \boldsymbol{n}_e) \\ &+ \frac{\partial \boldsymbol{h}}{\partial \boldsymbol{x}}\boldsymbol{\delta}_x + \frac{\partial \boldsymbol{h}}{\partial \boldsymbol{w}}\boldsymbol{\delta}_w + \frac{\partial \boldsymbol{h}}{\partial \boldsymbol{n}}\boldsymbol{\delta}_n \\ &+ \frac{1}{2!}\frac{\partial^2 \boldsymbol{h}}{\partial \boldsymbol{x}^2}\boldsymbol{\delta}_x^2 + \frac{1}{2!}\frac{\partial^2 \boldsymbol{h}}{\partial \boldsymbol{w}^2}\boldsymbol{\delta}_w^2 + \frac{1}{2!}\frac{\partial^2 \boldsymbol{h}}{\partial \boldsymbol{n}^2}\boldsymbol{\delta}_n^2 + ...\end{aligned}$$

Output equation about equilibrium points is $\boldsymbol{h}(\boldsymbol{x}_e, \boldsymbol{w}_e, \boldsymbol{n}_e) = \boldsymbol{y}_e$ and the higher-order derivative terms are neglected. Furthermore, output equation is linearized as Jacobian method as follows:

$$\boldsymbol{\delta}_y = \boldsymbol{C}\boldsymbol{\delta}_x + \boldsymbol{P}\boldsymbol{\delta}_w + \boldsymbol{\delta}_n$$

where $\boldsymbol{\delta}_y = \boldsymbol{y} - \boldsymbol{y}_e$ and $\boldsymbol{\delta}_n = \boldsymbol{n} - \boldsymbol{n}_e$ express the output and noise deviation variables, respectively. Output matrix $\boldsymbol{C}$ and disturbance output matrix $\boldsymbol{P}$ are:

$$\boldsymbol{C} = \left.\frac{\partial \boldsymbol{h}}{\partial \boldsymbol{x}}\right|_{\boldsymbol{x}_e, \boldsymbol{w}_e, \boldsymbol{n}_e} = \begin{bmatrix} \frac{\partial h_1}{\partial x_1} & \cdots & \frac{\partial h_1}{\partial x_n} \\ \cdots & \cdots & \cdots \\ \frac{\partial h_p}{\partial x_1} & \cdots & \frac{\partial h_p}{\partial x_n} \end{bmatrix}_{\boldsymbol{x}_e, \boldsymbol{w}_e, \boldsymbol{n}_e}$$

$$\boldsymbol{P} = \left.\frac{\partial \boldsymbol{h}}{\partial \boldsymbol{w}}\right|_{\boldsymbol{x}_e, \boldsymbol{w}_e, \boldsymbol{n}_e} = \begin{bmatrix} \frac{\partial h_1}{\partial w_1} & \cdots & \frac{\partial h_1}{\partial w_k} \\ \cdots & \cdots & \cdots \\ \frac{\partial h_p}{\partial w_1} & \cdots & \frac{\partial h_p}{\partial w_k} \end{bmatrix}_{\boldsymbol{x}_e, \boldsymbol{w}_e, \boldsymbol{n}_e}$$

where n is the number of state variables, p is the number of output variables and k is the number of disturbance input variables.

According to the clustering analysis explained in previous section, both coupled and decoupled inner gimbals have two LTI subsystems, on the other hand, decoupled outer gimbal has three LTI subsystems. Firstly, state space representation of a linear time invariant subsystem of the coupled gimbal is:

$$\dot{\boldsymbol{x}}_G = \boldsymbol{A}_G\boldsymbol{x}_G + \boldsymbol{B}_G\boldsymbol{u}_G + \boldsymbol{G}_G\boldsymbol{w}_G \tag{2.81}$$

$$\boldsymbol{y}_G = \boldsymbol{C}_G\boldsymbol{x}_G + \boldsymbol{P}_G\boldsymbol{w}_G + \boldsymbol{n}_G \tag{2.82}$$

where $\boldsymbol{x}_G$ is 6×1 state vector, $\boldsymbol{u}_G$ is 2×1 control input vector, $\boldsymbol{w}_G$ is 8×1 disturbance vector, $\boldsymbol{y}_G$ is 4×1 measured output vector, $\boldsymbol{n_G}$ is 4×1 sensor noise vector, $\boldsymbol{A}_G$ is

6×6 constant state matrix, $\boldsymbol{B}_G$ is 6×2 constant input matrix, $\boldsymbol{G}_G$ is 6×8 constant disturbance state matrix, $\boldsymbol{C}_G$ is 4×6 constant output matrix and $\boldsymbol{P}_G$ is 4×8 constant disturbance output matrix.

Secondly, state space representation of a linear time invariant subsystem of the decoupled inner gimbal is:

$$\dot{\boldsymbol{x}}_I = \boldsymbol{A}_I \boldsymbol{x}_I + \boldsymbol{B}_I u_I + \boldsymbol{G}_I \boldsymbol{w}_I \tag{2.83}$$

$$\boldsymbol{y}_I = \boldsymbol{C}_I \boldsymbol{x}_I + \boldsymbol{P}_I \boldsymbol{w}_I + \boldsymbol{n}_I \tag{2.84}$$

where $\boldsymbol{x}_I$ is 3×1 state vector, u_I is a scalar control input, $\boldsymbol{w}_I$ is 8×1 disturbance vector, $\boldsymbol{y}_I$ is 2×1 measured output vector, $\boldsymbol{n_I}$ is 2×1 sensor noise vector, $\boldsymbol{A}_I$ is 3×3 constant state matrix, $\boldsymbol{B}_I$ is 3×1 constant input matrix, $\boldsymbol{G}_I$ is 3×8 constant disturbance state matrix, $\boldsymbol{C}_I$ is 2×3 constant output matrix and $\boldsymbol{P}_I$ is 2×8 constant disturbance output matrix.

Lastly, state space representation of a linear time invariant subsystem of the decoupled outer gimbal is:

$$\dot{\boldsymbol{x}}_O = \boldsymbol{A}_O \boldsymbol{x}_O + \boldsymbol{B}_O u_O + \boldsymbol{G}_O \boldsymbol{w}_O \tag{2.85}$$

$$\boldsymbol{y}_O = \boldsymbol{C}_O \boldsymbol{x}_O + \boldsymbol{P}_O \boldsymbol{w}_O + \boldsymbol{n}_O \tag{2.86}$$

where $\boldsymbol{x}_O$ is 3×1 state vector, u_O is a scalar control input, $\boldsymbol{w}_O$ is 8×1 disturbance vector, $\boldsymbol{y}_O$ is 2×1 measured output vector, $\boldsymbol{n_O}$ is 2×1 sensor noise vector, $\boldsymbol{A}_O$ is 3×3 constant state matrix, $\boldsymbol{B}_O$ is 3×1 constant input matrix, $\boldsymbol{G}_O$ is 3×8 constant disturbance state matrix, $\boldsymbol{C}_O$ is 2×3 constant output matrix and $\boldsymbol{P}_O$ is 2×8 constant disturbance output matrix.

Controllability has a great importance for the control systems in state space. Controllability matrix of the LTI system is defined as $\left[\begin{array}{c:c:c:c:c} \boldsymbol{B} & \boldsymbol{AB} & \boldsymbol{A}^2\boldsymbol{B} & ... & \boldsymbol{A}^{n-1}\boldsymbol{B} \end{array} \right]$. The LTI system, given by Eq. 2.79, may be called completely state controllable if and only if rank of the controllability matrix is equal to n which is the number of state variables. Analysis of controllability of LTI subsystems of the coupled and decoupled gimbals results that all linear subsystems of the gimbals are full state controllable.

Even though all LTI subsystems of the gimbals are controllable, it does not guarantee the controllability of gimbal models. A partially controllable linear system can be called a stabilizable if its all uncontrollable subsystems are stable or its all unstable subsystems are controllable [36]. Thus, first, we analyzed the controllability and stability of all LTI subsystems of the coupled and decoupled gimbals. Result of the these analyses is that all subsystems of the gimbals are controllable and unstable. Furthermore, it is verified that linear state space models of all gimbals are stabilizable.

CHAPTER 3

CONTROLLER DESIGN

The design procedures of the two control methods, cascade PI and linear quadratic integral (LQI), of the 2-DOF gimbal system are introduced in this chapter. After that, all controllers are compared between each other and the best performed control method will be used for target tracking and stabilization. All of these studies are made on the MATLAB/Simulink platform.

During controller design study, parameters of the cascade PI controller are tuned with the nonlinear system, which includes friction, static and dynamic mass unbalance, directly. In contrast, the linear quadratic controllers are designed for the linearized state space models of both coupled and decoupled gimbals and these controllers are implemented in the nonlinear system model.

Global linear quadratic integral (LQI) control is used to yield the stabilization and tracking control problems of the coupled 2-DOF gimbal. Diversely, decoupled inner and outer gimbals have two separate linear quadratic controllers, called local LQI. Structure of the LQI controllers for the decoupled gimbals has some difference from the global LQI controller. Global LQI controller produces two control signals (motor torques). On the other hand, decoupled gimbals are controlled by own local LQI compensators.

Angular position references of the inner and outer gimbals are applied as step functions within the first order pre-filters for tracking with less control effort and lower position overshoot. On the other hand, when we implemented pre-filters of rate com-

mands, it has been observed that pre-filters of rate loops have no contribution to the performance. Controller parameters and cut-off frequency of the pre-filters are tuned with respect to the aim of achieving the desired conditions which are less than or equal to 2 seconds settling time, 10% maximum overshoot and 2% settling limit for position step responses.

3.1 Cascade PI Control

It can be said that the most used control strategy in the industrial applications is proportional integral derivative (PID) control. In many implementations of PID controllers, derivative term is generally set to zero due to raise of the high frequency sensor noise. In this study, we use only the proportional and integral terms of this controller. Integral term of the controller overcomes the steady state error for step responses. In addition, proportional term is used to adjust the system response time [29].

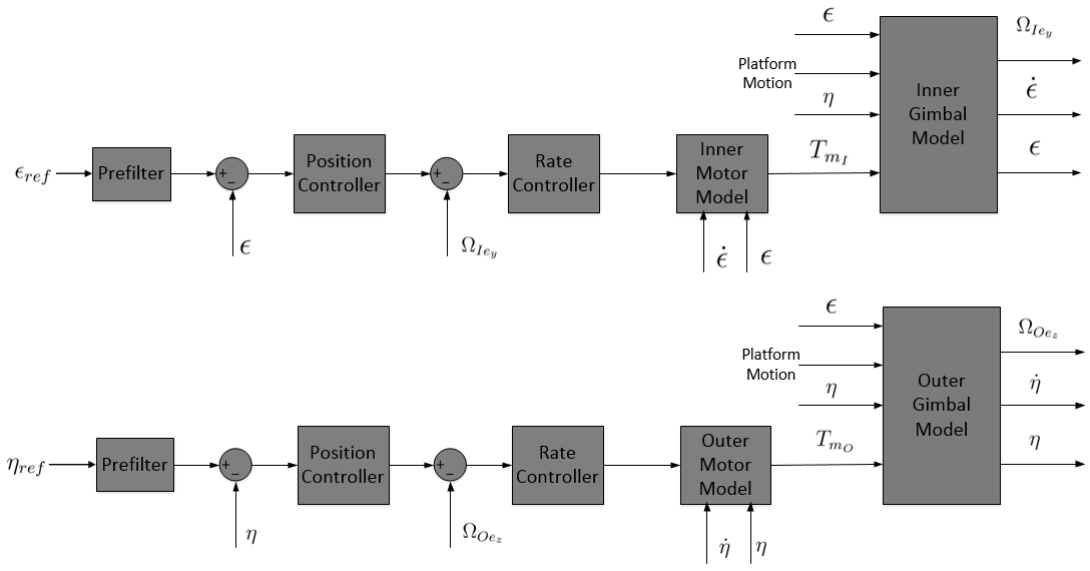

Figure 3.1: Block diagram of cascade PI control

Cascade PI control consists of one PI controller for position loop to track the target and one PI controller for rate loop to eliminate disturbances. Block diagram of

cascade PI control for the coupled 2-DOF gimbal is given in Figure 3.1. In this section, the continuous time position and rate PI controllers are tuned for both gimbals. Transfer function of the continuous time PI controller is:

$$C_{PI}(s) = K_p + \frac{K_i}{s} \tag{3.1}$$

where K_p and K_i express the proportional and integral gain of controller, respectively. First step of design procedure is that only PI controllers of the rate loops are tuned for different K_p and K_i values and the best performed controllers are chosen. After we designed the rate controllers of the system, position controllers are tuned with respect to the desired conditions. Lastly, pre-filters are designed for different cut-off frequency values to decrease overshoot and control effort for tracking.

3.1.1 Inner Gimbal

In cascade PI control design of the inner gimbal for different K_p and K_i values, performances of the rate controllers (Table 3.1, 3.2) and performances of position controllers (Table 3.3, 3.4) are given below. According to these results, when parameters of rate controller are selected as $K_p = 750$ and $K_i = 50$ and parameters of position controller are chosen $K_p = 8$ and $K_i = 0.1$, position step response has 1.7% overshoot, 1.0 seconds settling time and less than 1% steady state error.

Table3.1: Performances of the rate PI controllers of the inner gimbal for different K_p values (K_i = 50)

K_p Values	Overshoot(%)	Settling Time(sec)	Steady State Error(%)
375	1.7	0.24	<1
500	1.3	0.23	<1
625	1.1	0.23	<1
750	1.0	0.23	<1
1000	1.6	0.23	<1

Table3.2: Performances of the rate PI controller of the inner gimbal for different K_i values (K_p = 750)

K_i Values	Overshoot(%)	Settling Time(sec)	Steady State Error(%)
50	1.0	0.23	<1
100	1.4	0.23	<1
150	1.7	0.23	<1
200	2.1	0.23	<1
250	2.5	0.23	<1

Table3.3: Performances of the position PI controller of the inner gimbal for different K_p values (K_i = 0.1)

K_p Values	Overshoot(%)	Settling Time(sec)	Steady State Error(%)
7	1.9	1.2	<1
8	1.7	1.0	<1
9	8.2	1.0	<1
10	15.4	1.1	<1

Table3.4: Performances of the position PI controller of the inner gimbal for different K_i values (K_p = 8)

K_i Values	Overshoot(%)	Settling Time(sec)	Steady State Error(%)
0.1	1.7	1.0	<1
1	3.0	2.1	<1
3	7.7	2.5	<1
5	13.2	2.4	<1

Position performances of the inner gimbal with cascade PI control for different position references and cutoff frequency values of the pre-filters are given below. It is clearly seen that, this control method only satisfies all desired conditions if cut-off frequency of pre-filter is selected 1 Hz. As a result, when we implement the best performed controllers and pre-filter into the inner gimbal model, system responses and motor torque of the inner gimbal with cascade PI control is shown in Figure 3.2.

Table3.5: Position performances of the inner gimbal with cascade PI control for different position commands

Reference	Pre-filter cutoff frequency	Overshoot(%)	Settling time(sec)
0.5 rad	1 Hz	4.0	2.1
1.0 rad		1.7	1.0
0.5 rad	2 Hz	3.3	2.8
1.0 rad		25.1	1.2
0.5 rad	10 Hz	3.4	2.9
1.0 rad		28.3	1.3

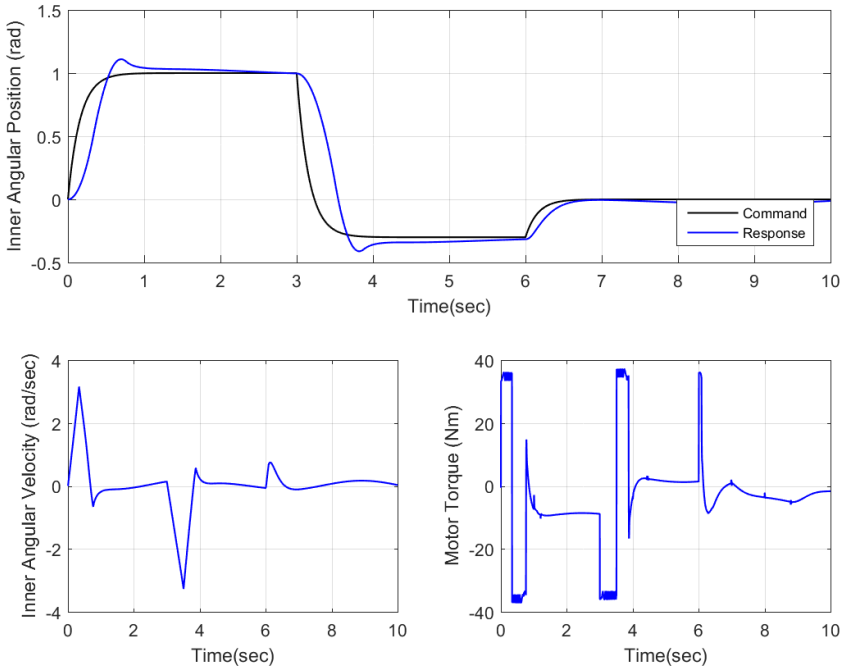

Figure 3.2: System responses and motor torque of the inner gimbal with cascade PI control

3.1.2 Outer Gimbal

In cascade PI control design of the outer gimbal for different K_p and K_i values, performances of the rate controllers (Table 3.6, 3.7) and performances of position controllers (Table 3.8, 3.9) are given below. If parameters of rate controller are selected as $K_p = 300$ and $K_i = 150$ and parameters of position controller are chosen $K_p = 5$ and $K_i = 0.05$, position step response has 1.8% overshoot, 1.1 seconds settling time and less than 1% steady state error.

Table3.6: Performances of the rate PI controller of the outer gimbal for different K_p values (K_i = 150)

K_p Values	Overshoot(%)	Settling Time(sec)	Steady State Error(%)
75	4.4	1.36	<1
150	1.1	0.38	<1
225	0.6	0.33	<1
300	0.5	0.32	<1
375	22.4	3.8	<1
450	26.6	>4	<1

Table3.7: Performances of the rate PI controller of the outer gimbal for different K_i values (K_p = 300)

K_i Values	Overshoot(%)	Settling Time(sec)	Steady State Error(%)
30	1.9	>4	<1
75	0.7	0.35	<1
150	0.5	0.32	<1
225	1.3	0.31	<1
300	2.8	0.57	<1

Table3.8: Performances of the position PI controller of the outer gimbal for different K_p values (K_i = 0.05)

K_p Values	Overshoot(%)	Settling Time(sec)	Steady State Error(%)
2	1.9	2.0	<1
3	2.0	1.5	<1
4	1.9	1.2	<1
5	1.8	1.1	<1

Table3.9: Performances of the position PI controller of the outer gimbal for different K_i values (K_p = 5)

K_i Values	Overshoot(%)	Settling Time(sec)	Steady State Error(%)
0.05	1.8	1.1	<1
0.1	2.5	1.2	<1
0.5	4.8	>4	<1
1.0	8.3	>4	<1

Position performances of the outer gimbal with cascade PI control for different position commands are given Table 3.10. Thus, all desired conditions are satisfied with the pre-filters whose cut-off frequency is 1 Hz for lower than 1.5 rad position reference. When we implement the best performed controllers and the pre-filter in the outer gimbal, system responses and motor torque of the outer gimbal with cascade PI control is shown in Figure 3.3.

Table3.10: Position performances of the outer gimbal with cascade PI control for different position commands

Reference	Pre-filter cutoff frequency	Overshoot(%)	Settling time(sec)
0.5 rad	1 Hz	1.3	1.6
1.0 rad		1.8	1.1
1.5 rad		11.6	2.4
2.0 rad		16.8	2.9
2.5 rad		22.6	>3.0
3.0 rad		30.3	2.6
0.5 rad	2 Hz	2.1	1.0
1.0 rad		18.6	2.9
1.5 rad		24.3	>3
2.0 rad		28.7	>3
2.5 rad		35.0	>3
3.0 rad		41.7	>3
0.5 rad	10 Hz	4.2	>3
1.0 rad		21.4	>3
1.5 rad		28.4	>3
2.0 rad		32.6	>3
2.5 rad		38.2	>3
3.0 rad		46.1	>3

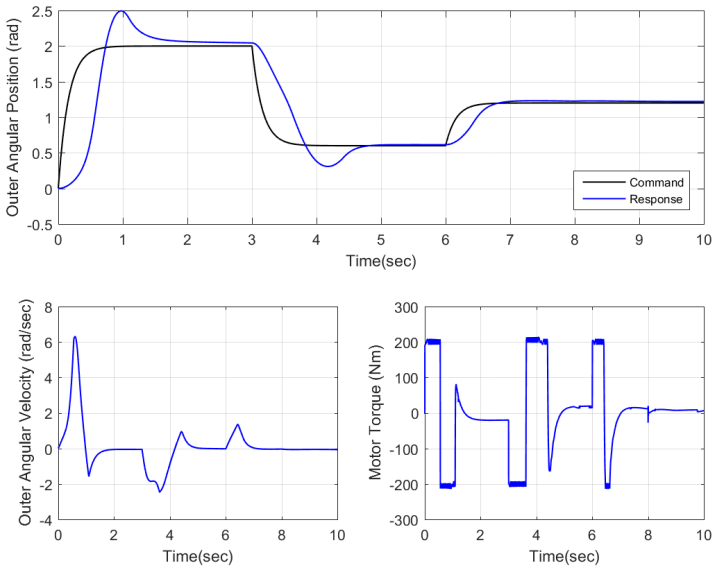

Figure 3.3: System responses and motor torque of the outer gimbal with cascade PI control

3.2 Linear Quadratic Integral (LQI) Control

The main benefits of the LQ controllers are that stability and robustness of system are guaranteed [41]. Aim of this problem is computing the state feedback gain matrix $\boldsymbol{K}$ of the optimal control vector $\boldsymbol{u}$ assumed as unconstrained in order to minimize the quadratic cost function J. In the design procedure of the LQ, it is required that system model has to be completely state controllable for the existence of $\boldsymbol{u}$ [36]. Block diagram of a linear quadratic (LQ) system is given below.

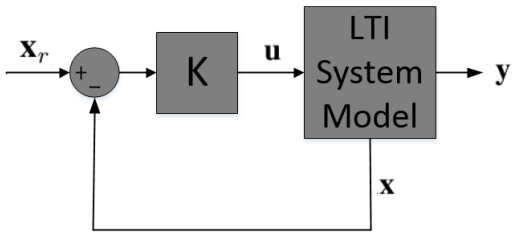

Figure 3.4: Block diagram of linear quadratic system

The optimal control law of linear quadratic problem is:

$$\boldsymbol{u} = -\boldsymbol{K}(\boldsymbol{x} - \boldsymbol{x}_r) \tag{3.2}$$

and the quadratic cost function is:

$$J = \int_0^\infty ((\boldsymbol{x} - \boldsymbol{x}_r)^T \boldsymbol{Q}(\boldsymbol{x} - \boldsymbol{x}_r) + \boldsymbol{u}^T \boldsymbol{R}\boldsymbol{u})dt \tag{3.3}$$

where $\boldsymbol{Q}$ and $\boldsymbol{R}$ are real symmetric or positive definite/semidefinite Hermitian matrices. Both $\boldsymbol{Q}$ and $\boldsymbol{R}$ are selected before the design procedure. On the right side of the quadratic cost function, the term

$$\int_0^\infty (\boldsymbol{u}^T \boldsymbol{R}\boldsymbol{u})dt$$

is the energy of control signal and the term

$$\int_0^\infty ((\boldsymbol{x} - \boldsymbol{x}_r)^T \boldsymbol{Q}(\boldsymbol{x} - \boldsymbol{x}_r))dt$$

is the energy of states. During the LQ controller design, there is a trade-off between minimization of these energy terms. If we would like to decrease the energy of control signal, the energy of states will be increased, or, conversely, large states are obtained

by small control signals [19].

Now, we defines an $\boldsymbol{N}$ matrix which is a real symmetric or positive definite/semidefinite Hermitian matrix. $\boldsymbol{N}$ matrix can be obtained by the reduced-matrix Riccati equation.

$$\boldsymbol{A}^T\boldsymbol{N} + \boldsymbol{N}\boldsymbol{A} - \boldsymbol{N}\boldsymbol{B}\boldsymbol{R}^{-}\boldsymbol{B}^T\boldsymbol{N} + \boldsymbol{Q} = 0.$$

Thus the optimal feedback gain matrix is:

$$\boldsymbol{K} = \boldsymbol{R}^{-}\boldsymbol{B}^T\boldsymbol{N} \tag{3.4}$$

It is examined that integrator effect exists in none of the linearized subsystems of the gimbals represented in state space. Hence integrators are inserted in the feed-forward path between the error signal ($\dot{\boldsymbol{\xi}}$), which is difference between reference and measured output signals, and the plant [36]. This configuration is called linear quadratic integrator (LQI) control which calculates the gain matrix $\hat{\boldsymbol{K}}$ for the tracking [28].

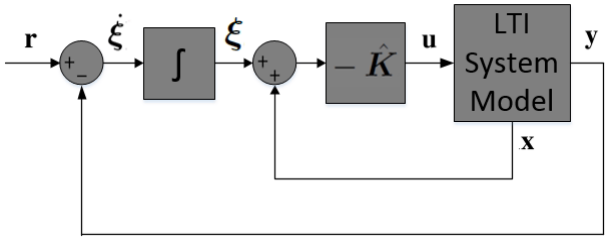

Figure 3.5: Block diagram of LQI control system with merged gain matrix $\hat{\boldsymbol{K}}$

In this problem, a new state vector arises by combining of state variables of the system $\boldsymbol{x}$ and integrator output of the error signal $\boldsymbol{\xi}$. As seen in Figure 3.6, $\hat{\boldsymbol{K}}$ gain matrix is obtained by merging of state feedback gain matrix $\boldsymbol{K}$ and error gain matrix $\boldsymbol{K_\xi}$.

$$\hat{\boldsymbol{K}} = \left[\begin{array}{c:c} \boldsymbol{K} & -\boldsymbol{K_\xi} \end{array}\right]_{k\times(n+m)}$$

In the design procedure, references are chosen as step functions. Hence $\boldsymbol{r}(t) = \boldsymbol{r}(\infty) = \boldsymbol{r}$ for $t > 0$ and the system is assumed asymptotically stable. As shown in Figure 3.6, error vector between references and outputs is:

$$\dot{\boldsymbol{\xi}} = \boldsymbol{r} - \boldsymbol{y} = \boldsymbol{r} - \boldsymbol{C}\boldsymbol{x} - \boldsymbol{P}\boldsymbol{w} - \boldsymbol{n} \tag{3.5}$$

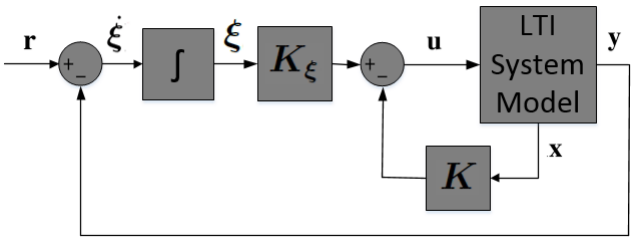

Figure 3.6: Block diagram of the LQI control system with separated gain matrix $\hat{\boldsymbol{K}}$

Thus the state error equation may be described as follows:

$$\begin{bmatrix} \dot{\boldsymbol{x}}_e(t) \\ \dot{\boldsymbol{\xi}}_e(t) \end{bmatrix} = \begin{bmatrix} \boldsymbol{A} & \boldsymbol{0} \\ -\boldsymbol{C} & \boldsymbol{0} \end{bmatrix} \begin{bmatrix} \boldsymbol{x}_e(t) \\ \boldsymbol{\xi}_e(t) \end{bmatrix} + \begin{bmatrix} \boldsymbol{B} \\ \boldsymbol{0} \end{bmatrix} \boldsymbol{u}_e(t) + \begin{bmatrix} \boldsymbol{G} \\ -\boldsymbol{P} \end{bmatrix} \boldsymbol{w}_e(t) + \begin{bmatrix} \boldsymbol{0} \\ -\mathbb{I}_1 \end{bmatrix} \boldsymbol{n}_e(t)$$

where $\dot{\boldsymbol{x}}_e(t)$ and $\dot{\boldsymbol{\xi}}_e(t)$ are state error vectors, $\boldsymbol{u}_e(t)$ is control input error vector, $\boldsymbol{w}_e(t)$ is disturbance error vector, $\boldsymbol{n}_e(t)$ is noise error vector and $\mathbb{I}_1$ is the identity matrix. $\dot{\boldsymbol{x}}_e(t)$ and $\dot{\boldsymbol{\xi}}_e(t)$ vectors are combined into $\boldsymbol{z}_e(t)$ vector. New definition of state equations with respect to state and input error vectors is:

$$\dot{\boldsymbol{z}}_e(t) = \hat{\boldsymbol{A}}\boldsymbol{z}_e(t) + \hat{\boldsymbol{B}}\boldsymbol{u}_e(t) + \hat{\boldsymbol{V}}\boldsymbol{w}_e(t) + \hat{\boldsymbol{E}}\boldsymbol{n}_e(t) \tag{3.6}$$

where state and input matrices are:

$$\hat{\boldsymbol{A}} = \begin{bmatrix} \boldsymbol{A} & \boldsymbol{0} \\ -\boldsymbol{C} & \boldsymbol{0} \end{bmatrix}_{(n+m)\times(n+m)}, \quad \hat{\boldsymbol{B}} = \begin{bmatrix} \boldsymbol{B} \\ \boldsymbol{0} \end{bmatrix}_{(n+m)\times k}$$

$$\hat{\boldsymbol{V}} = \begin{bmatrix} \boldsymbol{G} \\ -\boldsymbol{P} \end{bmatrix}_{(n+m)\times j}, \quad \hat{\boldsymbol{E}} = \begin{bmatrix} \boldsymbol{0} \\ -\mathbb{I}_1 \end{bmatrix}_{(n+m)\times l}$$

where n is the number of state variables of system and m is the number of error signal, k is the number of control input variables, j is the number of disturbance variables, l is the number of noise variables. From Eq. 3.4, optimal feedback gain matrix $\hat{\boldsymbol{K}}$ is:

$$\hat{\boldsymbol{K}} = \hat{\boldsymbol{R}}^{-}\hat{\boldsymbol{B}}^T\hat{\boldsymbol{N}} \tag{3.7}$$

where $\hat{\boldsymbol{N}}$ matrix is found by the reduced-matrix Riccati equation

$$\hat{\boldsymbol{A}}^T\hat{\boldsymbol{N}} + \hat{\boldsymbol{N}}\hat{\boldsymbol{A}} - \hat{\boldsymbol{N}}\hat{\boldsymbol{B}}\hat{\boldsymbol{R}}^{-}\hat{\boldsymbol{B}}^T\hat{\boldsymbol{N}} + \hat{\boldsymbol{Q}} = 0.$$

Consequently, the optimal control law of LQ tracking problem can be formulated by:

$$\begin{aligned} \boldsymbol{u}_e &= -\hat{\boldsymbol{K}}\boldsymbol{z}_e(t) = -\begin{bmatrix}\boldsymbol{K} & -\boldsymbol{K}_{\boldsymbol{\xi}}\end{bmatrix}\begin{bmatrix}\boldsymbol{x}_e \\ \boldsymbol{\xi}_e\end{bmatrix} \\ &\quad -\boldsymbol{K}\boldsymbol{x}_e(t) + \boldsymbol{K}_{\boldsymbol{\xi}}\boldsymbol{\xi}_e \end{aligned} \tag{3.8}$$

Determination of $\hat{\boldsymbol{Q}}$ and $\hat{\boldsymbol{R}}$ matrices by Bryson's rule [5] is a very successful method in order to minimize the quadratic cost function. According to this signal normalization method, $\hat{\boldsymbol{Q}}$ and $\hat{\boldsymbol{R}}$ matrices are:

$$\hat{\boldsymbol{Q}} = \begin{bmatrix} \frac{1}{(z_{e_1})^2_{max}} & & & \\ & \frac{1}{(z_{e_2})^2_{max}} & & \\ & & \ddots & \\ & & & \frac{1}{(z_{e_{(n+m)}})^2_{max}} \end{bmatrix}_{(n+m)\times(n+m)} \tag{3.9}$$

$$\hat{\boldsymbol{R}} = \rho \begin{bmatrix} \frac{1}{(u_{e_1})^2_{max}} & & \\ & \ddots & \\ & & \frac{1}{(u_{e_k})^2_{max}} \end{bmatrix}_{k\times k} \tag{3.10}$$

where diagonal terms $\hat{\boldsymbol{Q}}_{ii} = (z_{e_i})_{max}$, $\hat{\boldsymbol{R}}_{jj} = (u_{e_j})_{max}$ and ρ express the maximum value of the state signal, input signal and a positive constant, respectively. The desired maximum values of position and velocity error states are determined in consideration of the system performance criteria. During controller design of the gimbal system, ρ is chosen very small in order to obtain large control inputs.

After we computed the feedback gain matrices for each linearized subsystems of the coupled and decoupled gimbals, gain scheduling method is used for nonlinear system model in order to weight control signals of LQI controllers. Total control input of the nonlinear gimbal system is:

$$\boldsymbol{u}(t) = \sum_{i=1}^{k} w_{u_i}(t)\boldsymbol{u}_i(t) \tag{3.11}$$

where k is the number of subsystems, $\boldsymbol{u}_i$ is the control signal of the subsystem i and w_{u_i} is the weight constant of the control signal of the subsystem i. Weight constant

of the subsystem may be computed by:

$$w_{u_i}(t) = \begin{cases} 1 & : d_i < \varepsilon \\ \dfrac{\frac{1}{d_i(t)}}{\sum_{j=1}^{k} \frac{1}{d_j(t)}} & : d_i \geq \varepsilon \end{cases} \tag{3.12}$$

where d_i is the Euclidean distance between the instant values of state variables and equilibrium points of the subsystem i and ε is a very small positive number. It can be seen that the sum of all weight constants are equal to 1. In case of $d_i < \varepsilon$, $w_{u_i} = 1$ and weight constants of the other subsystems reach zero.

3.2.1 Global LQI Control

Mathematical model of the coupled 2-DOF gimbal contains kinematics and dynamics of both inner and outer gimbals. Coupled gimbal model has four inputs and four outputs: two input-outputs of them are related to the angular positions of each gimbal, and the other two input-outputs represents the angular velocity. In this way, to yield tracking and stabilization control problem of this MIMO system model, a linear quadratic controller, called global LQI, is designed. In global LQI control, two control signals (motor torques) are applied to coupled inner and outer gimbal. Block diagram of coupled 2-DOF gimbal with global LQI controller is shown in Figure 3.7.

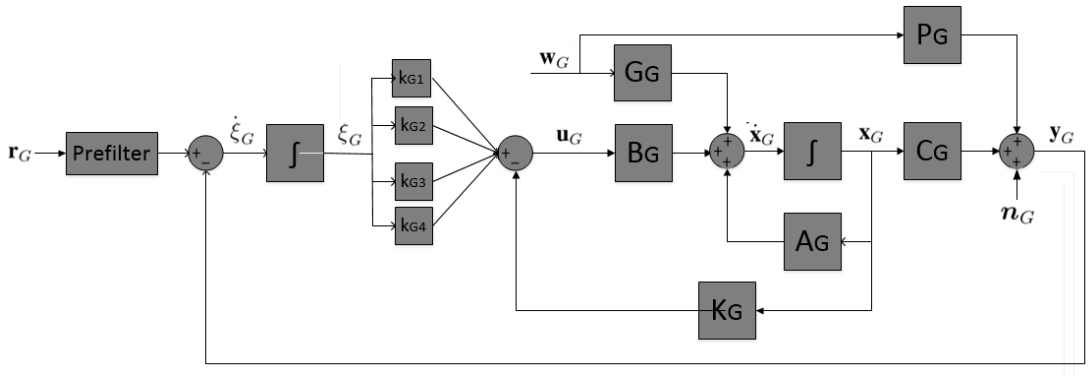

Figure 3.7: Linear quadratic integral control structure of a LTI subsystem of the coupled 2-DOF gimbal

State space representation of a LTI subsystem of the coupled gimbal, given by Eq

2.81 and 2.82, is:

$$\dot{\boldsymbol{x}}_G = \boldsymbol{A}_G\boldsymbol{x}_G + \boldsymbol{B}_G\boldsymbol{u}_G + \boldsymbol{G}_G\boldsymbol{w}_G$$

$$\boldsymbol{y}_G = \boldsymbol{C}_G\boldsymbol{x}_G + \boldsymbol{P}_G\boldsymbol{w}_G + \boldsymbol{n}_G$$

and according to the control structure, shown in Figure 3.7, error vector between references and outputs $\dot{\boldsymbol{\xi}}_G$ is:

$$\dot{\boldsymbol{\xi}}_G = \boldsymbol{r}_G - \boldsymbol{y}_G = \boldsymbol{r}_G - \boldsymbol{C}_G\boldsymbol{x}_G - \boldsymbol{P}_G\boldsymbol{w}_G - \boldsymbol{n}_G \tag{3.13}$$

where $\boldsymbol{\xi}_G$ is integral of error vector and $\boldsymbol{r}_G$ is reference vector. Output vector of integrator can be separated into four scalar variables $\boldsymbol{\xi}_G = \begin{bmatrix} \xi_{G_1} & \xi_{G_2} & \xi_{G_3} & \xi_{G_4} \end{bmatrix}^T$ and new state vector is $\boldsymbol{z}_G = \begin{bmatrix} \boldsymbol{x}_G \\ \hdashline \boldsymbol{\xi}_G \end{bmatrix}_{10\times 1}$. By using the new state vector, state equation of the coupled gimbal can be described by:

$$\dot{\boldsymbol{z}}_G = \hat{\boldsymbol{A}}_G\boldsymbol{z}_G + \hat{\boldsymbol{B}}_G\boldsymbol{u}_G + \hat{\boldsymbol{V}}_G\boldsymbol{w}_G + \hat{\boldsymbol{E}}_G\boldsymbol{n}_G \tag{3.14}$$

where state and input matrices are:

$$\hat{\boldsymbol{A}}_G = \begin{bmatrix} \boldsymbol{A}_G & \boldsymbol{0} \\ -\boldsymbol{C}_G & \boldsymbol{0} \end{bmatrix}_{10\times 10}, \quad \hat{\boldsymbol{B}}_G = \begin{bmatrix} \boldsymbol{B}_G \\ \boldsymbol{0} \end{bmatrix}_{10\times 2}, \quad \hat{\boldsymbol{V}}_G = \begin{bmatrix} \boldsymbol{G}_G \\ -\boldsymbol{P}_G \end{bmatrix}_{10\times 8}, \quad \hat{\boldsymbol{E}}_G = \begin{bmatrix} \boldsymbol{0} \\ -\mathbb{I}_1 \end{bmatrix}_{10\times 4}$$

Optimal control gain matrix of a LTI subsystem of the coupled gimbal $\hat{\boldsymbol{K}}_G$ can be described by:

$$\hat{\boldsymbol{K}}_G = \left[\begin{array}{c:c} \boldsymbol{K}_G & -\boldsymbol{K}_{\boldsymbol{\xi}_G} \end{array}\right]_{2\times 10}$$

where state feedback gain matrix $\boldsymbol{K}_G$ is:

$$\boldsymbol{K}_G = \begin{bmatrix} \boldsymbol{k}_{G_1} & \boldsymbol{k}_{G_2} & \boldsymbol{k}_{G_3} & \boldsymbol{k}_{G_4} & \boldsymbol{k}_{G_5} & \boldsymbol{k}_{G_6} \end{bmatrix}$$

and gain matrix $\boldsymbol{K}_{\boldsymbol{\xi}_G}$ is:

$$\boldsymbol{K}_{\boldsymbol{\xi}_G} = \begin{bmatrix} \boldsymbol{k}_{G_1} & \boldsymbol{k}_{G_2} & \boldsymbol{k}_{G_3} & \boldsymbol{k}_{G_4} \end{bmatrix}$$

Consequently, control input vector of the coupled gimbal can be written as:

$$\begin{aligned} \boldsymbol{u}_G = &- \hat{\boldsymbol{K}}_G\boldsymbol{z}_G \\ &- \boldsymbol{K}_G\boldsymbol{x}_G + \boldsymbol{k}_{G_1}\xi_{G_1} + \boldsymbol{k}_{G_2}\xi_{G_2} + \boldsymbol{k}_{G_3}\xi_{G_3} + \boldsymbol{k}_{G_4}\xi_{G_4} \end{aligned} \tag{3.15}$$

Controller design matrices $\hat{\boldsymbol{Q}}_G$ and $\hat{\boldsymbol{R}}_G$ are defined by Eq. 3.9 and Eq. 3.10, respectively. The maximum values of the system state and control input variables are given in Tables 2.5, 2.6.

$$\hat{\boldsymbol{Q}}_G = \begin{bmatrix} \frac{1}{(z_{G_{e_1}})^2_{max}} & & & \\ & \frac{1}{(z_{G_{e_2}})^2_{max}} & & \\ & & \ddots & \\ & & & \frac{1}{(z_{G_{e10}})^2_{max}} \end{bmatrix}_{10\times 10}$$

$$\hat{\boldsymbol{R}}_G = \rho_G \begin{bmatrix} \frac{1}{(u_{G_{e_1}})^2_{max}} & \\ & \frac{1}{(u_{G_{e_2}})^2_{max}} \end{bmatrix}_{2\times 2}$$

Maximum values of the position error states $z_{G_{e_7}\,max}$ and $z_{G_{e_8}\,max}$ are selected 10% of $z_{G_{e_1}\,max}$ and $z_{G_{e_2}\,max}$. In addition, maximum values of the velocity error states $z_{G_{e_9}\,max}$ and $z_{G_{e10}\,max}$ are the same with $z_{G_{e_3}\,max}$ and $z_{G_{e_4}\,max}$. Lastly, ρ_G is tuned manually in order to get the best performance.

From Eq. 3.11, the sum of the control inputs of all subsystems is:

$$\boldsymbol{u}_G = w_{u_1}\boldsymbol{u}_{G_1} + w_{u_2}\boldsymbol{u}_{G_2}$$

Angular position commands are applied as step function references within the pre-filters which are at first order low-pass filters. On the other hand, angular velocity commands are zero to stabilize the system. When we implemented global LQI control in the nonlinear gimbal system, performances of the global LQI controller for different position commands are given in Table 3.11. It can be seen that global LQI controller satisfies the desired tracking performances for the outer gimbal when cut-off frequency of the pre-filter is 1 Hz. Likewise if the cut-off frequency of the pre-filter is increased for the outer gimbal, global LQI controller is unable to control the system for position commands higher than 2.0 rad. Moreover, inner gimbal has the best system performances by means of 10 Hz cut-off frequency of the pre-filter. System responses and motor torques of the nonlinear coupled 2-DOF gimbal with global LQI control are shown in Figure 3.8 and 3.9.

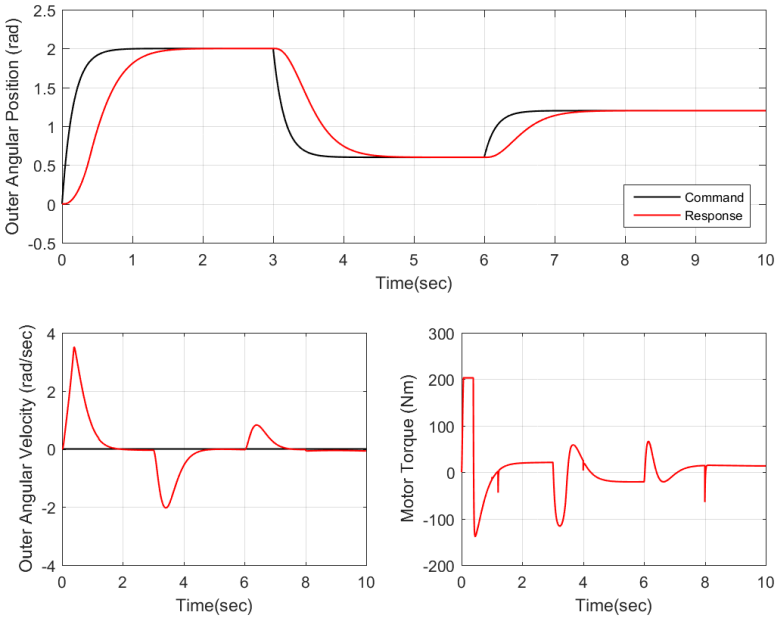

Figure 3.8: System responses and motor torque of the outer gimbal with global LQI control

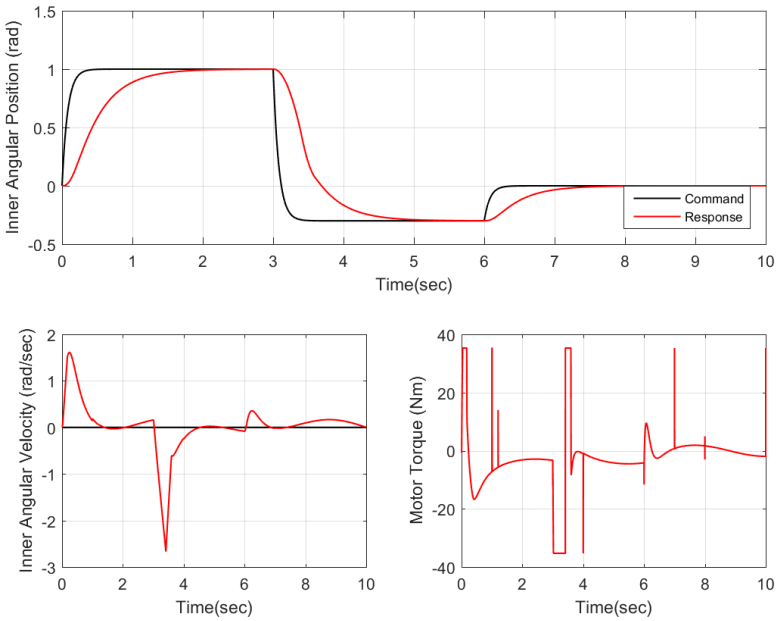

Figure 3.9: System responses and motor torque of the inner gimbal with global LQI control

Table3.11: Position performances of the gimbals with global LQI control for different position commands

Gimbal	Reference	Pre-filter cutoff frequency	Overshoot(%)	Settling time(sec)
Outer gimbal	0.5 rad	1 Hz	0.0	1.3
	1.0 rad		0.0	1.3
	1.5 rad		0.0	1.3
	2.0 rad		0.0	1.3
	2.5 rad		0.0	1.3
	3.0 rad		9.6	1.9
	0.5 rad	2 Hz	0.0	1.2
	1.0 rad		0.0	1.2
	1.5 rad		0.0	1.2
	2.0 rad		25.9	1.9
	2.5 rad		Unstable	Unstable
	3.0 rad		Unstable	Unstable
	0.5 rad	10 Hz	0.0	1.1
	1.0 rad		0.0	1.1
	1.5 rad		0.0	1.1
	2.0 rad		23.5	1.3
	2.5 rad		Unstable	Unstable
	3.0 rad		Unstable	Unstable
Inner gimbal	0.5 rad	1 Hz	0.0	1.7
	1.0 rad		0.0	1.7
	0.5 rad	2 Hz	0.0	1.6
	1.0 rad		0.0	1.6
	0.5 rad	10 Hz	0.0	1.5
	1.0 rad		0.0	1.5

3.2.2 Local LQI Control

In control of the decoupled inner and outer gimbals, local linear quadratic integral (LQI) method is implemented. Different from global LQI control, there are two separate compensators to control decoupled inner and outer gimbal models having two inputs and two outputs. Control structures of the decoupled gimbals with local LQI controllers, gain-scheduling algorithm and LTI subsystems of the gimbals are examined in this section. Then quadratic controller matrices and cut-off frequencies of the pre-filters are tuned to satisfy system performance requirements. Similar to the global LQI control method, angular position commands are applied as step function references within the pre-filters and angular velocity commands are zero.

3.2.2.1 Inner Gimbal

Linear quadratic integral control structure of a LTI subsystem of the decoupled inner gimbal is given in Figure 3.10.

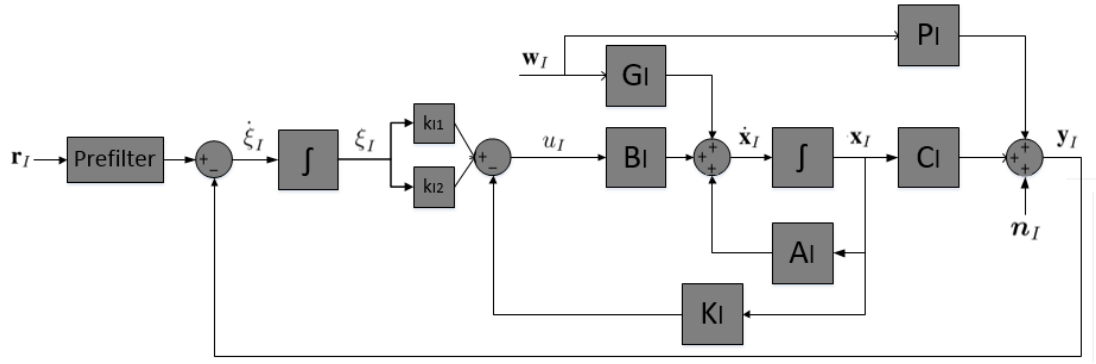

Figure 3.10: Block diagram of a decoupled inner gimbal control subsystem model

State space representation of linearized decoupled inner gimbal, given by Eq 2.83 and 2.84, is:

$$\dot{\boldsymbol{x}}_I = \boldsymbol{A}_I\boldsymbol{x}_I + \boldsymbol{B}_I u_I + \boldsymbol{G}_I\boldsymbol{w}_I$$

$$\boldsymbol{y}_I = \boldsymbol{C}_I\boldsymbol{x}_I + \boldsymbol{P}_I\boldsymbol{w}_I + \boldsymbol{n}_I$$

Error vector between references and outputs $\dot{\boldsymbol{\xi}}_I$ is:

$$\dot{\boldsymbol{\xi}}_I = \boldsymbol{r}_I - \boldsymbol{y}_I = \boldsymbol{r}_I - \boldsymbol{C}_I\boldsymbol{x}_I - \boldsymbol{P}_I\boldsymbol{w}_I - \boldsymbol{n}_I \tag{3.16}$$

where $\boldsymbol{\xi}_I$ is integral of error vector and $\boldsymbol{r}_I$ is reference vector. Output vector of integrator can be separated into two scalar variables $\boldsymbol{\xi}_I = \begin{bmatrix}\xi_{I_1} & \xi_{I_2}\end{bmatrix}^T$ and new state vector is: $\boldsymbol{z}_I = \begin{bmatrix}\boldsymbol{x}_I \\ \hdashline \boldsymbol{\xi}_I\end{bmatrix}_{5\times1}$. Hence new state equation of inner gimbal is:

$$\dot{\boldsymbol{z}}_I = \hat{\boldsymbol{A}}_I\boldsymbol{z}_I + \hat{\boldsymbol{B}}_I u_I + \hat{\boldsymbol{V}}_I\boldsymbol{w}_I + \hat{\boldsymbol{E}}_I\boldsymbol{n}_I \tag{3.17}$$

where state and input matrices are:

$$\hat{\boldsymbol{A}}_I = \begin{bmatrix}\boldsymbol{A}_I & \boldsymbol{0} \\ -\boldsymbol{C}_I & \boldsymbol{0}\end{bmatrix}_{5\times5}, \quad \hat{\boldsymbol{B}}_I = \begin{bmatrix}\boldsymbol{B}_I \\ \boldsymbol{0}\end{bmatrix}_{5\times1}, \quad \hat{\boldsymbol{V}}_I = \begin{bmatrix}\boldsymbol{G}_I \\ -\boldsymbol{P}_I\end{bmatrix}_{5\times8}, \quad \hat{\boldsymbol{E}}_G = \begin{bmatrix}\boldsymbol{0} \\ -\mathbb{I}_1\end{bmatrix}_{5\times2}$$

Optimal control gain matrix of decoupled LTI inner gimbal system $\hat{\boldsymbol{K}}_I$ is:

$$\hat{\boldsymbol{K}}_I = \left[\begin{array}{c:c} \boldsymbol{K}_I & -\boldsymbol{K}_{\boldsymbol{\xi}_I} \end{array} \right]_{1\times 5}$$

where state feedback gain matrix is $\boldsymbol{K}_I = \begin{bmatrix} k_{I_1} & k_{I_2} & k_{I_3} \end{bmatrix}$ and error gain matrix is $\boldsymbol{K}_{\boldsymbol{\xi}_I} = \begin{bmatrix} k_{I_1} & k_{I_2} \end{bmatrix}$. Thus control input scalar of inner gimbal is:

$$\begin{aligned} u_I = &- \hat{\boldsymbol{K}}_I \boldsymbol{z}_I \\ &- \boldsymbol{K}_I \boldsymbol{x}_I + k_{I_1}\xi_{I_1} + k_{I_2}\xi_{I_2} \end{aligned} \tag{3.18}$$

Terms of inner gimbal local LQI controller, $\hat{\boldsymbol{Q}}_I$ and $\hat{R}_I$, are:

$$\hat{\boldsymbol{Q}}_I = \begin{bmatrix} \frac{1}{(z_{I_{e_1}})^2_{max}} & & & \\ & \frac{1}{(z_{I_{e_2}})^2_{max}} & & \\ & & \ddots & \\ & & & \frac{1}{(z_{I_{e_5}})^2_{max}} \end{bmatrix}_{5\times 5}$$

$$\hat{R}_I = \rho_I \frac{1}{(u_I)^2_{max}}$$

where parameter values of decoupled inner gimbal and coupled gimbal are the same.

By means of gain scheduling, sum of control inputs of all inner subsystems is:

$$u_I = w_{u_1} u_{I_1} + w_{u_2} u_{I_2}$$

System performances of the coupled inner gimbal with local LQI controller for different position commands are given in Table 3.12. Results of this analysis show that coupled inner gimbal has the best performance with local LQI control if cut-off frequency of the pre-filter is chosen as 2 Hz. Motor torque, angular position and velocity responses of the coupled nonlinear inner gimbal with local LQI control is shown in Figure 3.11.

Table3.12: Position performances of the coupled nonlinear inner gimbal with local LQI control for different position commands

Reference	Pre-filter cutoff frequency	Overshoot(%)	Settling time(sec)
0.5 rad	1 Hz	0.0	2.0
1.0 rad		0.0	2.0
0.5 rad	2 Hz	0.0	1.8
1.0 rad		0.0	1.8
0.5 rad	10 Hz	0.0	1.8
1.0 rad		2.9	2.2

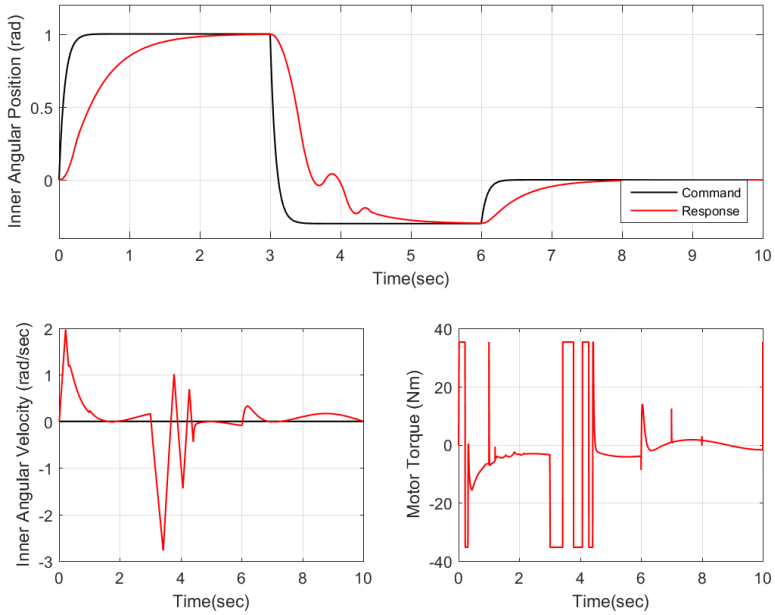

Figure 3.11: System responses and motor torque of the coupled nonlinear inner gimbal with local LQI control

3.2.2.2 Outer Gimbal

Linear quadratic integral control structure of a LTI subsystem of the decoupled outer gimbal is given in Figure 3.12. State space representation of linearized outer gimbal, given by Eq 2.85 and 2.86, is:

$$\dot{\boldsymbol{x}}_O = \boldsymbol{A}_O\boldsymbol{x}_O + \boldsymbol{B}_O u_O + \boldsymbol{G}_O\boldsymbol{w}_O$$

$$\boldsymbol{y}_O = \boldsymbol{C}_O\boldsymbol{x}_O + \boldsymbol{P}_O\boldsymbol{w}_O + \boldsymbol{n}_O$$

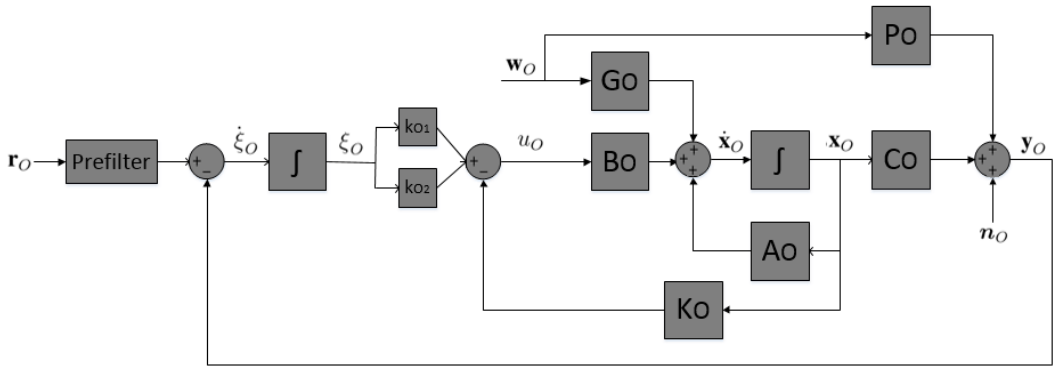

Figure 3.12: Block diagram of a decoupled outer gimbal control subsystem model

Error vector between references and outputs $\dot{\boldsymbol{\xi}}_O$ is:

$$\dot{\boldsymbol{\xi}}_O = \boldsymbol{r}_O - \boldsymbol{y}_O = \boldsymbol{r}_O - \boldsymbol{C}_O\boldsymbol{x}_O - \boldsymbol{P}_O\boldsymbol{w}_O - \boldsymbol{n}_O \tag{3.19}$$

where $\boldsymbol{\xi}_O$ is integral of error vector and $\boldsymbol{r}_O$ is reference vector. Output vector of integrator is $\boldsymbol{\xi}_O = \begin{bmatrix} \xi_{O_1} & \xi_{O_2} \end{bmatrix}^T$ and new state vector is $\boldsymbol{z}_O = \begin{bmatrix} \boldsymbol{x}_O \\ \hdashline \boldsymbol{\xi}_O \end{bmatrix}_{5\times 1}$. New state equation of the decoupled outer gimbal can be described by:

$$\dot{\boldsymbol{z}}_O = \hat{\boldsymbol{A}}_O\boldsymbol{z}_O + \hat{\boldsymbol{B}}_O u_O + \hat{\boldsymbol{V}}_O\boldsymbol{w}_O + + \hat{\boldsymbol{E}}_O\boldsymbol{n}_O \tag{3.20}$$

where state and input matrices are:

$$\hat{\boldsymbol{A}}_O = \begin{bmatrix} \boldsymbol{A}_O & \boldsymbol{0} \\ -\boldsymbol{C}_O & \boldsymbol{0} \end{bmatrix}_{5\times 5}, \quad \hat{\boldsymbol{B}}_O = \begin{bmatrix} \boldsymbol{B}_O \\ \boldsymbol{0} \end{bmatrix}_{5\times 1}, \quad \hat{\boldsymbol{V}}_O = \begin{bmatrix} \boldsymbol{G}_O \\ -\boldsymbol{P}_O \end{bmatrix}_{5\times 8}, \quad \hat{\boldsymbol{E}}_O = \begin{bmatrix} \boldsymbol{0} \\ -\mathbb{I}_1 \end{bmatrix}_{5\times 2}$$

and optimal control gain matrix of a LTI subsystems of the decoupled outer gimbal is:

$$\hat{\boldsymbol{K}}_O = \left[\begin{array}{ccc:cc} k_{O_1} & k_{O_2} & k_{O_3} & -k_{O_1} & -k_{O_2} \end{array}\right]_{1\times 5}$$

Thus control input scalar of the outer gimbal is:

$$\begin{aligned} u_O = &- \hat{\boldsymbol{K}}_O\boldsymbol{z}_O \\ &- \boldsymbol{K}_O\boldsymbol{x}_O + k_{O_1}\xi_{O_1} + k_{O_2}\xi_{O_2} \end{aligned} \tag{3.21}$$

Controller matrices of the local LQI controller for the decoupled outer gimbal, $\hat{\boldsymbol{Q}}_O$

and $\hat{R}_O$, are given below. Values of parameters of the decoupled outer and coupled gimbals are the same.

$$\hat{\boldsymbol{Q}}_O = \begin{bmatrix} \frac{1}{(z_{O_{e_1}})^2_{max}} & & & & \\ & \frac{1}{(z_{O_{e_2}})^2_{max}} & & & \\ & & \ddots & & \\ & & & \frac{1}{(z_{O_{e_5}})^2_{max}} \end{bmatrix}_{5\times 5}$$

$$\hat{R}_O = \rho_O \frac{1}{(u_O)^2_{max}}$$

Decoupled outer gimbal model consists of three subsystems. By means of gain scheduling, sum of control inputs of all outer subsystems is:

$$u_O = w_{u_1} u_{O_1} + w_{u_2} u_{O_2} + w_{u_3} u_{O_3}$$

System performances of the coupled nonlinear outer gimbal with local LQI controller for different position commands are given in Table 3.13.

Table3.13: Position performances of the coupled nonlinear outer gimbal with local LQI control for different position commands

Reference	**Pre-filter cutoff frequency**	**Overshoot(%)**	**Settling time(sec)**
0.5 rad	1 Hz	0.0	2.0
1.0 rad		0.0	2.0
1.5 rad		0.0	2.0
2.0 rad		1.1	2.8
2.5 rad		Unstable	Unstable
3.0 rad		Unstable	Unstable
0.5 rad	2 Hz	0.0	1.9
1.0 rad		2.1	1.9
1.5 rad		Unstable	Unstable
2.0 rad		Unstable	Unstable
2.5 rad		Unstable	Unstable
3.0 rad		Unstable	Unstable
0.5 rad	10 Hz	0.0	1.8
1.0 rad		11.8	1.8
1.5 rad		Unstable	Unstable
2.0 rad		Unstable	Unstable
2.5 rad		Unstable	Unstable
3.0 rad		Unstable	Unstable

We can say that the coupled outer gimbal goes to instability when position command is higher than 2.0 rad for all pre-filters. This controller satisfies the most desired performance conditions for the coupled outer gimbal if cut-off frequency of the pre-filter is 1 Hz. Motor torque and system responses of the coupled nonlinear outer gimbal with local LQI control are shown in Figure 3.13.

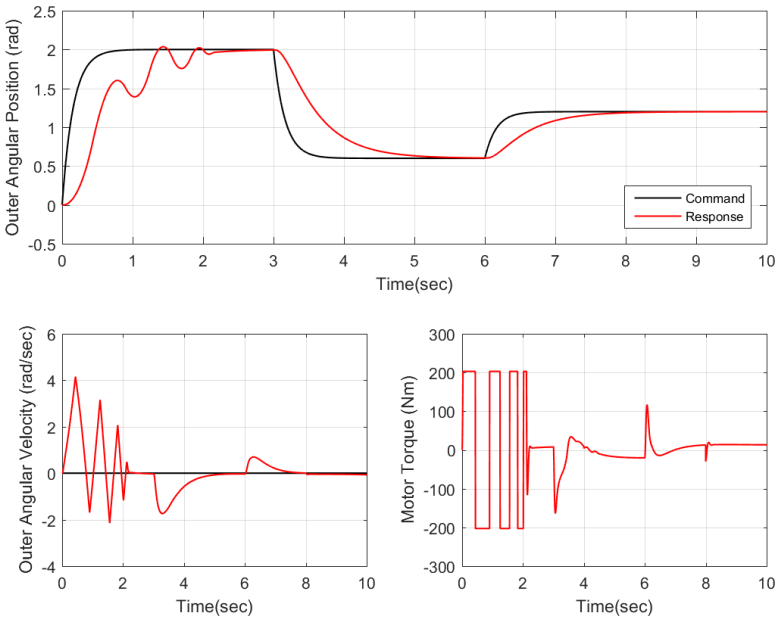

Figure 3.13: System responses and motor torque of the coupled nonlinear outer gimbal with local LQI control

3.3 Performance Comparison of Controllers

Before construction study of the virtual world, we have to choose the best performed control method for nonlinear 2-DOF gimbal in order to stabilize the system and track the target. During controller design study, parameters of the cascade PI controller are tuned with the nonlinear system directly. On the other hand, LQI controllers are implemented in the nonlinear system after their gain matrices are computed for the linear gimbal models. In this section, we have examined performances of all control methods for nonlinear 2-DOF gimbal model.

First performance comparison of the controllers is about their tracking and stabilization performances when different position commands are applied to the nonlinear 2-DOF gimbal model. Second comparison is about some performance measures related to the position and rate error signals such as the integrated square error (ISE), the integrated absolute value of the error (IAE) and the integrated time-weighted absolute error (ITAE). These performance measures are formulated by:

$$ISE = \int_0^\infty e(t)^2 dt \tag{3.22}$$

$$IAE = \int_0^\infty |e(t)| dt \tag{3.23}$$

$$ITAE = \int_0^\infty t|e(t)| dt \tag{3.24}$$

where $e(t)$ represents error signal. In this analysis, a controller having the lowest measure value of a criterion has the best performance in regard to the criterion.

3.3.1 Global and Local LQI Control

As it is explained in the previous sections, both global and local LQI controllers are designed for the linear subsystems of coupled and decoupled gimbals. Although local LQI controllers are designed for decoupled linear inner and outer gimbal subsystems, these models are actually coupled in the linearization procedure.

Position performances of inner gimbal with global and local LQI control methods are given in Table 3.11, 3.12. Analysis of results show that both controllers guarantee the stability of the system and satisfy the desired conditions. In addition, we can say that global LQI controller with 10 Hz cut-off frequency of the pre-filter has the best performance. On the purpose of examining the system behaviors in more detail, system responses and motor torque of the system are simulated for both controllers in Figure 3.14. As a result, target tracking and elimination of disturbances abilities of the global LQI position response is better than local LQI controller. Moreover, although continuous motor torques of both controllers are about the same, local LQI frequently reaches the peak motor torque values.

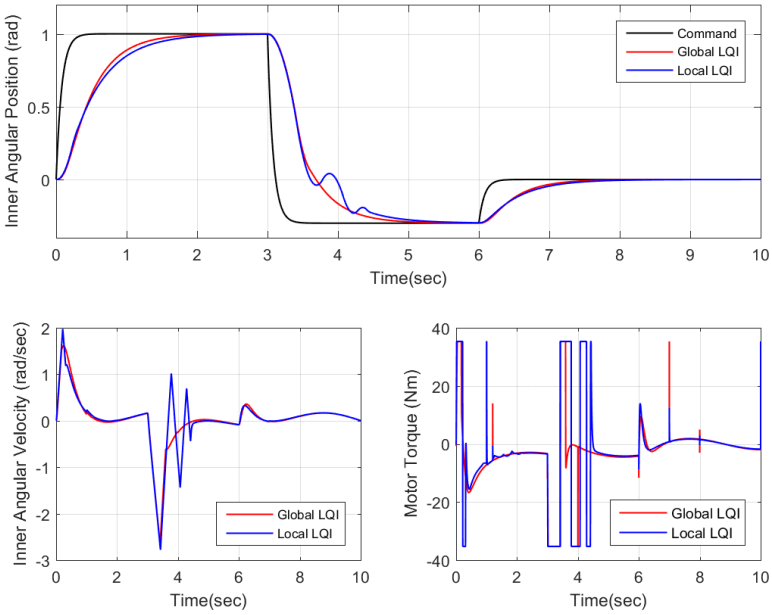

Figure 3.14: System responses and motor torques of inner gimbal with global and local LQI control methods

For the outer gimbal control, performance results of global and local LQI controllers are given in Table 3.11, 3.13, respectively. These tables shows that global LQI controller with 1 Hz cut-off frequency of the pre-filter is only successful method in all desired conditions. Likewise the best performed local LQI controller with 1 Hz cut-off frequency of the pre-filter is unstable when position command higher than 2.0 radians is applied to the outer gimbal. Figure 3.15 shows that global LQI has no overshoot and less settling time than local LQI controller. Further, global LQI eliminates disturbances faster than local LQI. Lastly, continuous motor torque values of both controllers are about the same even though local LQI frequently reaches the peak motor torques.

In addition to these examinations, comparison of global and local LQI controllers with respect to ISE, IAE and ITAE performance measures is given above. Table 3.14 shows that all of performance measures of the global LQI controller are lower than local LQI's. In conclusion, success of the global LQI controller in not only tracking and stabilization control problems but also performance measures is higher than local LQI controllers for both gimbals.

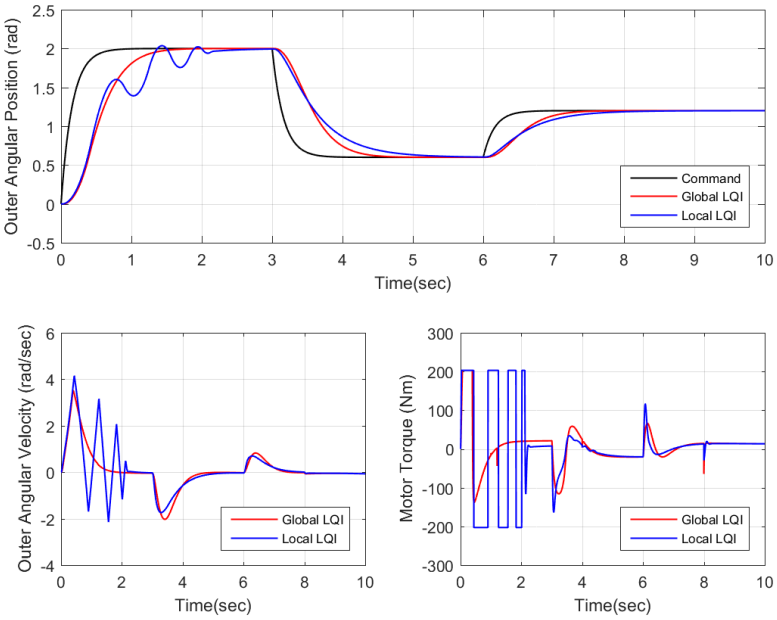

Figure 3.15: System responses and motor torques of outer gimbal with global and local LQI control methods

Table3.14: Performance comparison of global and local LQI control with respect to ISE, IAE and ITAE measures

Gimbal	Controller	Command	ISE	IAE	ITAE
Outer gimbal	Global LQI	Position	0.188	0.413	0.188
		Rate	1.03	1.03	0.62
	Local LQI	Position	0.290	0.536	0.299
		Rate	3.99	2.34	2.02
Inner gimbal	Global LQI	Position	0.261	0.454	0.180
		Rate	1.27	0.81	0.27
	Local LQI	Position	0.272	0.538	0.346
		Rate	3.02	2.21	2.16

3.3.2 Global LQI and Cascade PI Control

According to the performance results of the inner gimbal with cascade PI, given in Table 3.5, and global LQI, given in Table 3.11, global LQI control has no overshoot and its settling time is less than 1.8 seconds whereas cascade PI satisfies the desired conditions only if cut-off frequency of the pre-filter is 1 Hz. In Figure 3.16, system responses and motor torques of the inner gimbal with both controllers are shown. When global LQI controller with 10 Hz cut-off frequency of the pre-filter and cascade

PI controller with 1 Hz cut-off frequency of the pre-filter are compared, cascade PI has overshoot for position commands higher than 0.5 rad although settling time and rise time of the cascade PI are lower than global LQI. Furthermore angular velocities of these methods reach to the zero velocity about the same time.

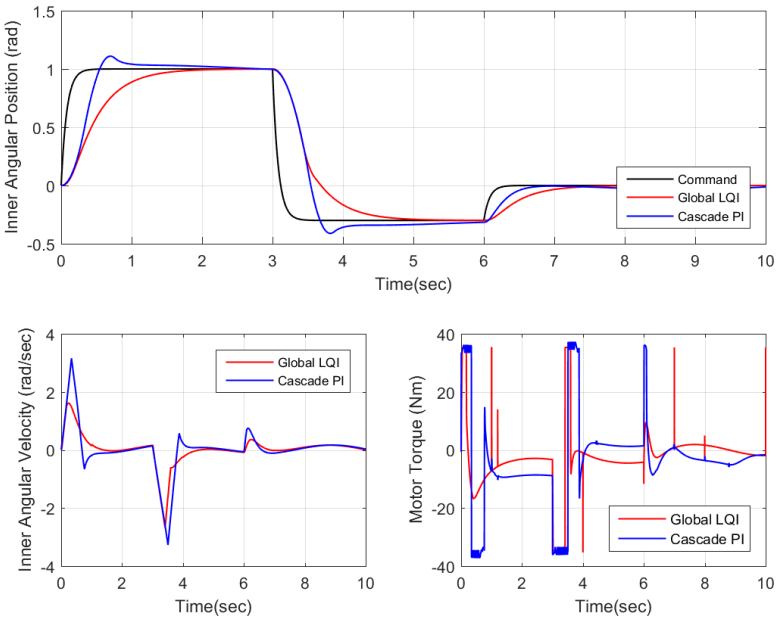

Figure 3.16: System responses and motor torques of inner gimbal with global LQI and cascade PI control methods

Position performances of outer gimbal with cascade PI and global LQI control methods are given in Table 3.10, 3.11, respectively. It is clearly seen that, global LQI controller with 1 Hz cut-ff frequency of the pre-filter is only compensator satisfying the desired conditions for all position commands. When we applied position commands higher than 1.0 rad to the outer gimbal with cascade PI, position outputs of gimbal have overshoot higher than %10 and their settling times rise. Position outputs, velocity outputs and motor torques of the outer gimbal with both controllers are shown in Figure 3.14.

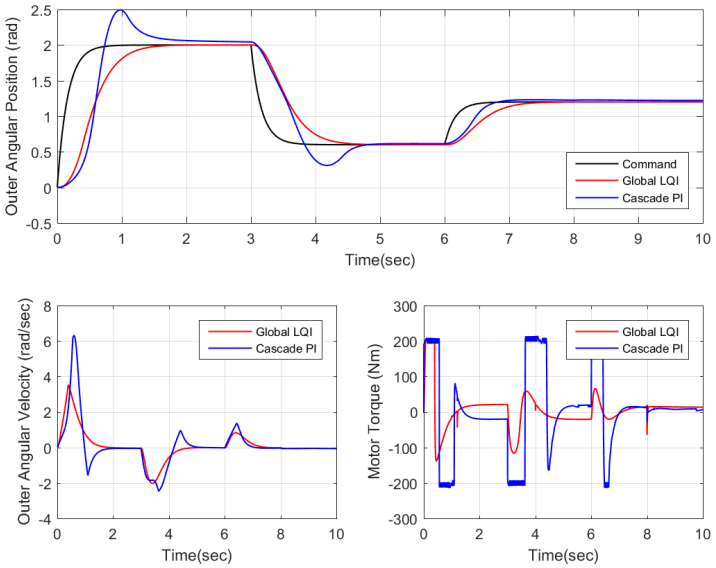

Figure 3.17: System responses and motor torques of the outer gimbal with global LQI and cascade PI control methods

Table3.15: Performance comparison of global LQI and cascade PI control with respect to ISE, IAE and ITAE measures

Gimbal	**Controller**	**Command**	**ISE**	**IAE**	**ITAE**
Outer gimbal	Global LQI	Position	0.773	0.824	0.369
		Rate	4.29	2.03	1.19
	Cascade PI	Position	1.02	1.05	0.67
		Rate	18.8	4.54	2.83
Inner gimbal	Global LQI	Position	0.259	0.454	0.182
		Rate	1.29	0.957	0.518
	Cascade PI	Position	0.08	0.26	0.16
		Rate	1.88	1.08	0.627

Comparison of the global LQI and cascade PI controllers with respect to the performance criteria is given in Table 3.15. Outer gimbal position, outer gimbal velocity and inner gimbal velocity performances of the global LQI controller is better than cascade PI controller. In spite of that cascade PI is seen more successful than global LQI for the inner gimbal.

3.3.3 Conclusion

In this chapter, cascade PI and linear quadratic integral control methods are compared between each other. Decoupling of the inner and outer gimbals is examined in Section 2.7. Result of this examination shows that our decoupling approaches are unable to respond with the same coupled 2-DOF gimbal. Although we can not obtain realistic decoupled models via these approaches, designed local LQI controllers satisfies the desired conditions for some position commands. When we compared global and local LQI controllers, it is clearly seen that stabilization and tracking performances of the global LQI is more successful than local LQI's. If global LQI control method is implemented in the nonlinear system model the 2-DOF gimbal with 10 Hz cut-off frequency of the prefilter for inner gimbal and 1 Hz cut-off frequency of the pre-filter for outer gimbal, outputs of both gimbals satisfy the desired conditions for all position commands.

When we compare cascade PI and global LQI control methods, both approaches are very successful and compatible in order to use in system simulator. Global LQI control has the lowest overshoot and settling time for step position commands and it reaches to zero velocity in a short time. Further, global LQI is the most successful controller with respect to the performance measures except position response of the inner gimbal. Even though global LQI controller overcomes target tracking and stabilization requirements, it has slow rise time so this control method is unable to give quick responses against instant changes of the position commands. Unlike global LQI, cascade PI controllers have the fastest position responses and their rise times are rather short. In addition, cascade PI controllers can handle disturbances in a short time and position performance of them are in desired conditions for lower position commands. In flight scenarios of the target for this study, position commands are lower than 0.5 rad and rise time, settling time and elimination of disturbances contain more importance. As a result, cascade PI control with pre-filters providing the best performance is preferred to be implemented in control system for system simulator although the other controllers are very successful.

CHAPTER 4

TARGET TRACKING AND ANIMATION

The main aim of building a virtual reality world is realization of the system scenarios when a plane is tracked by the gimbal looking from a distance and platform motion is carried out in the gimbal base. Structure of simulation framework is shown in Figure 4.1.

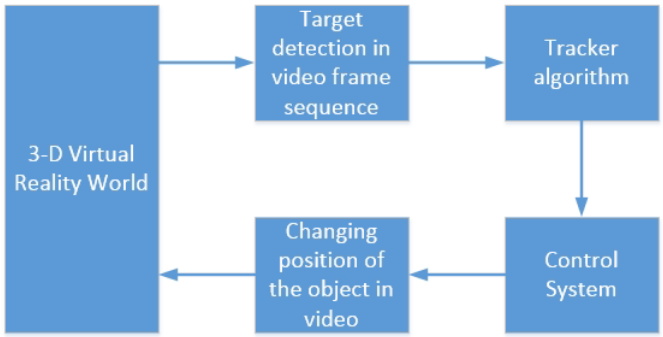

Figure 4.1: Structure of simulation framework

Video output of the VRML sink produces images in sequence and each image is used by target tracking algorithm with the discrete Kalman filter [9]. Tracking algorithm computes angular position commands for the gimbal and later position responses of the system is converted to the orientation of camera view in the VRML coordinate system. Simulink blocks of control system, tracker algorithm, VRML sinks and the other functions are shown in Figure B.6.

4.1 Construction of the Virtual World

Virtual Reality Modeling Language (VRML) is a file format, which is saved with .wrl file extension, for visualizing interactive 3-D virtual worlds. On the purpose of creating and modifying the virtual worlds, VREALM Builder [32] produced by MATLAB is used in this study. The objects in a virtual world can be created by MPEG images, MIDI data, 3-D aggregates and their interactions [45]. Libraries of VREALM Builder give lots of options for inserting navigation screens, backgrounds and various objects. In order to simulate the sky and ground in the virtual worlds, at background objects defining a color backdrop can be implemented. In addition, some features of the objects such as scale, translational position and orientation can be modified both statically and dynamically. In this study, scale and orientation of all objects are described as static. On the other hand, translational position of the plane is changed dynamically in order to move the target.

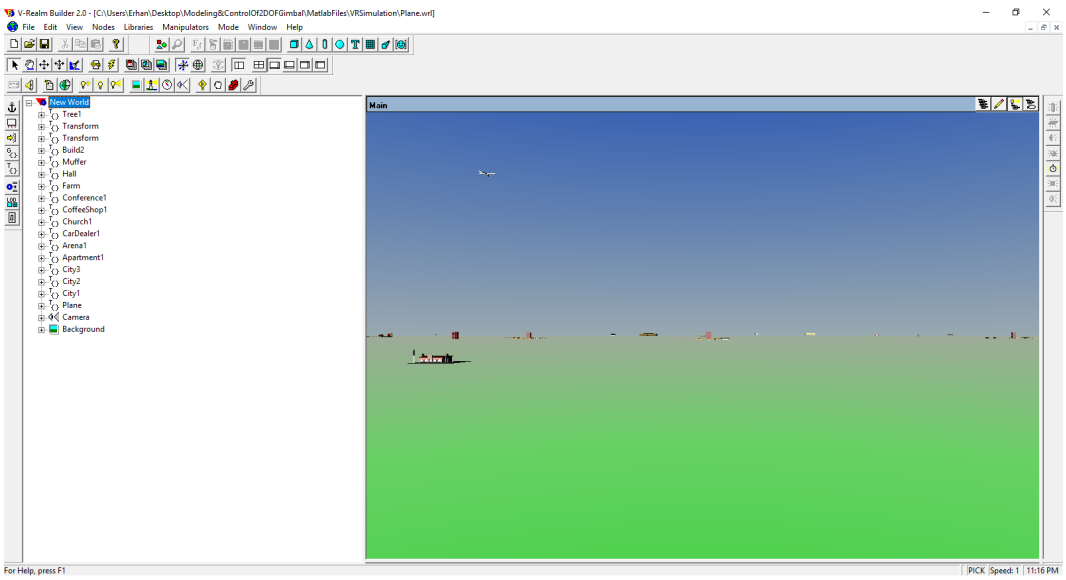

Figure 4.2: VRealm Builder

VRML coordinate system on MATLAB/Simulink (Figure 4.3) and the earth coordinate system are identical. Objects are placed farther or nearer from the point of view on the z axis and altitude of objects are pointed on the y axis. In addition, rotation angles are described by the right hand rule. Units of all translation distances and an-

gular measurements are in meters and radians, respectively [32].

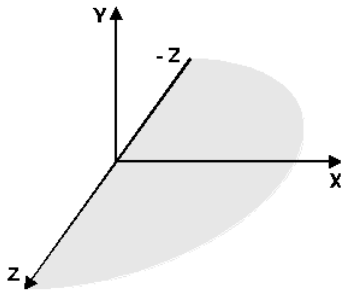

Figure 4.3: VRML coordinate system on MATLAB/Simulink [32]

Viewpoints are used to display the objects from different position and orientation. There are two types of viewpoint options: Static viewpoint is independent from the objects and its position and orientation remains the same during simulation whereas dynamic viewpoint can move at both, tranlationally and rotationally [32]. In this study, camera view must be the dynamic viewpoint on the purpose of orienting the gimbal to the target.

Target detection is an image processing study that requires an image sequence to compute target velocity between video frames. Video outputs of the VR sink blocks are able to produce images in sequence from the our virtual world having 1080-by-800 pixel resolution and 50 Hz frame rate. In VR sink block, translational position of the plane and orientation of the camera view are described dynamically, diversely, position of the camera is fixed.

Initial distance between the virtual world and the camera view, camera orientation and field of view (FOV) can be determined by viewpoints. The gimbal is located away at constant 5000 meters from the plane along the +z axis and initial position of the center of the camera view is (0, 0) on the horizontal and vertical axes. The plane flies along the horizontal and vertical axes of the virtual world and initial position of the plane is (x, y, z) = (-2000, 1500, 0) in meters. The other objects such as apartments, houses, markets etc. are located arbitrarily. Appearance of the virtual world from the camera is shown in Figure 4.4.

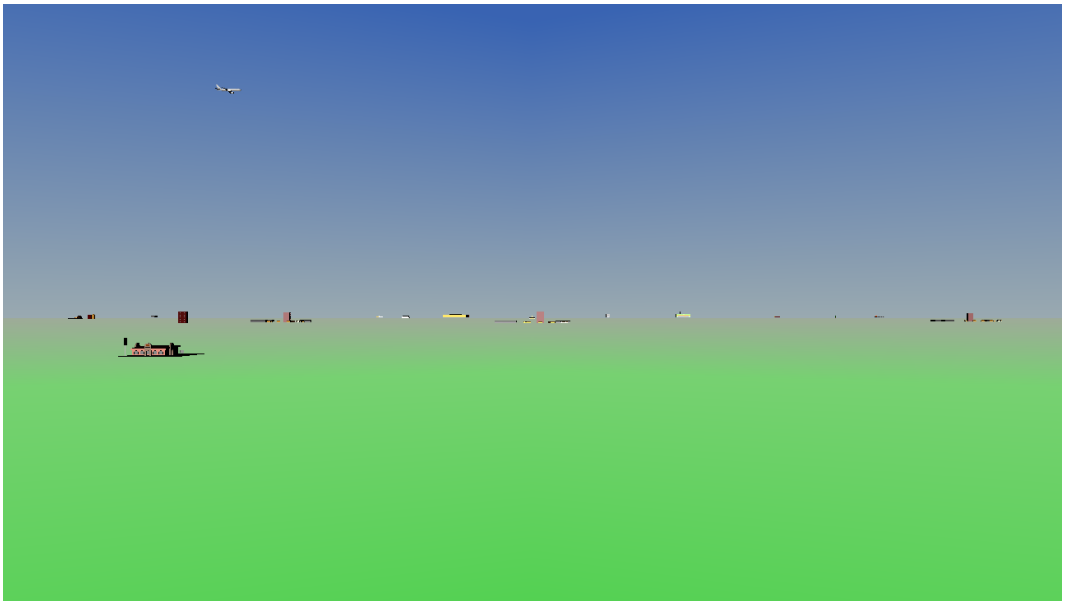

Figure 4.4: Appearance of the virtual world from the camera

4.2 Tracking of an Object with the Discrete Kalman Filter

Target tracking technology is very important for engineering applications of computer vision such as military guidance, navigation and surveillance. It focuses on following the target, also called tracking, in an image sequence [23]. A tracking algorithm with the discrete Kalman filter was designed with the intend of computing position and velocity of the plane. Input of the algorithm is a sequence of images which are produced by the virtual reality sink block. After that, the target is segmented from the image by applying image processing methods and then position of the target is computed in the image [11]. Hence the state of the system, expressed by $\boldsymbol{x}_k$, is taken as the horizontal and vertical components of position and velocity of the target at the instant k. Lastly, position of the target in pixel is projected onto the virtual world with respect to the translational position in meters.

The Kalman filter which looks for the target in a search window, centered in the predicted value of the filter, is a very efficient method for tracking [11]. In this study, it uses the measurement which is the real position of the target and estimates the velocity and position of the target. Besides, the constant velocity model is used for the

motion model of the Kalman filter. The state and the output equations are formulated by:

$$\boldsymbol{x}_{k+1} = \boldsymbol{A}\boldsymbol{x}_k + \boldsymbol{w}_k \tag{4.1}$$

$$\boldsymbol{y}_k = \boldsymbol{C}\boldsymbol{x}_k + \boldsymbol{v}_k \tag{4.2}$$

where $\boldsymbol{x}_k$ is the state vector, $\boldsymbol{A}$ is the state matrix, $\boldsymbol{w}_k \sim N(0, \boldsymbol{Q})$ is the process noise, $\boldsymbol{y}_k$ is the measurement vector, $\boldsymbol{C}$ is the measurement matrix and $\boldsymbol{v}_k \sim N(0, \boldsymbol{R})$ is the measurement noise. When a constant velocity model is implemented, the system matrices given in Eq. 4.1 and Eq. 4.2 are:

$$\boldsymbol{A} = \begin{bmatrix} 1 & 0 & 0.02 & 0 \\ 0 & 1 & 0 & 0.02 \\ 0 & 0 & 1 & 0 \\ 0 & 0 & 0 & 1 \end{bmatrix}, \qquad \boldsymbol{C} = \begin{bmatrix} 1 & 0 & 0 & 0 \\ 0 & 1 & 0 & 0 \end{bmatrix} \tag{4.3}$$

Kalman filter starts with initial covariance and state values. It predicts the state and covariance based on the equations given in 4.4 and 4.5.

$$\boldsymbol{x}_{k+1|k} = \boldsymbol{A}_k \boldsymbol{x}_{k|k} \tag{4.4}$$

$$\boldsymbol{P}_{k+1|k} = \boldsymbol{A}_k \boldsymbol{P}_{k|k} {\boldsymbol{A}_k}^T + \boldsymbol{Q}_k \tag{4.5}$$

In our cases, the initial state estimation error covariance matrix is:

$$\begin{bmatrix} 100 & 0 & 0 & 0 \\ 0 & 100 & 0 & 0 \\ 0 & 0 & 10000 & 0 \\ 0 & 0 & 0 & 10000 \end{bmatrix}$$

and the process covariance matrix is:

$$\boldsymbol{Q} = \begin{bmatrix} 25 & 0 & 0 & 0 \\ 0 & 25 & 0 & 0 \\ 0 & 0 & 10 & 0 \\ 0 & 0 & 0 & 10 \end{bmatrix}$$

Then, Kalman filter uses the measurement to update the filter based on the equations given in 4.6 and 4.7 [9].

$$\boldsymbol{x}_{k|k} = \boldsymbol{x}_{k|k-1} + \boldsymbol{K}_k(\boldsymbol{y}_k - \boldsymbol{C}\boldsymbol{x}_{k|k-1}) \tag{4.6}$$

$$\boldsymbol{P}_{k|k} = \boldsymbol{P}_{k|k-1} - \boldsymbol{K}_k\boldsymbol{C}\boldsymbol{P}_{k|k-1} \tag{4.7}$$

where the gain matrix is:

$$\boldsymbol{K}_k = \boldsymbol{P}_{k|k-1}\boldsymbol{C}^T(\boldsymbol{C}\boldsymbol{P}_{k|k-1}\boldsymbol{C}^T + \boldsymbol{R}_k)^{-1}$$

and the measurement noise covariance is:

$$\boldsymbol{R} = \begin{bmatrix} 25 & 0 \\ 0 & 25 \end{bmatrix}$$

4.3 Simulation Results

There are two VR sink blocks using the same .wrl file in simulation: One of them is used to produce the images in sequence on the purpose of detection and estimation of the moving target via target tracking algorithm. Besides the camera can be oriented to the target by means of the other VR sink block. As explained in Section 4.1, location of the camera is (0, 0, 5000) and initial location of plane is (-2000, 1500, 0) in the direction of x, y and z axes, respectively. When we implemented the tracking algorithm in the system simulator, the flight of the target and trajectory of the outputs of the algorithm are shown in the Figure 4.5. Position of the plane and estimation of the tracker algorithm are simulated in Figure 4.6. It is clearly seen that the tracking algorithm captures the object in the image and estimates position and velocity of the target successfully.

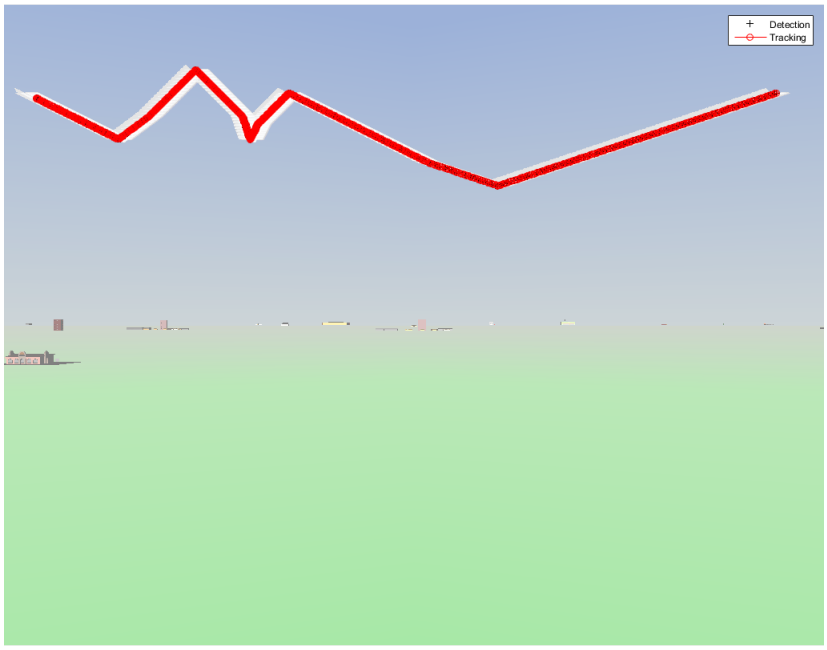

Figure 4.5: Trajectories of the outputs of the tracker algorithm

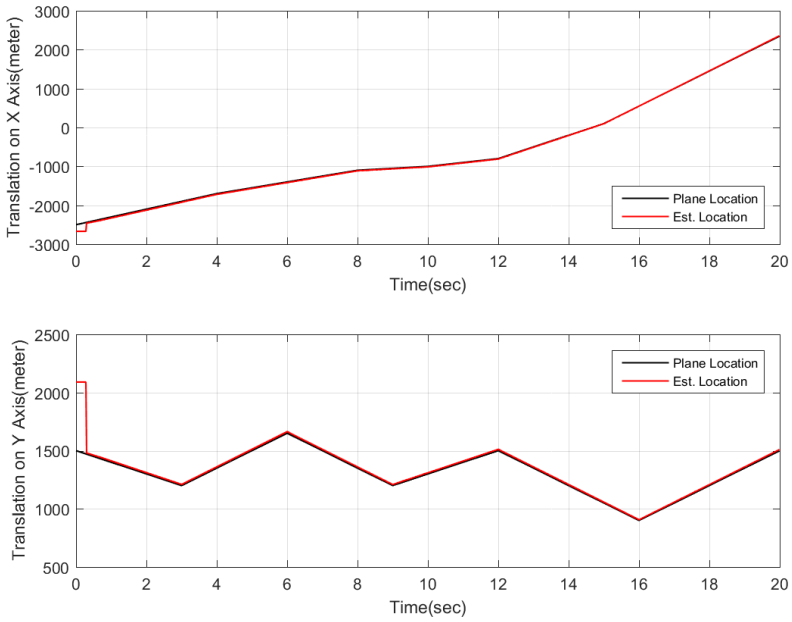

Figure 4.6: Position of the moving plane and estimation of the target tracking algorithm

Output of the tracker algorithm expresses the estimated translational position of the plane. In order to compute angular position references of the gimbal, these locational

data must be projected onto the angular displacements. Projection of LOS onto the virtual world is shown in figure 4.7.

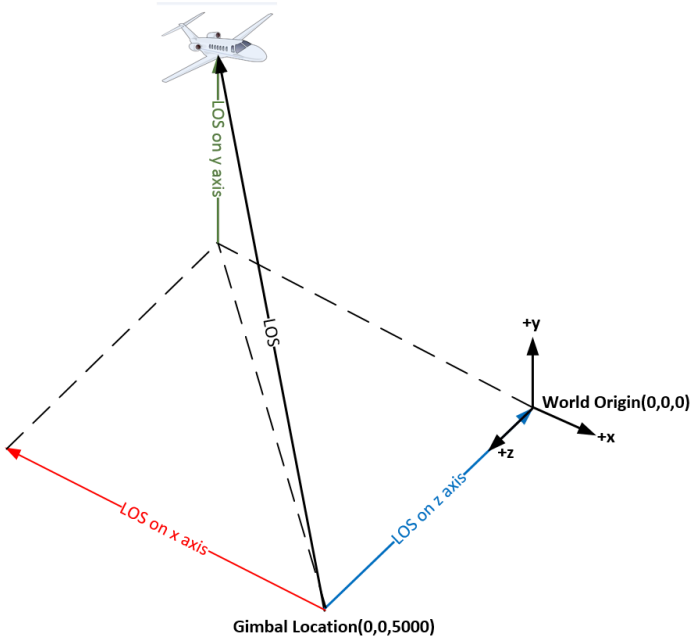

Figure 4.7: Projection of LOS onto the virtual world

From Figure 4.7, angular position references of outer and inner gimbals, expressed by η_{ref} and ϵ_{ref}, respectively, can be formulated by:

$$\eta_{ref} = \tan\left(\frac{x_{Est.PlaneLoc}}{z_{Est.PlaneLoc}}\right) = \tan\left(\frac{x_{Est.PlaneLoc}}{5000}\right)$$

$$\epsilon_{ref} = \tan\left(\frac{y_{Est.PlaneLoc}}{z_{Est.PlaneLoc}}\right) = \tan\left(\frac{y_{Est.PlaneLoc}}{5000}\right)$$

According to the performance comparison of cascade PI, global and local linear quadratic control methods in Section 3.3, cascade PI control has the best stabilization and positioning performance for the flight scenario of the target. Hence cascade PI is implemented in the visual tracking simulator. When angular tracker position commands are applied to the nonlinear gimbal model containing platform motions and sensor noise, system responses and motor torques of both outer and inner gimbals are shown in Figure 4.8 and 4.9, respectively.

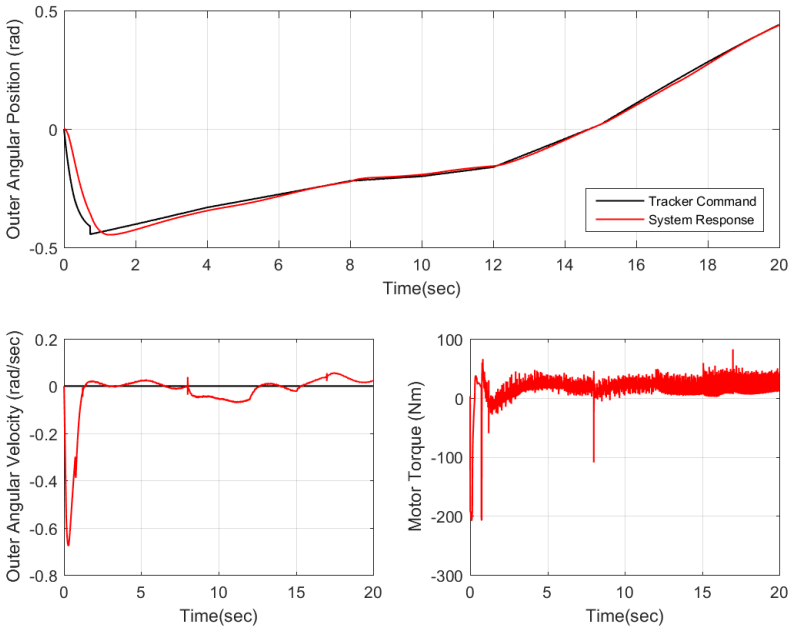

Figure 4.8: System responses and motor torque of outer gimbal when the system tracks a target in a virtual world

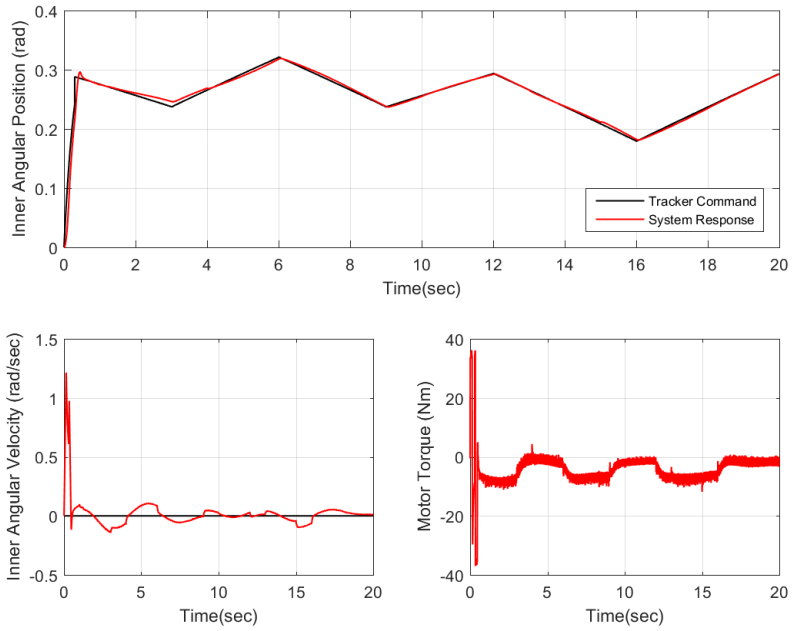

Figure 4.9: System responses and motor torque of inner gimbal when the system tracks a target in a virtual world

After tracker commands η_{ref} and ϵ_{ref} are computed and applied to the coupled 2-DOF gimbal model, angular position responses of outer (η) and inner (ϵ) gimbals are converted to the translational positions in the virtual world in order to view the target in the center of camera screen. Conversion of angular position responses of gimbals to the translational positions are computed by:

$$x_{LOS} = z_{LOS} \tan^{-}(\eta) = 5000 \tan^{-}(\eta)$$

$$y_{LOS} = z_{LOS} \tan^{-}(\epsilon) = 5000 \tan^{-}(\epsilon)$$

It must be stated that the center of the camera view is oriented by the translational projection of the outputs of the gimbal system onto the virtual world, or namely LOS, if the positions of the LOS is applied to the VR sink block. Virtual camera view of a 2-DOF gimbal tracking a plane is shown in Figure 4.10.

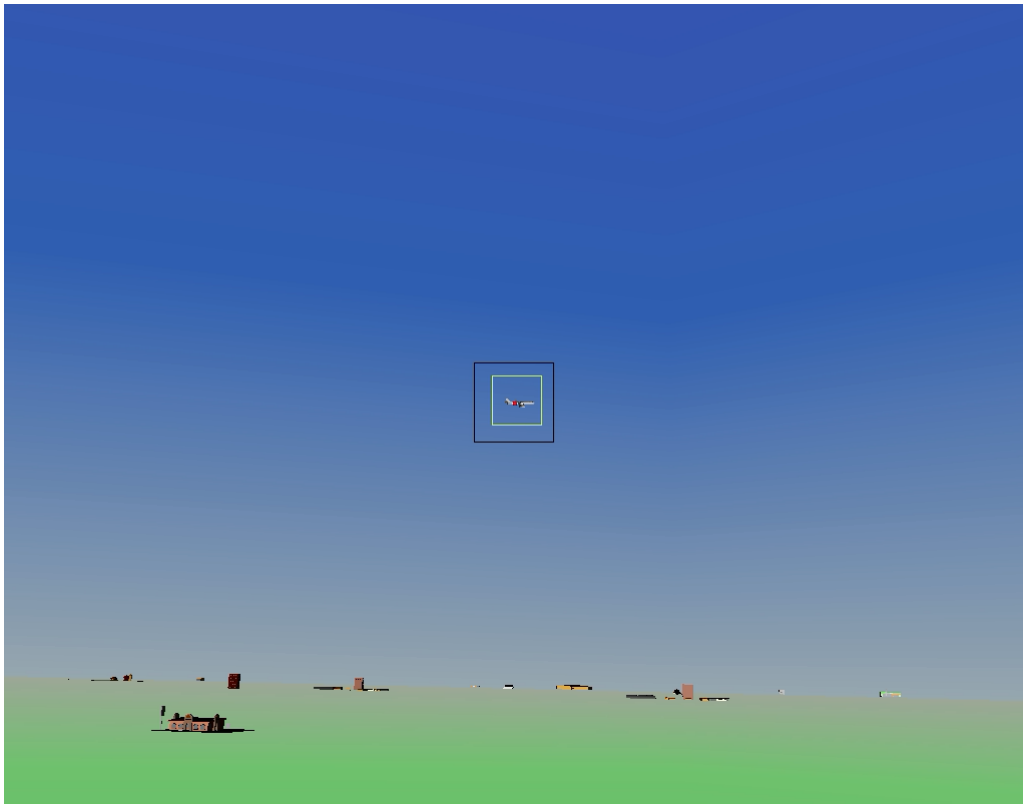

Figure 4.10: Virtual camera view of a 2-DOF gimbal system tracking a plane

In this figure, red point with a 80-by-80 pixel black square expresses the center of the

camera view and 60-by-60 pixel green square refers to the track gate. As a conclusion, we have constructed a realistic system simulator having a detailed system model, control method rejecting disturbances and pointing to the target, tracker algorithm detecting and estimating position and velocity of the target and a virtual reality world to observe flight scenarios.

CHAPTER 5

CONCLUSION AND FUTURE WORKS

This chapter is organized in a summary of the main results of this thesis and some recommendations for future studies have been suggested.

5.1 Summary

Simulation environment gives lots of opportunities for control system designers. For instance, system scenarios can be replicated multiple times, since computational times of simulations are very short and obtaining desired data using encoders and gyroscopes is very easy. This study focuses mainly on the detailed mathematical modeling of a 2-DOF gimbal on the purpose of obtaining a mathematical model as realistic as possible. The other purpose is to design different controllers and compare their performances. Finally, the best controller have been tested for its tracking performance in a virtual world. Parameters of the system model are obtained by a CAD analysis, because the physical system is yet to be constructed. It is to be noted that certain assumptions have been made in modeling, controller design and visualization of the virtual world.

Chapter 2 focuses on the detailed mathematical model of the gimbal system on the purpose of observing disturbance effects and obtaining a realistic system model by using Newton-Euler approach. Nonlinear effects of this system are friction between inner and outer gimbals, friction between outer gimbal and gimbal base, static and dynamic mass unbalances of inner and outer gimbals, motor friction and torque ripple.

Before dynamic equations and nonlinearities are formulated, first, reference frames and transformation matrices of this system are described. By means of transformation matrices between each reference frame, angular velocity and acceleration variables of frames are expressed. Then Dahl friction model is determined to be the most convenient model. In modeling of a DC brushed actuator, ripple torque and Coulomb friction torque are added to the basic motor model having electrical and mechanical parts. After kinematic equations are obtained, motor and friction models are expressed, dynamic equations of gimbal are written and system model is constructed. Apart from this conventional approach, modern control theory allows to construct a MIMO system model in state space. Therefore coupled 2-DOF gimbal, decoupled inner and decoupled outer gimbals are represented in state space to determine which approach is more convenient in control studies. Platform motions, sensor noise, kinematic and dynamic equations are defined in state space except motor models. After nonlinear models of gimbal are written in state space, linearization has been performed around too-many equilibrium points, which are clustered according to their similarities by means of the K-means algorithm and Calinski-Harabatz criterion. As a result, there are two LTI subsystems of both coupled 2-DOF and decoupled inner gimbal and three LTI subsystems of the decoupled outer gimbal.

Cascade PI control, which is a conventional technique, and linear quadratic integral (LQI), which is a relatively new technique, for the gimbal system are examined in Chapter 3. Both control methods are implemented in the nonlinear system models and their system performances are compared for different position commands. In state space, there are some differences between controls of the coupled and decoupled gimbals which are global and local LQI. Global LQI control yields the stabilization and tracking control problems of coupled system model by using one controller whereas two local LQI controllers have been designed for decoupled inner and outer gimbals, separately. Hence global LQI control applies two control signals (motor torques) to the coupled gimbal and each local LQI control carries out one control signal to drive its own gimbal. In the design procedure of cascade PI controllers of coupled gimbals, firstly rate controller parameters of both gimbals are tuned. Then position controllers and pre-filters are designed together to obtain the best performed control system. In LQI design, controller matrices $\hat{\boldsymbol{Q}}$ and $\hat{\boldsymbol{R}}$ are determined by us-

ing Bryson's rule allowing to weight state variables and optimal gain matrices $\hat{\boldsymbol{K}}$ are computed for all LTI subsystems of the coupled and decoupled gimbals. Next, control signals are weighted by a gain scheduling algorithm for each subsystem and sum of their outputs gives the overall system controller outputs. Last step of LQI design is determining the cut-off frequency of the pre-filter to satisfy the desired performance. In system simulator study, position commands are lower than 0.5 rad and rise time, settling time and elimination of disturbances contain more importance. For these position commands, all control methods have success in stabilization and tracking problems. Global LQI controller is the most successful controller for higher position commands. However, cascade PI control has the fast positioning and elimination performances for disturbances for lower position commands. Even though all control strategies are very successful for lower position commands, cascade PI control with pre-filters providing the best performance is preferred to implement in control system for system simulator.

Chapter 4 explains building of a virtual reality world to observe system scenarios when a plane is tracked by a gimbal looking from a constant distance and platform motion is carried out at the gimbal base. In the construction of this simulation environment, Simulink 3-D toolbox is used not only to create a virtual reality world by means of VREALM Builder, but also to implement the gimbal model, tracker and control algorithms. VR sink blocks can produce video frames and rotates the screen to the desired location. Hence two VR sink blocks are used in this study: One of them creates images in sequence for the tracker algorithm with the discrete Kalman filter to detect and estimate the target velocity, the other is used to move camera view of the gimbal to the target by means of position commands produced by the tracker algorithm. In conclusion, it has been obtained a realistic simulation environment which consists of a system model containing dynamics in detail, control method rejecting disturbances and pointing to a target, a tracker algorithm detecting location and flight of the target and a virtual reality world to observe system scenarios.

5.2 Future Works

This thesis study provides the requirements of system simulation; however there are still many theoretical and practical matters have been left untouched or not sufficiently discussed yet. In this section, some recommendations are given so as to obtain more realistic system simulator and compare their performances with control and tracker methods mentioned in previous sections.

Theoretical future works can improve system performance to eliminate disturbances or react faster to the reference signals as well as they may improve robustness, tracking and stabilization abilities. Firstly, some disturbance rejection algorithms can be implemented with the system model such as friction compensation and disturbance observer. Secondly, there are lots of reference-signals-shaping methods which may achieve faster and more robust system responses. In addition, linear controllers have been designed in this study; instead, different nonlinear controllers may be designed such as sliding mode control, and their performances can be compared with LQI and cascade PI control. Lastly, even though our tracker algorithm can be work successfully, it can not be guaranteed for every flight scenarios so that a new tracker algorithm can be designed for different cases.

In the simulation study, there are some assumptions for system model parameters so controllers are designed for this system models. All of system parameters may be identified via some optimization algorithms when physical system is completed. After system parameters are identified, they are implemented to the system model and controller can be designed again, theoretical and physical system performances can be compared between each other to check how realistic system simulator is. If there are differences between behaviors of physical and modeled systems, modeling study can be improved to implement the other unknown dynamics on the purpose of taking advantages of simulation studies.

REFERENCES

[1] M. Abdo, A. Toloei, A. R. Vali, and M. R. Arvan. Cascade Control System for Two Axes Gimbal System with Mass Unbalance. *International Journal of Scientific & Engineering Research*, 4:903–912, 2013.

[2] B. Armstrong-Hélouvry, P. Dupont, and C. C. De Wit. A Survey of Models, Analysis Tools and Compensation Methods for the Control of Machines with Friction. *Automatica*, 30(7):1083–1138, 1994.

[3] P. Bliman and M. Sorine. Easy-to-use Realistic Dry Friction Models for Automatic Control. In *Proceedings of 3rd European Control Conference*, volume 113, pages 267–272, 1995.

[4] J.-L. Boiffier. *The Dynamics of Flight: The Equations*, Volume 1. John Wiley & Sons, 1998.

[5] A. E. Bryson and W. F. Denham. A Steepest-ascent Method for Solving Optimum Programming Problems. *Journal of Applied Mechanics*, 29(2):247–257, 1962.

[6] M. S. Büyüksarıkulak. Autopilot Design for a Quadrator. Master's Thesis, METU, 2014.

[7] T. Caliński and J. Harabasz. A Dendrite Method for Cluster Analysis. *Communications in Statistics-theory and Methods*, 3(1):1–27, 1974.

[8] R. Carrey and G. Bell. The Annotated VRML97 Reference Manual, 1997.

[9] J. L. Crassidis and J. L. Junkins. *Optimal Estimation of Dynamic Systems*. CRC Press, 2011.

[10] I. E. Şener. Stabilization of an Image Based Tracking System. Master's Thesis, METU, 2015.

[11] E. V. Cuevas, D. Zaldivar, and R. Rojas. Kalman Filter For Vision Tracking. 2005.

[12] P. Dahl. A Solid Friction Model. Technical Report, DTIC Document, 1968.

[13] D. L. Davies and D. W. Bouldin. A Cluster Separation Measure. *IEEE Transactions on Pattern Analysis and Machine Intelligence*, PAMI-1(2):224–227, 1979.

[14] C. C. De Wit, H. Olsson, K. J. Astrom, and P. Lischinsky. A New Model for Control of Systems with Friction. *Automatic Control, IEEE Transactions on*, 40(3):419–425, 1995.

[15] D. Domínguez. VRML and Simulink Interface for the Development of 3-D Simulator for Mobile Robots. In *Proceedings of World Academy of Science, Engineering and Technology*, volume 25. Citeseer, 2007.

[16] B. Ekstrand. Equations of Motion for A Two Axes Gimbal System. *Aerospace and Electronic Systems, IEEE Transactions on*, 37(3):1083–1091, 2001.

[17] C. A. Ganzaroli, D. F. de Carvalho, R. N. Dias, M. R. Reis, A. J. Alves, J. L. Domingos, and W. P. Calixto. Heuristic and Deterministic Strategies Applied on Cascade PI Controller Tuning for Speed Control of a DC Motor. In *2015 CHILEAN Conference on Electrical, Electronics Engineering, Information and Communication Technologies (CHILECON)*, pages 101–106. IEEE, 2015.

[18] D. A. Haessig and B. Friedland. On the Modeling and Simulation of Friction. *Journal of Dynamic Systems, Measurement, and Control*, 113(3):354–362, 1991.

[19] J. Hespanha. Lecture Notes on LQR/LQG Controller Design. *notes, http://www. uz. zgora. pl/˜ wpaszke/materialy/kss/lqrnotes.pdf*, 2005.

[20] J. Hilkert. Inertially Stabilized Platform Technology Concepts and Principles. *IEEE Control Systems*, 28(1):26–46, 2008.

[21] B. K. Horn and B. G. Schunck. Determining Optical Flow. *Artificial intelligence*, 17(1-3):185–203, 1981.

[22] G. D. Illeperuma and U. J. Sonnadara. An Autonomous Robot Navigation System Based on Optical Flow. In *2011 6th International Conference on Industrial and Information Systems*, pages 489–492. IEEE, 2011.

[23] X. Jianbo and L. Jingwei. Moving Target Tracking Algorithm Based on Scale Invariant Optical Flow Method. *Information Science and Control Engineering (ICISCE), 2016 3rd International Conference on*, pages 468–472, 2016.

[24] D. Karnopp. Computer Simulation of Stick-slip Friction in Mechanical Dynamic Systems. *Journal of dynamic systems, measurement, and control*, 107(1):100–103, 1985.

[25] P. J. Kennedy and R. L. Kennedy. Direct Versus Indirect Line of Sight (LoS) Stabilization. *Control Systems Technology, IEEE Transactions on*, 11(1):3–15, 2003.

[26] H. K. Khalil. *Nonlinear Systems*. Prentice Hall, 3rd ed edition, 2002.

[27] H. Khodadadi, M. R. J. Motlagh, and M. Gorji. Robust Control and Modeling a 2-DOF Inertial Stabilized Platform. In *Electrical, Control and Computer Engineering (INECCE), 2011 International Conference on*, pages 223–228. IEEE, 2011.

[28] D. E. Kirk. *Optimal Control Theory: An Introduction*. Courier Corporation, 2012.

[29] C. Knospe. PID Control. *IEEE Control Systems Magazine*, 26(1):30–31, 2006.

[30] S. Lloyd. Least Squares Quantization in PCM. *IEEE transactions on information theory*, 28(2):129–137, 1982.

[31] Mathworks. Computer Vision System Toolbox User's Guide. Accessed: 2016-11-05.

[32] Mathworks. Simulink 3D Animation User's Guide. Accessed: 2016-11-03.

[33] Mathworks. Statistics and Machine Learning Toolbox User's Guide. Accessed: 2016-11-03.

[34] U. Maulik and S. Bandyopadhyay. Performance Evaluation of Some Clustering Algorithms and Validity Indices. *IEEE Transactions on Pattern Analysis and Machine Intelligence*, 24(12):1650–1654, 2002.

[35] K. I. Motor. Direct Drive DC Motors Catalogue. *Radford, VA, USA: Kollmorgen Corporation*.

[36] K. Ogata and Y. Yang. *Modern Control Engineering*. Prentice-Hall Englewood Cliffs, 5 edition, 2010.

[37] H. Olsson, K. J. Åström, C. C. De Wit, M. Gäfvert, and P. Lischinsky. Friction Models and Friction Compensation. *European journal of control*, 4(3):176–195, 1998.

[38] D. R. Otlowski, K. Wiener, and B. A. Rathbun. Mass Properties Factors in Achieving Stable Imagery from a Gimbal Mounted Camera. In *SPIE Defense and Security Symposium*, pages 69460B–69460B. International Society for Optics and Photonics, 2008.

[39] T. Öztürk. Angular Acceleration Assisted Stabilization of a 2-DOF Gimbal Platform. Master's Thesis, METU, 2010.

[40] O. Ravn, T. D. Larsen, and N. Andersen. Simulation and Animation in Simulink and VRML. In *Computer Aided Control System Design, 1999. Proceedings of the 1999 IEEE International Symposium on*, pages 120–125. IEEE, 1999.

[41] J. D. Robinson. A Linear Quadratic Regulator Weight Selection Algorithm for Robust Pole Assignment. Technical Report, DTIC Document, 1990.

[42] E. Sincar. Friction Identification and Compensation in Stabilized Platforms. Master's Thesis, METU, 2013.

[43] K. Xia, J. Lu, C. Bi, Y. Tan, and B. Dong. Dynamic Commutation Torque-ripple Reduction for Brushless DC Motor Based on Quasi-z-source Net. *IET Electric Power Applications*, 2016.

[44] H. Xinjian, J. Ruiqing, C. Li, and Z. Zhaohua. The Realization of Simulation of Vehicle Dynamics Model Visualization Based on Simulink and VR Toolbox. In *Education Technology and Computer Science (ETCS), 2010 Second International Workshop on*, volume 3, pages 224–227. IEEE, 2010.

[45] L. Zheng-wen, Z. Guo-liang, Z. Wei-ping, and J. Bin. A Simulation Platform Design of Humanoid Robot Based on Simmechanics and VRML. *Procedia Engineering*, 15:215–219, 2011.

APPENDIX A

DETAILED MATHEMATICAL EXPRESSIONS

A.1 Angular Acceleration

Component of $\boldsymbol{\alpha}_{Oe}$ about the x axis is:

$$\begin{aligned}\alpha_{Oe_x} = &+ \ddot{\phi}\cos\eta + \ddot{\theta}\cos\phi\sin\eta - \ddot{\psi}(\cos\eta\sin\theta + \cos\theta\sin\eta\sin\phi) \\ &+ \dot{\eta}(\dot{\phi}\sin\eta - \dot{\psi}(\sin\eta\sin\theta + \cos\eta\cos\theta\sin\phi) - \dot{\theta}\cos\eta\cos\phi) \\ &+ \dot{\psi}\dot{\theta}((\cos^2\eta - \cos\phi\sin^2\eta)\cos\theta + (1+\cos\eta)\sin\eta\sin\phi\sin\theta)\cos\phi \\ &+ \dot{\phi}(\dot{\theta}(\sin\phi\cos\eta + \cos\phi\sin\eta)\sin\phi - \dot{\psi}(\cos\phi\sin\eta + \cos\eta\sin\phi)\cos\phi\cos\theta)\end{aligned} \tag{A.1}$$

, component of $\boldsymbol{\alpha}_{Oe}$ about the y axis is:

$$\begin{aligned}\alpha_{Oe_y} = &+ \ddot{\theta}\cos\eta\cos\phi - \ddot{\phi}\sin\eta + \ddot{\psi}(\sin\eta\sin\theta + \cos\eta\cos\theta\sin\phi) \\ &+ \dot{\eta}(\dot{\phi}\cos\eta + \dot{\theta}\cos\phi\sin\eta + \dot{\psi}(\cos\theta\sin\eta\sin\phi - \cos\eta\sin\theta)) \\ &+ \dot{\phi}\dot{\theta}(\cos\eta\cos\phi\sin\phi - \sin\eta - \cos^2\phi\sin\eta) \\ &+ \dot{\phi}\dot{\psi}(\sin\eta\sin\phi - \cos\eta\cos\phi)\cos\theta\cos\phi \\ &+ \dot{\psi}\dot{\theta}(\sin\phi\sin\theta(1+\cos\eta) - \cos\theta\sin\eta(1+\sin\eta))\cos\eta\cos\phi\end{aligned} \tag{A.2}$$

and component of $\boldsymbol{\alpha}_{Oe}$ about the z axis is:

$$\alpha_{Oe_z} = \ddot{\eta} + \alpha_{dist_{O_z}} \tag{A.3}$$

where $\alpha_{dist_{O_z}}$ is disturbance acceleration effect on the z axis of outer gimbal

$$
\begin{aligned}
\alpha_{dist_{O_z}} = & -\ddot{\theta}\sin\phi + \ddot{\psi}\cos\phi\cos\theta \\
& + \dot{\psi}\dot{\theta}(\cos\phi\cos\theta\sin\eta\sin\phi - \sin^2\phi\sin\theta + \cos\eta\cos^2\phi\sin\theta) \\
& + \dot{\phi}(\dot{\psi}(\cos\phi\cos\theta\sin\phi - \sin\phi\sin\theta) + \dot{\theta}\cos^2\phi)
\end{aligned}
$$

In addition, component of $\boldsymbol{\alpha}_{Ie}$ about the x axis is:

$$
\alpha_{Ie_x} = -\ddot{\eta}\sin\epsilon + \alpha_{dist_{I_x}} \tag{A.4}
$$

where $\alpha_{dist_{I_x}}$ representing the disturbance acceleration effect on the x axis of inner gimbal is:

$$
\begin{aligned}
\alpha_{dist_{I_x}} = & + \ddot{\phi}\cos\epsilon\cos\eta + \ddot{\theta}(\sin\epsilon\sin\phi + \cos\epsilon\cos\phi\sin\eta) \\
& - \ddot{\psi}(\cos\epsilon\cos\eta\sin\theta - \cos\phi\cos\theta\sin\epsilon + \cos\epsilon\cos\theta\sin\eta\sin\phi) \\
& + \dot{\eta}\dot{\epsilon}\cos\epsilon - \dot{\phi}\dot{\theta}\cos^2\phi\sin\epsilon + \dot{\phi}\dot{\theta}\cos\epsilon\cos\eta + \dot{\eta}\dot{\phi}\cos\epsilon\sin\eta + \dot{\epsilon}\dot{\phi}\cos\eta\sin\epsilon \\
& - \dot{\epsilon}\dot{\theta}\cos\epsilon\sin\phi + \dot{\psi}\dot{\theta}\sin\epsilon\sin^2\phi\sin\theta - \dot{\eta}\dot{\theta}\cos\epsilon\cos\eta\cos\phi + \dot{\epsilon}\dot{\psi}\cos\epsilon\cos\phi\cos\theta \\
& + \dot{\epsilon}\dot{\theta}\cos\phi\sin\epsilon\sin\eta - \dot{\eta}\dot{\psi}\cos\epsilon\sin\eta\sin\theta - \dot{\epsilon}\dot{\psi}\cos\eta\sin\epsilon\sin\theta + \dot{\phi}\dot{\psi}\sin\epsilon\sin\phi\sin\theta \\
& - \dot{\phi}\dot{\theta}\cos\epsilon\cos\eta\cos\phi^2 - \dot{\psi}\dot{\theta}\cos\epsilon\cos^2\phi\cos\theta\sin^2\eta - \dot{\eta}\dot{\psi}\cos\epsilon\cos\eta\cos\theta\sin\phi \\
& + \dot{\phi}\dot{\theta}\cos\epsilon\cos\phi\sin\eta\sin\phi - \dot{\phi}\dot{\psi}\cos\phi\cos\theta\sin\epsilon\sin\phi + \dot{\epsilon}\dot{\psi}\cos\theta\sin\epsilon\sin\eta\sin\phi \\
& + \dot{\psi}\dot{\theta}\cos\epsilon\cos^2\eta\cos\phi\cos\theta - \dot{\phi}\dot{\psi}\cos\epsilon\cos^2\phi\cos\theta\sin\eta - \dot{\psi}\dot{\theta}\cos\eta\cos^2\phi\sin\epsilon\sin\theta \\
& + \dot{\psi}\dot{\theta}(\cos\epsilon\sin\theta - \cos\theta\sin\epsilon + \cos\epsilon\cos\eta\sin\theta)\cos\phi\sin\phi\sin\eta \\
& - \dot{\phi}\dot{\psi}\cos\epsilon\cos\eta\cos\phi\cos\theta\sin\phi
\end{aligned}
$$

, component of $\boldsymbol{\alpha}_{Ie}$ about the y axis is:

$$
\alpha_{Ie_y} = \ddot{\epsilon} + \alpha_{dist_{I_y}} \tag{A.5}
$$

where $\alpha_{dist_{I_y}}$ representing the disturbance acceleration effect on the y axis of inner gimbal is:

$$
\begin{aligned}
\alpha_{dist_{I_y}} =& -\ddot{\phi}\sin\eta + \ddot{\psi}(\cos\eta\cos\theta\sin\phi + \sin\eta\sin\theta) + \ddot{\theta}\cos\eta\cos\phi \\
&- \dot{\phi}\dot{\theta}\sin\eta + \dot{\eta}\dot{\phi}\cos\eta + \dot{\phi}\dot{\theta}\cos^2\phi\sin\eta + \dot{\psi}\dot{\theta}\cos^2\eta\cos\phi\sin\phi\sin\theta \\
&+ \dot{\eta}\dot{\theta}\cos\phi\sin\eta - \dot{\eta}\dot{\psi}\cos\eta\sin\theta + \dot{\phi}\dot{\theta}\cos\eta\cos\phi\sin\phi \\
&+ \dot{\eta}\dot{\psi}\cos\theta\sin\eta\sin\phi - \dot{\phi}\dot{\psi}\cos\eta\cos^2\phi\cos\theta - \dot{\psi}\dot{\theta}\cos\eta\cos\phi\cos\theta\sin\eta \\
&+ \dot{\phi}\dot{\psi}\cos\phi\cos\theta\sin\eta\sin\phi + \dot{\psi}\dot{\theta}\cos\eta\cos\phi\sin\phi\sin\theta \\
&- \dot{\psi}\dot{\theta}\cos\eta\cos^2\phi\cos\theta\sin\eta
\end{aligned}
$$

and component of $\boldsymbol{\alpha}_{Ie}$ about the z axis is:

$$
\alpha_{Ie_z} = \ddot{\eta}\cos\epsilon + \alpha_{dist_{I_z}} \tag{A.6}
$$

where $\alpha_{dist_{I_z}}$ representing the disturbance acceleration effect on the z axis of inner gimbal is:

$$
\begin{aligned}
\alpha_{dist_{I_z}} =& \ddot{\phi}\cos\eta\sin\epsilon + \ddot{\theta}(\cos\phi\sin\epsilon\sin\eta - \cos\epsilon\sin\phi) \\
&+ \ddot{\psi}(\cos\epsilon\cos\phi\cos\theta - \cos\eta\sin\epsilon\sin\theta + \cos\theta\sin\epsilon\sin\eta\sin\phi) \\
&+ \dot{\eta}(\dot{\epsilon} + \dot{\phi}\sin\eta - \dot{\psi}\sin\eta\sin\theta - \dot{\psi}\cos\eta\cos\theta\sin\phi - \dot{\theta}\cos\eta\cos\phi)\sin\epsilon \\
&+ \dot{\epsilon}\dot{\psi}(\cos\epsilon\cos\eta\sin\theta + \cos\phi\cos\theta\sin\epsilon - \cos\epsilon\cos\theta\sin\eta\sin\phi) \\
&- \dot{\epsilon}\dot{\phi}\cos\epsilon\cos\eta - \dot{\epsilon}\dot{\theta}(\sin\epsilon\sin\phi + \cos\epsilon\cos\phi\sin\eta) \\
&+ \dot{\phi}\dot{\theta}(\cos\phi\sin\epsilon\sin\eta\sin\phi + \cos\epsilon\cos^2\phi + \cos\eta\sin\epsilon - \cos\eta\cos^2\phi\sin\epsilon) \\
&+ \dot{\psi}\dot{\theta}(\cos\epsilon\cos\eta\cos^2\phi\sin\theta + \cos^2\eta\cos\phi\cos\theta\sin\epsilon - \cos\epsilon\sin\phi^2\sin\theta \\
&- \cos^2\phi\cos\theta\sin\epsilon\sin^2\eta + \cos\epsilon\cos\phi\cos\theta\sin\eta\sin\phi \\
&+ \cos\phi\sin\epsilon\sin\eta\sin\phi\sin\theta + \cos\eta\cos\phi\sin\epsilon\sin\eta\sin\phi\sin\theta) \\
&+ \dot{\phi}\dot{\psi}(\cos\epsilon\cos\phi\cos\theta\sin\phi - \cos\epsilon\sin\phi\sin\theta - \cos^2\phi\cos\theta\sin\epsilon\sin\eta \\
&- \cos\eta\cos\phi\cos\theta\sin\epsilon\sin\phi)
\end{aligned}
$$

A.2 Dynamic Equations

Firstly, dynamic equations of outer gimbal can be written as three scalar equations by Eq. 2.36. Dynamic equations of inner gimbal on x, y and z axes with respect to angular velocity and acceleration terms are given below, respectively.

$$\begin{aligned} & I^I_{xx}\alpha_{Ie_x} + I^I_{xy}\alpha_{Ie_y} + I^I_{xz}\alpha_{Ie_z} - \Omega_{Ie_z}(I^I_{xy}\Omega_{Ie_x} + I^I_{yy}\Omega_{Ie_y} + I^I_{yz}\Omega_{Ie_z}) \\ & \quad + \Omega_{Ie_y}(I^I_{xz}\Omega_{Ie_x} + I^I_{yz}\Omega_{Ie_y} + I^I_{zz}\Omega_{Ie_z}) \\ & \quad = -gm_I r_{PG_{I_y}}(\cos(\epsilon)\cos(\theta) - \sin(\epsilon)\sin(\theta)) \end{aligned} \tag{A.7}$$

$$\begin{aligned} & I^I_{xy}\alpha_{Ie_x} + I^I_{yy}\alpha_{Ie_y} + I^I_{yz}\alpha_{Ie_z} + \Omega_{Ie_z}(I^I_{xx}\Omega_{Ie_x} + I^I_{xy}\Omega_{Ie_y} + I^I_{xz}\Omega_{Ie_z}) \\ & \quad - \Omega_{Ie_x}(I^I_{xz}\Omega_{Ie_x} + I^I_{yz}\Omega_{Ie_y} + I^I_{zz}\Omega_{Ie_z}) \\ & \quad = T_{m_I} + T_{fr_{OI}} + gm_I r_{PG_{I_x}}(\cos(\epsilon)\cos(\theta) - \sin(\epsilon)\sin(\theta)) \\ & \quad + gm_I r_{PG_{I_z}}(\cos(\epsilon)\sin(\theta) + \cos(\theta)\sin(\epsilon)) \end{aligned} \tag{A.8}$$

$$\begin{aligned} & I^I_{xz}\alpha_{Ie_x} + I^I_{yz}\alpha_{Ie_y} + I^I_{zz}\alpha_{Ie_z} - \Omega_{Ie_y}(I^I_{xx}\Omega_{Ie_x} + I^I_{xy}\Omega_{Ie_y} + I^I_{xz}\Omega_{Ie_z}) \\ & \quad + \Omega_{Ie_x}(I^I_{xy}\Omega_{Ie_x} + I^I_{yy}\Omega_{Ie_y} + I^I_{yz}\Omega_{Ie_z}) \\ & \quad = -gm_I r_{PG_{I_y}}(\cos(\epsilon)\sin(\theta) + \sin(\epsilon)\cos(\theta)) \end{aligned} \tag{A.9}$$

Secondly, in order to obtain dynamic equations of the outer gimbal, Eq. 2.47 is described as three scalar equations. Dynamic equations of the outer gimbal on x, y and z axes with respect to angular velocity and acceleration terms are given below, respectively.

$$\begin{aligned} & I^O_{xx}\alpha_{Oe_x} + I^O_{xy}\alpha_{Oe_y} + I^O_{xz}\alpha_{Oe_z} \\ & + \alpha_{Ie_x}(I^I_{xx}\cos\epsilon - I^I_{xz}\sin\epsilon) + \alpha_{Ie_y}(I^I_{xy}\cos\epsilon - I^I_{yz}\sin\epsilon) + \alpha_{Ie_z}(I^I_{xz}\cos\epsilon - I^I_{zz}\sin\epsilon) \\ & - \Omega_{Oe_z}(I^I_{xy}\Omega_{Oe_x} + I^O_{xy}\Omega_{Oe_x} + I^I_{yy}\Omega_{Oe_y} + I^O_{yy}\Omega_{Oe_y} + I^I_{yz}\Omega_{Oe_z} + I^O_{yz}\Omega_{Oe_z}) \\ & + \Omega_{Oe_y}(I^O_{xz}\Omega_{Oe_x} + I^O_{yz}\Omega_{Oe_y} + I^O_{zz}\Omega_{Oe_z} + \Omega_{Oe_x}(I^I_{xz}\cos\epsilon + I^I_{xx}\sin\epsilon) \\ & + \Omega_{Oe_y}(I^I_{yz}\cos\epsilon + I^I_{xy}\sin\epsilon) + \Omega_{Oe_z}(I^I_{zz}\cos\epsilon + I^I_{xz}\sin\epsilon)) \\ & + \Omega_{Ie_x}\dot{\epsilon}(I^I_{xz}\cos\epsilon + I^I_{xx}\sin\epsilon) + \Omega_{Ie_y}\dot{\epsilon}(I^I_{yz}\cos\epsilon + I^I_{xy}\sin\epsilon) \\ & + \Omega_{Ie_z}\dot{\epsilon}(I^I_{zz}\cos\epsilon + I^I_{xz}\sin\epsilon) \\ & = g(m0 + m1)((\sin\eta\sin\theta + \cos\eta\sin\phi\cos\theta)r_{PG_{O_z}} - (\cos\phi\cos\theta)r_{PG_{O_y}}) \end{aligned} \tag{A.10}$$

$$
\begin{aligned}
&I^I_{xy}\alpha_{Ie_x} + I^O_{xy}\alpha_{Oe_x} + I^I_{yy}\alpha_{Ie_y} + I^O_{yy}\alpha_{Oe_y} + I^I_{yz}\alpha_{Ie_z} + I^O_{yz}\alpha_{Oe_z} \\
&+ \Omega_{Oe_z}(I^O_{xx}\Omega_{Oe_x} + I^O_{xy}\Omega_{Oe_y} + I^O_{xz}\Omega_{Oe_z} + \Omega_{Oe_x}(I^I_{xx}\cos\epsilon - I^I_{xz}\sin\epsilon) \\
&+ \Omega_{Oe_y}(I^I_{xy}\cos\epsilon - I^I_{yz}\sin\epsilon) + \Omega_{Oe_z}(I^I_{xz}\cos\epsilon - I^I_{zz}\sin\epsilon)) \\
&- \Omega_{Oe_x}(I^O_{xz}\Omega_{Oe_x} + I^O_{yz}\Omega_{Oe_y} + I^O_{zz}\Omega_{Oe_z} + \Omega_{Oe_x}(I^I_{xz}\cos\epsilon + I^I_{xx}\sin\epsilon) \\
&+ \Omega_{Oe_y}(I^I_{yz}\cos\epsilon + I^I_{xy}\sin\epsilon) + \Omega_{Oe_z}(I^I_{zz}\cos\epsilon + I^I_{xz}\sin\epsilon)) \\
&= g(m_O + m_I)(\cos\phi\cos\theta r_{PG_{O_x}} - (-\cos\eta\sin\theta + \sin\eta\sin\phi\cos\theta)r_{PG_{O_z}})
\end{aligned}
\tag{A.11}
$$

$$
\begin{aligned}
&I^O_{xz}\alpha_{Oe_x} + I^O_{yz}\alpha_{Oe_y} + I^O_{zz}\alpha_{Oe_z} + \alpha_{Ie_x}(I^I_{xz}\cos\epsilon + I^I_{xx}\sin\epsilon) + \alpha_{Ie_y}(I^I_{yz}\cos\epsilon + I^I_{xz}\sin\epsilon) \\
&+ \alpha_{Ie_z}(I^I_{zz}\cos\epsilon + I^I_{xz}\sin\epsilon) \\
&+ \Omega_{Oe_x}(I^I_{xy}\Omega_{Oe_x} + I^O_{xy}\Omega_{Oe_x} + I^I_{yy}\Omega_{Oe_y} + I^O_{yy}\Omega_{Oe_y} + I^I_{yz}\Omega_{Oe_z} + I^O_{yz}\Omega_{Oe_z}) \\
&- \Omega_{Oe_y}(I^O_{xx}\Omega_{Oe_x} + I^O_{xy}\Omega_{Oe_y} + I^O_{xz}\Omega_{Oe_z} + \Omega_{Oe_x}(I^I_{xx}\cos\epsilon - I^I_{xz}\sin\epsilon) \\
&+ \Omega_{Oe_y}(I^I_{xy}\cos\epsilon - I^I_{yz}\sin\epsilon) + \Omega_{Oe_z}(I^I_{xz}\cos\epsilon - I^I_{zz}\sin\epsilon)) - \Omega_{Ie_x}\dot{\epsilon}(I^I_{xx}\cos\epsilon - I^I_{xz}\sin\epsilon) \\
&- \Omega_{Ie_y}\dot{\epsilon}(I^I_{xy}\cos\epsilon - I^I_{yz}\sin\epsilon) - \Omega_{Ie_z}\dot{\epsilon}(I^I_{xz}\cos\epsilon - I^I_{zz}\sin\epsilon) \\
&= T_{m_O} + T_{fr_{BO}} + T_{fr_{IO}} + g(m_O + m_I)((-\cos\eta\sin\theta + \sin\eta\sin\phi\cos\theta)r_{PG_{O_y}} \\
&- (\sin\eta\sin\theta + \cos\eta\sin\phi\cos\theta)r_{PG_{O_x}})
\end{aligned}
\tag{A.12}
$$

APPENDIX B

SIMULINK BLOCKS

B.1 Friction and DC Motor Models

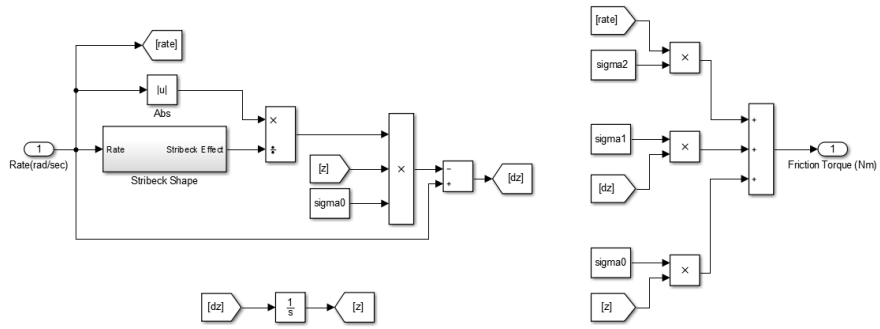

Figure B.1: Simulink block of LuGre friction model

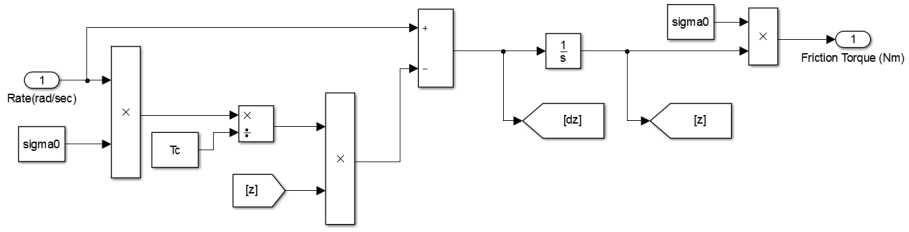

Figure B.2: Simulink block of Dahl friction model

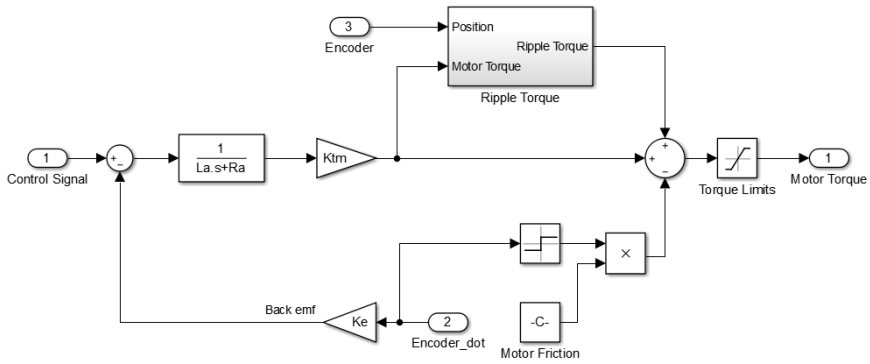

Figure B.3: Simulink block of a brushed DC motor model

B.2 Cascade PI Control

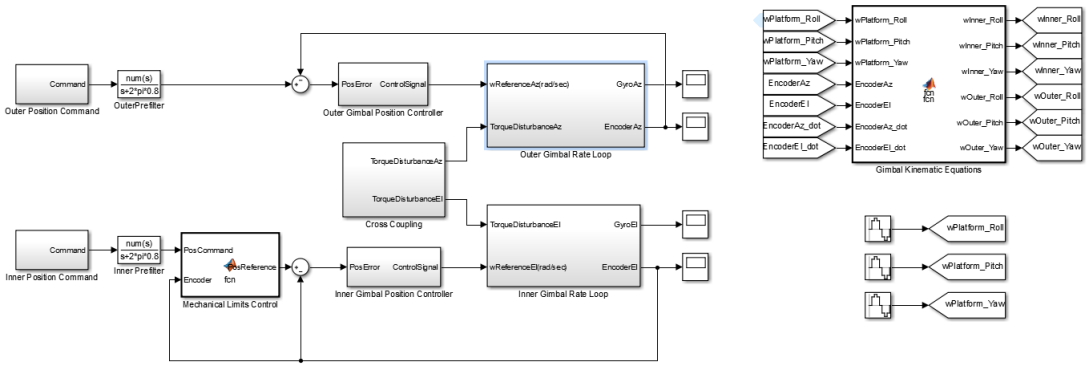

Figure B.4: Simulink block of cascade PI control

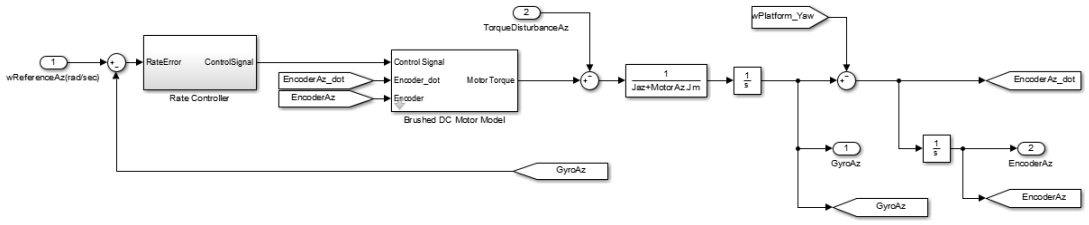

Figure B.5: Simulink block of outer gimbal cascade PI control rate loop

B.3 System Simulator

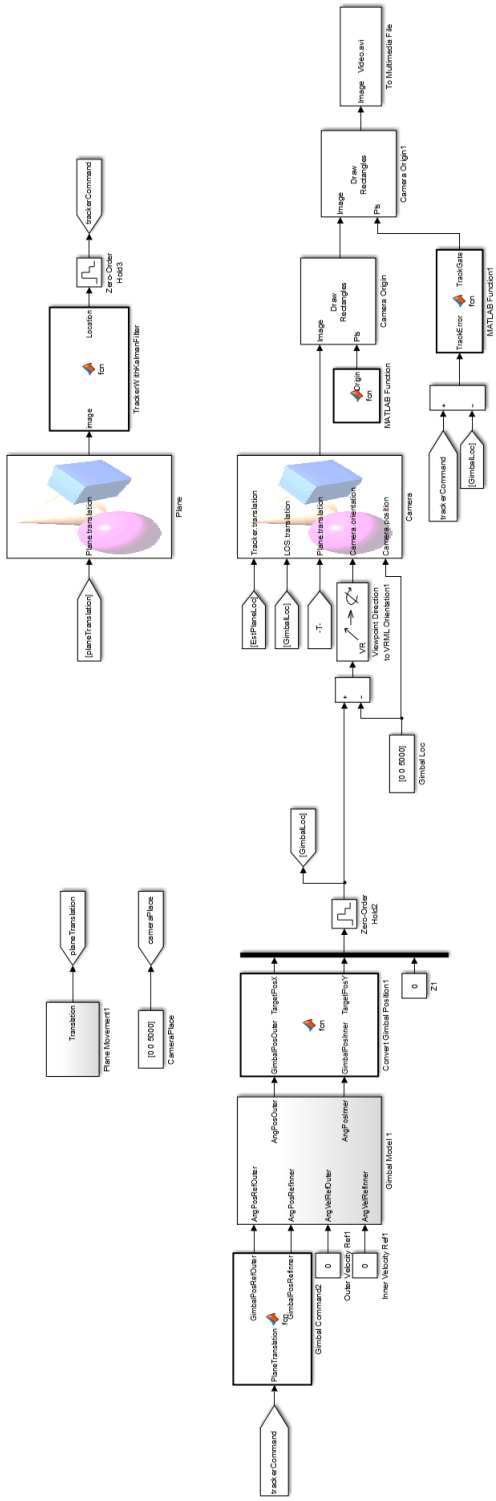

Figure B.6: Simulink model of the system simulator